Coherent control and manipulation of electromagnetic fields in novel quantum optical systems

A thesis submitted in partial fulfilment of the requirements for the award of

DOCTOR OF PHILOSOPHY

by

Sandeep Sharma

Department of Physics
Indian Institute of Technology Guwahati
Guwahati 781039, India.

March 2018

TH-1819_11612116

Dedicated to my family

TH-1819_11612116

TH-1819_11612116

Declaration

I hereby declare that the contents of this thesis are original and have not been submitted for consideration for any other degree or qualification in this, or any other university. This dissertation is my own work and contains nothing which is the outcome of work done by others, except for the collaboration as specified in the text and Acknowledgements.

Sandeep Sharma
March 2018

TH-1819_11612116

TH-1819_11612116

Certificate

This is to certify that the work contained in the thesis entitled "**Coherent control and manipulation of electromagnetic fields in novel quantum optical systems**" submitted by Sandeep Sharma in the partial fulfillment of the requirement for the award of the degree of Doctor of Philosophy in Physics, Department of Physics, Indian Institute of Technology Guwahati, is a record of the candidate's own work carried out by him under my supervision and guidance. The matter embodied in this report has not been submitted in part or full to any other university or institute for the award of any degree.

Dr. Tarak Nath Dey
Associate Professor
Department of Physics
Indian Institute of Technology Guwahati
Guwahati - 781039
Assam, India.

March 2018

TH-1819_11612116

TH-1819_11612116

Acknowledgements

First and foremost, I take this opportunity to express my heartfelt gratitude to my thesis supervisor Dr. Tarak Nath Dey for his guidance, encouragement, help and support in accomplishing this research work. His enthusiasm and insightful criticism has been inspiring and motivating throughout the period of my research. I am deeply indebted to him for giving me the opportunity to carry out my research work under his guidance.

I would like to extend my sincerest gratitude to my doctoral committee members, Prof. Girish S. Setlur, Dr. Ashwini K. Sharma and Dr. Vinay Wagh for their insightful comments and suggestion during my review seminars.

I take immense pleasure to express my deep sense of gratitude to Prof. Bimalendu Deb, Department of Material Science, Indian Association for the Cultivation of Science (IACS), Jadavpur, Kolkata for providing me an opportunity to work with him. I am grateful to him for his kind care and hospitality during my visit to IACS. I wish to acknowledge his Ph.D. students Arpita Rakshit, Biswajit Das, Somnath Naskar, Debashree Chakraborty for their kind help and discussion during my stay at IACS.

I sincerely acknowledge Dr. Charudatt Y. Kadolkar, Department of Physics, IIT Guwahati for his consistent support and indispensable suggestions during the course of my research work.

I take this opportunity to sincerely acknowledge the financial assistance from MHRD which helped me in completing of my research work successfully.

I extend my special thanks to my seniors Dr. O. N. Verma and Dr. Rajitha K.V. for their insightful comments and suggestions on different topics related to my research work. I would also like to thank my group members Nawaz and Nilamoni for their support during the course of my work.

I thank all my batch-mates Arnab, Biplob, Debashish, Dhrubajyoti, Kartik, Gyan, Raushan, and Tapas for their encouragement and entertaining company during my Ph.D. period.

I am greatly indebted to my parents, my brother and my sister-in-law for their constant support and encouragement throughout this period. Without their support and encouragement, this work would not have been possible.

TH-1819_11612116

Finally, I bow my head before God almighty for his blessings in the successful completion of this work.

Sandeep Sharma

TH-1819_11612116

Abstract

The present thesis deals with coherent control of optical fields by using coherent optical media. We utilize different quantum interference effects such as electromagnetically induced transparency (EIT), double dark resonances (DDR), phase induced transparency (PIT) and Fano resonance (FR) arising in various atomic and atom-molecule systems to control various properties of the optical fields. In chapter 1, we build the semiclassical formalism for light-matter interaction to study the above quantum effects. We provide the density matrix formalism to study the effect of optical fields on the atomic medium. We next present the basic propagation equation for optical fields using Maxwell's equations. Later in this chapter the derivation of interaction Hamiltonian is discussed and is used to describe various coherence effects arising in the two-level and three level atomic medium.

In chapter 2, we propose an efficient scheme for the generation of tunable optical waveguide based on atomic vapor in N-type configuration. We make use of both control field induced transparency and Kerr field induced absorption to create a flexible probe transparency window. We employ a suitable spatial profile of control and Kerr beams to create a high contrast refractive index modulation that holds the key to guiding a weak narrow probe beam. Further we numerically demonstrate that high contrast tunable waveguide can guide different modes of probe beam to several Rayleigh lengths without diffraction.

In chapter 3, we present a phase induced transparency based scheme to generate structured beam patterns in a closed four level atomic system. We employ phase structured probe beam and a transverse magnetic field (TMF) to create phase dependent medium susceptibility. We use a full density matrix formalism to explain the experiments of Radwell *et al.* [Phys. Rev. Lett. 114, 123603 (2015)] at weak probe limits. Our numerical results on beam propagation show that phase-dependent medium susceptibility creates petal-like structures in the probe profile. The contrast of the formed structured beam can be enhanced by changing the strength of TMF as well as of the probe intensity. Further we also notice that the profile of the structured beam can be rotated by changing the probe field intensity owing to nonlinear magneto-optical rotation (NMOR).

TH-1819_11612116

In chapter 4, we introduce a novel scheme based on electromagnetically induced transparency and phase induced transparency to create various structured beam patterns in a closed-loop five level atomic system. We employ a phase structured probe beam and a transverse magnetic field (TMF) to create phase dependent medium susceptibility. Additionally, a suitable azimuthally inhomogeneous control field is used to further manipulate the phase varying susceptibility. We show that different control beam structures create different phase structured absorption profile. Such manipulation of the absorption is the key to the creation of various structured beam patterns. Our numerical results on beam propagation confirms that the phase information from specific spatial position of the absorption profile gets encoded on the spatial probe envelope creating beam structures with different petal forms.

In chapter 5, we demonstrate how fano resonance can induce an EIT like feature in a Feshbach-resonant atom-molecule coupled *Lambda*−system. We show that, by controlling the strength of control field and the Feshbach resonance width, a very narrow transparency window can be created for the probe. Our numerical results on probe pulse propagation displays ultra slow group velocity owing to the narrow EIT features. Furthermore, manipulation of the EIT feature by the Feshbach resonance width can lead to enhancement of the delay-bandwidth product (DBP) of the atom-molecule coupled system.

TH-1819_11612116

Contents

TH-1819_11612116

TH-1819_11612116

TH-1819_11612116

TH-1819_11612116

List of figures

TH-1819_11612116

TH-1819_11612116

TH-1819_11612116

TH-1819_11612116

TH-1819_11612116

TH-1819_11612116

List of tables

TH-1819_11612116

TH-1819_11612116

Chapter 1

Introduction

Interactions of electromagnetic(em) fields with atomic medium have been studied in great detail in the past few decades. The ability to control the optical properties of an atomic medium using coherent em fields has attracted much attention of the researchers in the recent years. The formation of atomic coherences holds the key of control over the optical properties of the medium. Generally atoms are characterized by different atomic states and coupling of em fields to these states leads to the creation of atomic coherence. This induced coherence not only changes the optical properties of the medium but also affects the interacting em fields. The effect of the induced coherence on an em field was first experimentally demonstrated by McCall and Hahn [1]. In their experiment, they studied the propagation of nanosecond pulse through a ruby crystal in a two-level configuration. They realized that a strongly absorptive ruby crystal becomes transparent to a 2π-pulse. The transparency is a result of coherent excitation and de-excitation of atoms by the 2π-pulse. This phenomena of creating a transparency for itself is known as self-induced transparency (SIT). However the above coherence effect occurs for a particular-shaped pulse and that too at high intensity regime, thus limiting their practical applicability. Moreover controlling atomic coherences using two coherent em fields can result in interesting coherence effects which have immense application in many areas of optics.

Interaction of two coherent em fields with an atomic media is studied using a three level configuration, where both the fields act on different transitions but share a common atomic state. These fields create atomic coherences between different transition pathways of the three level configuration which can interfere with each other. The interference among the atomic coherences lead to exciting quantum optical phenomena such as coherent population trapping (CPT) [2, 3], electromagnetically induced transparency (EIT) [4, 5], lasing without inversion (LWI) [6–9] and saturated absorption techniques (SAT) [10, 11]. Among the above quantum effects CPT was the first novel phenomena to be observed. CPT was first experimentally observed by Alzetta

TH-1819_11612116

et al. in sodium vapor in a three level atomic configuration [12]. In this phenomena the atoms are prepared in coherent superposition of states which is immune to absorption of radiation *i.e.,* the atoms gets trapped in the superposed state and cannot be excited to any other state [2]. In CPT both the fields are of comparable strength whereas one of the field becomes weak in case of EIT. EIT is a technique for making an otherwise optically thick gaseous medium transparent to a resonant weak(probe) field by applying another strong(control) field. This induced transparency is a result of destructive interference between two excitation paths of a weak probe field interacting with the three level system. The reduced absorption of the probe field near the atomic resonance is also accompanied by a rapidly varying atomic dispersion. In 1990, Harris *et al.* [13] first proposed the EIT phenomena in three level atomic system. The first experimental observation of EIT was reported by Boller *et al.* [14] in 1991. Since then EIT has become a versatile tool for creating and manipulating various optical properties of the medium as well as that of em fields.

Manipulation of optical properties of the medium in both space and time domain by using EIT can lead to many interesting application in optics. Spectral modification of the medium absorption and dispersion can be accomplished by a strong light pulse, which induces a steep dispersion near the atomic resonance due to EIT. Tailoring of this steep dispersion has remarkable application in the slowing and stopping of light[16, 17], storage and retrieval of light [18, 19]. In different mechanisms, spatial modulation of the optical properties of the medium can be achieved by using a spatially modulated control beam. A suitable control beam can induce a waveguide like structure by modulating refractive index in transverse directions. This modulation of refractive index leads to confinement and diffractionless propagation of a weak probe beam. Such type of induced waveguides have been experimentally demonstrated by Truscott *et al.* in a V-type three level system [20]. Spatial inhomogeneity induced by the control beam in the refractive index of the medium has been used in focusing/defocusing [21, 22], steering [23, 24] and splitting [25] the probe beam. In recent years large number of theoretical predictions and experimental realizations to achieve all-optical waveguiding in EIT medium have been carried out [20, 21, 26–29].

Recently, manipulation of medium absorption with standing-wave control field has gathered lot of attraction. A standing-wave control field creates alternating regions of high and low absorption. This oscillating absorption can trap atoms in a very narrow spatial region (of the order of wavelength) [30, 31]. The localization techniques have immense application in laser cooling and trapping of atoms [32], atom nanolithography [33], etc. Further the periodic variation of absorption and refractive index of the medium can also result in creation of a grating like pattern in the medium. This

TH-1819_11612116

induced grating structure in the atomic medium has major applications in beam splitting and steering [34, 35].

In the recent years EIT in three level atomic system has shown a very rich variety of applications in many areas starting from information processing to spectroscopy. Modification of three level systems to four level atomic systems or a closed loop systems can result in new type of quantum interference effects such as Double dark resonance (DDR) [36, 37] and phase-dependent EIT (PDEIT) [38]. DDR has been demonstrated in four-level system, where the probe absorption spectrum is characterized by two EIT windows, separated by a sharp absorption peak. The appearance of the central narrow structure is due to the coherent interaction between the two dark states, which greatly enhances the Kerr nonlinearity [39]. Modification of the medium susceptibility by DDR also has many applications in imaging [40], optical switching [41], and high precision atom localization [42]. Further, relative phase difference of the em fields can dramatically modify the EIT features in a closed-loop atomic system and create PDEIT. PDEIT is an effective tool in achieving high precision atom localization [43], frequency conversion [4], generation of structured beams [44], etc. In general, open and closed-loop multi-level atomic systems allow us to manipulate both the medium and the em fields in a more sophisticated manner than in conventional EIT systems [39, 42, 43] and can have greater applications in various areas of optics.

Spatio-temporal evolution of em fields through either open or closed loop multilevel atomic systems without loss of generality poses a major challenge in quantum optics. The propagation dynamics of em fields through a medium can be governed by the Maxwell's wave equation. The complete evolution of the em fields through these multi-level system can be investigated by solving coupled Bloch and Maxwell's equation. In this chapter, we first discuss the semiclassical theory to describe light-matter interaction. We start by giving a general quantum description of matter followed by classical theory for em fields. Next, we derive the Hamiltonian for the atomic system in presence of fields. We then use this Hamiltonian to study various induced coherence effects in two-level and three level atomic systems.

1.1 Theoretical background of atom-field interaction

In this section, we review the formulation of light-matter interaction in the semiclassical framework. In this framework, light is described as a classical field that satisfies the Maxwell's equations whereas the matter is treated as a quantum system having discrete energy levels. Most of the experimental findings related to light-matter interaction in quantum optics has been successfully explained using the semiclassical theory. Hence in this thesis, we use this semiclassical theory to study various phe-

TH-1819_11612116

nomena arising due to the interaction between light and matter. In the following subsection we provide quantum description of matter by considering time-dependent Schrödinger and density matrix equations.

1.1.1 Quantum description of matter

Atomic vapor is a good candidate to explore various quantum effects experimentally. This is made possible due to the presence of low coherence dephasing rates of the atomic vapors. From quantum mechanics, we know that atom consists of discrete energy levels and each level is associated with a unique wave function. The wave function and the corresponding energy of a state can be estimated by solving the Schrödinger equation. The Schrödinger equation for an electron bound to an atom is expressed as

$$i\hbar\frac{\partial|\psi\rangle}{\partial t} = H|\psi\rangle \tag{1.1}$$

where H is the Hamiltonian of the system and it contains the unperturbed and perturbation part. The explicit form of the Hamiltonian will be discussed in detail in the next subsections. We can know all the information about the atomic system by solving Eq. (1.1). However calculations become complicated when the system is affected by incoherent processes such as damping due to radiative and non-radiative processes. In such cases the wave function $|\psi\rangle$ cannot give the complete information about the system. Use of density matrix can overcome all the above mentioned disadvantages while using the wave function approach. Density matrix is a well suited technique for dealing with all the coherence and decoherence effects present in isolated or interactive systems.

Density matrix formalism:

In most of the real problems we have an ensemble of similar atoms which obeys the same equation of motion but exhibits different stages of evolution. The density matrix for this ensemble of atom is expressed as

$$\rho = \sum_j P_j|\psi_j\rangle\langle\psi_j| \tag{1.2}$$

where P_j are the fraction of atoms in state $|\psi_j\rangle$ at time t in the ensemble. This is described as a mixed case. If all the atoms in the ensemble are in same state say $|\psi\rangle$, then it is known as a pure case and the density matrix can be written as $\rho = |\psi\rangle\langle\psi|$. The advantage of density matrix is that the time evolution and expectation can be

TH-1819_11612116

calculated in the same way as before even after introducing the statistical concept. The expectation value of an observable is expressed as

$$\begin{aligned}\langle \mathbf{O} \rangle &= \sum_j P_j \langle \psi_j | \mathbf{O} | \psi_j \rangle \\ &= \sum_j P_j \sum_k \langle \psi_j | \mathbf{O} | k \rangle \langle k | \psi_j \rangle \\ &= \sum_k \sum_j P_j \langle k | \psi_j \rangle \langle \psi_j | \mathbf{O} | k \rangle \\ &= \sum_k \langle k | \sum_j P_j | \psi_j \rangle \langle \psi_j | \mathbf{O} | k \rangle \\ &= \sum_k (\rho \mathbf{O})_{kk} \\ &= Tr[\rho \mathbf{O}] \ .\end{aligned} \tag{1.3}$$

It is evident fro the above Eq. (1.3) that knowing the density matrix element is sufficient to find the expectation value of any observable. The density matrix approach is a very robust technique for extracting all the information about the system without the requirement of a detail expression of the wave function.

To derive the equation of motion for the density matrix, we take a time derivative of Eq. (1.2) and subsequently use the Schrödinger equation Eq. (1.1) to write the density matrix equation in the following manner

$$\begin{aligned}\dot{\rho} &= \sum_j P_j (|\dot{\psi_j}\rangle \langle \psi_j| + |\psi_j\rangle \langle \dot{\psi_j}|) \\ &= -\frac{i}{\hbar} \sum_j P_j (H|\psi_j\rangle \langle \psi_j| - |\psi_j\rangle \langle \psi_j| H) \\ &= -\frac{i}{\hbar} [H, \rho] \ .\end{aligned} \tag{1.4}$$

The above equation is called Liouville or Von Neumann equation. However, the above form of the Liouville equation describes only the coherent interaction processes. In a physical system, there exists various incoherent processes, such as spontaneous emission, collisional mechanism, etc. So to completely understand the light-matter interaction, one has to account for all these incoherent processes in the Liouville equation. Thus the modified Liouville equation takes the following form [45]:

$$\frac{\partial \rho}{\partial t} = -\frac{i}{\hbar} [\mathcal{H}, \rho] + \mathcal{L}\rho \, . \tag{1.5}$$

TH-1819_11612116

The last term $\mathcal{L}\rho$ is Liouville operator which describes all the incoherent processes. The above equation is used throughout the thesis to study the dynamics of atomic populations and coherences in different atom-field systems.

1.1.2 Classical theory for Electromagnetic fields

In the framework of classical electrodynamics, the propagation of electromagnetic fields through a medium is governed by the following Maxwell's equations:

$$\nabla.\ \mathbf{D} = 4\pi\rho, \qquad \text{(Gauss's law)} \tag{1.6a}$$

$$\nabla.\ \mathbf{B} = 0, \tag{1.6b}$$

$$\nabla \times \mathbf{E} = -\frac{1}{c}\frac{\partial \mathbf{B}}{\partial t}, \qquad \text{(Faraday's law)} \tag{1.6c}$$

$$\nabla \times \mathbf{H} = \frac{4\pi}{c}\mathbf{J} + \frac{1}{c}\frac{\partial \mathbf{D}}{\partial t}, \qquad \text{(Ampere's law)} \tag{1.6d}$$

where ρ is the free charge density, $\mathbf{J}$ is the free current density, and c is the speed of light in vacuum. The fundamental electric and magnetic field vectors are represented by $\mathbf{E}$ and $\mathbf{H}$, respectively. The electric displacement and the magnetic induction vectors in material medium are denoted by $\mathbf{D}$ and $\mathbf{B}$, respectively. Both the vectors $\mathbf{D}$ and $\mathbf{B}$ are related to the basic electric and magnetic field vectors by the following relation

$$\mathbf{D} = \mathbf{E} + 4\pi\mathbf{P}, \tag{1.7}$$

$$\mathbf{B} = \mathbf{H} + 4\pi\mathbf{M}. \tag{1.8}$$

where $\mathbf{P}$ is the electric polarization and $\mathbf{M}$ is the magnetization of the medium.

Propagation of EM fields:

For the case of simplicity, we consider the medium to be nonmagnetic ($\mathbf{M} = 0$), non-conducting ($\mathbf{J} = 0$) and free of charges ($\rho = 0$). To derive the propagation equation for em fields, we take the curl of Eq. (1.6c) and use the relation for $\mathbf{B}$ as in Eq. (1.6d) and $\mathbf{D}$ as in Eq. (1.7), to obtain the following equation:

$$\nabla \times \nabla \times \mathbf{E} + \frac{1}{c^2}\frac{\partial^2}{\partial t^2}(\mathbf{E} + 4\pi\mathbf{P}) = 0. \tag{1.9}$$

Next, we use the vector identity

$$\nabla \times \nabla \times \mathbf{A} = \nabla(\nabla \cdot \mathbf{A}) - \nabla^2\mathbf{A}, \tag{1.10}$$

TH-1819_11612116

in order to simplify Eq. (1.9) to the following form

$$\nabla^2\mathbf{E} - \frac{1}{c^2}\frac{\partial^2\mathbf{E}}{\partial t^2} = \frac{4\pi}{c^2}\frac{\partial^2\mathbf{P}}{\partial t^2}. \tag{1.11}$$

This equation is known as Maxwell's wave equation for propagation of electromagnetic field through a dielectric medium. The term on the right hand side of the equation is the source term and represents the response of the medium. In order to simplify the wave Eq. (1.11), we make some approximation by writing an explicit form of the electric field and the polarization. We consider a nearly monochromatic wave propagating in the z-direction. Its electric field and induced polarization can be described as

$$\mathbf{E}(x,y,z,t) = \hat{\mathbf{e}}\mathcal{E}(x,y,z,t)e^{i(kz-\omega t)} + c.c., \tag{1.12}$$

$$\mathbf{P}(x,y,z,t) = \hat{\mathbf{e}}\mathcal{P}(x,y,z,t)e^{i(kz-\omega t)} + c.c., \tag{1.13}$$

where $\mathcal{E}(x,y,z,t)$ and $\mathcal{P}(x,y,z,t)$ are the envelope functions of the field. The unit vector $\hat{\mathbf{e}}$ shows the direction of polarization, k is the wave number and ω is the carrier frequency of the field. The required derivatives of Eq. (1.11) are given by

$$\nabla^2\mathbf{E} = \hat{\mathbf{e}}(\nabla_\perp^2\mathcal{E} + \frac{\partial^2\mathcal{E}}{\partial z^2} + 2ik\frac{\partial\mathcal{E}}{\partial z} - k^2\mathcal{E})e^{i(kz-\omega t)} + c.c., \tag{1.14}$$

$$\frac{\partial^2\mathbf{E}}{\partial t^2} = \hat{\mathbf{e}}(\frac{\partial^2\mathcal{E}}{\partial t^2} - 2i\omega\frac{\partial\mathcal{E}}{\partial t} - \omega^2\mathcal{E})e^{i(kz-\omega t)} + c.c., \tag{1.15}$$

$$\frac{\partial^2\mathbf{P}}{\partial t^2} = \hat{\mathbf{e}}(\frac{\partial^2\mathcal{P}}{\partial t^2} - 2i\omega\frac{\partial\mathcal{P}}{\partial t} - \omega^2\mathcal{P})e^{i(kz-\omega t)} + c.c., \tag{1.16}$$

where $\nabla_\perp^2 = \partial^2/\partial x^2 + \partial^2/\partial y^2$ is the Laplacian operator and represents the variation of the field in the transverse direction. Now, we make an approximation by assuming that the envelope functions $\mathcal{E}$ and $\mathcal{P}$ vary very slowly in space and time within the optical period and optical wavelength. This assumption is mathematically represented by the following inequalities:

$$\left|\frac{\partial^2\mathcal{E}}{\partial z^2}\right| \ll \left|k\frac{\partial\mathcal{E}}{\partial z}\right| \ll |k^2\mathcal{E}|, \quad \left|\frac{\partial^2\mathcal{E}}{\partial t^2}\right| \ll \left|\omega\frac{\partial\mathcal{E}}{\partial t}\right| \ll |\omega^2\mathcal{E}|, \tag{1.17}$$

$$\left|\frac{\partial^2\mathcal{P}}{\partial z^2}\right| \ll \left|k\frac{\partial\mathcal{P}}{\partial z}\right| \ll |k^2\mathcal{E}|, \quad \left|\frac{\partial^2\mathcal{P}}{\partial t^2}\right| \ll \left|\omega\frac{\partial\mathcal{P}}{\partial t}\right| \ll |\omega^2\mathcal{E}|. \tag{1.18}$$

The above approximation is known as the **slowly varying envelope approximation (SVEA)**. Substituting above derivatives into Eq. (1.11) and neglecting the higher order derivatives with respect to z and t, we arrive at the wave equation for a slowly

TH-1819_11612116

varying electric field envelope as follows:

$$\frac{1}{2ik}\nabla_{\perp}^{2}\mathcal{E}+\frac{\partial\mathcal{E}}{\partial z}+\frac{1}{c}\frac{\partial\mathcal{E}}{\partial t}=2\pi ik\mathcal{P}. \tag{1.19}$$

Beam propagation:

We now derive the wave equation depicting the propagation of a monochromatic laser field. In this regard, we consider the laser field to be continuous wave i.e., $\frac{\partial\mathcal{E}}{\partial t}=0$. With this assumption the Eq. (1.19) can be written as

$$\frac{1}{2ik}\nabla_{\perp}^{2}\mathcal{E}+\frac{\partial\mathcal{E}}{\partial z}=2\pi ik\mathcal{P}. \tag{1.20}$$

This wave equation is known as a paraxial wave equation. Almost all forms of laser fields satisfy this beam equation. The first term in the left hand side of the equation describes the diffraction of the beam. The term on the right hand side accounts for the dispersion and absorption of the beam inside the medium.

Pulse propagation:

Next we derive the propagation equation for an em pulse. For this we consider the transverse variation of the field envelope to be very small in comparison with the variation in z and t. Hence the first term on the left hand side of Eq. (1.19) can be ignored. Under this approximation the equation for propagation of a pulse through a dispersive medium is given by

$$\frac{\partial\mathcal{E}}{\partial z}+\frac{1}{c}\frac{\partial\mathcal{E}}{\partial t}=2\pi ik\mathcal{P}. \tag{1.21}$$

We simplify the above equation by using the following set of transformation:

$$\tau=t-z/c,\ \ \zeta=z. \tag{1.22}$$

so that ,

$$\partial/\partial z+c^{-1}\partial/\partial t=\partial/\partial\zeta,\ \partial/\partial t=\partial/\partial\tau. \tag{1.23}$$

Hence, the wave equation Eq. (1.21) is simplified into the following form:

$$\frac{\partial\mathcal{E}}{\partial\zeta}=2\pi ik\mathcal{P}. \tag{1.24}$$

TH-1819_11612116

The above equation signifies how light pulse propagates through a dielectric medium with polarization $\mathcal{P}$. The imaginary and real parts of the complex polarization represents the absorption and dispersion of the medium, respectively. In this thesis, we use Eq. (1.20) and Eq. (1.24) to study the propagation of the different em fields through the multi-level atomic system.

1.1.3 Polarization of the medium

The electron cloud is distributed uniformly around the nucleus in atoms and molecules with no permanent dipole moment. However in presence of an external electric field, an asymmetry is created in the distribution of electron cloud around the nucleus. This asymmetry in the charge distribution result in creation of an electric dipole. The strength of the dipole moment $\boldsymbol{p}$ is directly proportional to the strength of the electric field $\boldsymbol{E}$ and is expressed as

$$\boldsymbol{p} = \alpha \boldsymbol{E} \tag{1.25}$$

where, α is the atomic polarizability. For a medium with an ensemble of n atoms per unit volume each with dipole moment $\boldsymbol{p}$, the total macroscopic polarization is given by

$$\boldsymbol{P} = n\langle \boldsymbol{p} \rangle \tag{1.26}$$

From classical theory of electromagnetism, the induced polarization can also be expressed in terms of the applied electric field. Most of our work is in the weak field regime. Hence we consider only the linear effects of the field and neglect all the higher order effects. The induced polarization $d\boldsymbol{P}(\boldsymbol{r}, t)$ in a homogeneous and isotropic medium at an interval t is induced by the electric field $\boldsymbol{E}(\boldsymbol{r}, t')$ before the moment $t' = t - dt'$. $d\boldsymbol{P}(\boldsymbol{r}, t)$ and $\boldsymbol{E}(\boldsymbol{r}, t')$ are related in the time interval dt' and can be expressed as

$$d\boldsymbol{P}(\boldsymbol{r}, t) = \chi(t - t')E(\boldsymbol{r}, t')dt' \tag{1.27}$$

Considering the contribution of $\boldsymbol{E}(\boldsymbol{r}, t')$ in $\boldsymbol{P}(\boldsymbol{r}, t)$ in all times before the moment t, we have

$$\boldsymbol{P}(\boldsymbol{r}, t) = \int_{-\infty}^{t} \chi(t - t')\boldsymbol{E}(\boldsymbol{r}, t')dt' \tag{1.28}$$

TH-1819_11612116

In the long time interaction limit, the Eq. (1.28) can be expressed in the following manner

$$\boldsymbol{P}(\boldsymbol{r},t) = \int_{-\infty}^{\infty} \chi(t-t')\boldsymbol{E}(\boldsymbol{r},t')dt' \tag{1.29}$$

We now take the fourier transform of $\boldsymbol{E}(\boldsymbol{r},t')$ and $\boldsymbol{P}(\boldsymbol{r},t)$, i.e.,

$$\boldsymbol{E}(\boldsymbol{r},t') = \int_{-\infty}^{+\infty} \boldsymbol{E}(\boldsymbol{r},\omega)e^{-i\omega t'}d\omega \tag{1.30}$$

$$\boldsymbol{P}(\boldsymbol{r},t) = \int_{-\infty}^{+\infty} \boldsymbol{P}(\boldsymbol{r},\omega)e^{-i\omega t}d\omega. \tag{1.31}$$

Next, we substitute Eq. (1.30)-(1.31) in Eq. (1.29) and eliminate the integral sign to arrive at

$$\boldsymbol{P}(\boldsymbol{r},\omega) = \chi(\omega)\boldsymbol{E}(\boldsymbol{r},\omega). \tag{1.32}$$

where

$$\chi(\omega) = \int_{-\infty}^{+\infty} \chi(t-t')e^{i\omega(t-t')}dt' \tag{1.33}$$

We use the polarization expression of Eq. (1.32) and Eq. (1.26) to derive an expression of the medium susceptibility.

1.2 Atom-field interaction Hamiltonian

We next consider the interaction between the em fields and alkali metal atoms. All alkali atoms have a single electron in their outermost shell. This single electron is bound to the nucleus by Coulomb interaction potential $V(\mathbf{r})$, $\mathbf{r}$ being the position vector of the electron with respect to the nucleus. The classical expression for Hamiltonian of a bound electron of mass m and charge $-e$ is expressed as

$$H_0 = \frac{\mathbf{p}^2}{2m} + V(\mathbf{r}), \tag{1.34}$$

where $\mathbf{p}$ is the canonical momentum of the electron. We now derive the Hamiltonian of the electron in the presence of an em field. From classical theory of radiation, the electric field $\mathbf{E}$ and magnetic induction $\mathbf{B}$ associated with an em field can be expressed

TH-1819_11612116

in terms of the scalar and vector potentials $\Phi(\mathbf{r},t)$ and $\mathbf{A}(\mathbf{r}$,t) as:

$$\mathbf{E}(\mathbf{r},t) = -\nabla\Phi(\mathbf{r},t) - \frac{1}{c}\frac{\partial}{\partial t}\mathbf{A}(\mathbf{r},t), \tag{1.35}$$

$$\mathbf{B}(\mathbf{r},t) = \nabla \times \mathbf{A}(\mathbf{r},t). \tag{1.36}$$

Using the above equations for the em fields in the Lorentz force equation: $\mathbf{F} = -e[\mathbf{E} + (\mathbf{V} \times \mathbf{B})/c]$ and comparing with the classical Lagrange's equation, one can write the total Hamiltonian of an atom-field system in the following manner

$$H' = \frac{1}{2m}\left[\mathbf{p} + \frac{e}{c}\mathbf{A}(\mathbf{r},t)\right]^2 - e\Phi(\mathbf{r},t). \tag{1.37}$$

Hence the total Hamiltonian of bound electron in the presence of an em fields takes the following form

$$H = \frac{1}{2m}\left[\mathbf{p} + \frac{e}{c}\mathbf{A}(\mathbf{r},t)\right]^2 - e\Phi(\mathbf{r},t) + V(\mathbf{r}). \tag{1.38}$$

In quantum mechanics, quantization of equation Eq. (1.38) is done by replacing the classical variables with the corresponding quantum operators. Thus, momentum $\mathbf{p} \rightarrow \hat{\mathbf{p}} = -i\hbar\nabla$, and the total energy $\mathbf{E} \rightarrow \hat{\mathbf{E}} = i\hbar\partial/\partial t$, where $\hbar = h/2\pi$ is the reduced Planck's constant. The same Hamiltonian can be derived for a quantum system from a gauge invariant point of view. In this regard, we first study the dynamics of the system using the non-relativistic Schrödinger equation:

$$i\hbar\frac{\partial}{\partial t}\Psi(\mathbf{r},t) = H\Psi, \tag{1.39}$$

where $\Psi(\mathbf{r},t)$ is the wave function of the quantum system so that quantity $|\Psi(\mathbf{r},t)|^2$ gives the probability density of finding an electron at position $\mathbf{r}$ and time t. The electronic motion under Coulomb potential is described by,

$$i\hbar\frac{\partial}{\partial t}\Psi(\mathbf{r},t) = \left[\frac{-\hbar^2}{2m_e}\nabla^2 + V(\mathbf{r})\right]\Psi(\mathbf{r},t). \tag{1.40}$$

The general solution of Eq. (1.39) can be written as:

$$\Psi(\mathbf{r},t) = \psi(\mathbf{r},t)e^{i\chi}, \tag{1.41}$$

where χ is an arbitrary scalar function and does not affect the probability density. However, if the phase is a function of both space and time variables, then the solution

TH-1819_11612116

of the form

$$\Psi(\mathbf{r},t) = \psi(\mathbf{r},t)e^{i\chi(\mathbf{r},t)}, \tag{1.42}$$

does not satisfy the Schrödinger equation Eq. (1.39), but the probability density still remains invariant under this transformation. Hence to satisfy the phase invariance the Schrödinger equation has to be modified in the following form

$$i\hbar\frac{\partial}{\partial t}\Psi(\mathbf{r},t) = \left\{\frac{1}{2m}\left[-i\hbar\nabla + \frac{e}{c}\mathbf{A}(\mathbf{r},t)\right]^2 - e\Phi(\mathbf{r},t) + V(\mathbf{r})\right\}\Psi(\mathbf{r},t), \tag{1.43}$$

where the functions $\mathbf{A}$(r,t) and $\Phi(\mathbf{r},t)$ on right hand side of Eq. (1.43) represent the usual vector and scalar potentials of the external electromagnetic field, respectively. In order to make Eq. (1.43) invariant under the transformation as in Eq. (1.42), the scalar and vector potentials $\Phi(\mathbf{r},t)$ and $\mathbf{A}$(r,t) has to be replaced by the following gauge transformations

$$\mathbf{A}(\mathbf{r},t) \rightarrow \mathbf{A}'(\mathbf{r},t) = \mathbf{A}(\mathbf{r},t) - \frac{\hbar c}{e}\nabla\chi(\mathbf{r},t), \tag{1.44}$$

$$\Phi(\mathbf{r},t) \rightarrow \Phi'(\mathbf{r},t) = \Phi(\mathbf{r},t) + \frac{\hbar}{e}\frac{\partial\chi(\mathbf{r},t)}{\partial t}. \tag{1.45}$$

It is to be noted that under the above gauge transformations the fields $\mathbf{E}$ and $\mathbf{B}$ remain invariant. We simplify the Hamiltonian in Eq. (1.43) using the Coulomb gauge or radiation gauge given by $\Phi(\mathbf{r},t) = 0$ and $\nabla\cdot\mathbf{A}(\mathbf{r},t) = 0$. The total Hamiltonian in radiation gauge reduces to,

$$\hat{H} = -\frac{\hbar^2}{2m}\nabla^2 - \frac{ie\hbar}{2mc}\mathbf{A}(\mathbf{r},t)\cdot\nabla + \frac{e^2}{2mc^2}\mathbf{A}(\mathbf{r},t)\cdot\mathbf{A}(\mathbf{r},t) + V(\mathbf{r}). \tag{1.46}$$

Now, we introduce a very well known approximation i.e., "dipole approximation" which leads to substantial simplification of the total Hamiltonian given by Eq. (1.46).

Electric dipole Approximation

A plane electromagnetic wave can be expressed by a vector potential $\mathbf{A}(\mathbf{r_0}+\mathbf{r},t)$, which has the following form:

$$\mathbf{A}(\mathbf{r_0}+\mathbf{r},t) = \mathbf{A}(t)exp[i\mathbf{k}\cdot(\mathbf{r_0}+\mathbf{r})], \tag{1.47}$$

where $\mathbf{r}_0$ is location of nucleus of the atom. Now we make use of the "electric dipole approximation", where we assume that the wavelength of the interacting em field is

TH-1819_11612116

much larger than the typical size of the atom, *i.e.,* $kr \ll 1$, where $|k| = 2\pi/\lambda$. Under this approximation, the vector potential can be written as

$$\begin{aligned}\mathbf{A}(\mathbf{r_0}+\mathbf{r},t) &= \mathbf{A}(t)exp[i\mathbf{k}\cdot(\mathbf{r_0}+\mathbf{r})] \\ &= \mathbf{A}(t)exp(i\mathbf{k}\cdot\mathbf{r_0})[1+i\mathbf{k}\cdot\mathbf{r}+\cdots] \\ &\approx \mathbf{A}(t)exp(i\mathbf{k}\cdot\mathbf{r_0}). \end{aligned} \tag{1.48}$$

The total atom-field interaction Hamiltonian in the dipole approximation is given by

$$\hat{H} = -\frac{\hbar^2}{2m}\nabla^2 + V(\mathbf{r}) - \frac{ie\hbar}{2mc}\mathbf{A}(\mathbf{r_0},t)\cdot\nabla + \frac{e^2}{2mc^2}\mathbf{A}^2(\mathbf{r}_0,t). \tag{1.49}$$

We now use a gauge transformation $\chi(\mathbf{r},t) = (-e/\hbar c)\mathbf{A}(r_0,t)\cdot\mathbf{r}$, to transform the wave function $\Psi(\mathbf{r},t)$ of Eq. (1.42) into the following form

$$\Psi(\mathbf{r},t) = exp\left[\frac{-ie}{\hbar c}\mathbf{A}(\mathbf{r_0},t)\cdot\mathbf{r}\right]\psi(\mathbf{r},t). \tag{1.50}$$

The electric field $\mathbf{E}$ at $\mathbf{r_0}$ in can be written in terms of the Coulomb potential as $\mathbf{E}(\mathbf{r}_0,t) = -\frac{1}{c}\frac{\partial}{\partial t}\mathbf{A}(\mathbf{r}_0,t)$. Putting this along with Eqs. (1.50) and (1.49) into Eq. (1.43) and simplifying,

$$i\hbar\frac{\partial}{\partial t}\psi(\mathbf{r},t) = \left\{-\frac{\hbar^2}{2m}\nabla^2 + V(\mathbf{r}) + e\mathbf{r}\cdot\mathbf{E}(\mathbf{r}_0,t)\right\}\psi(\mathbf{r},t) \tag{1.51}$$

$$= (H_0 + H_I)\psi(\mathbf{r},t), \tag{1.52}$$

where H_0 and H_I represents the unperturbed and interaction parts of the Hamiltonian respectively. The simplified interaction Hamiltonian can be expressed in terms of the dipole operator $\mathbf{d} = -e\mathbf{r}$ as

$$H_I = e\mathbf{r}\cdot\mathbf{E} = -\mathbf{d}\cdot\mathbf{E}. \tag{1.53}$$

Throughout this thesis, we use the above expression for interaction Hamiltonian to study various atom-field interaction problems. One of the simplest problems involving atom-field interaction is a two-level atomic system. In the next section, we present the basic theory and results of a two-level atom interacting with a near resonant em field.

TH-1819_11612116

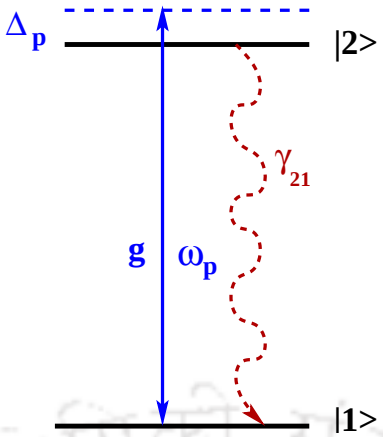

Fig. 1.1 (Color online) Shows a schematic diagram of the level system. A probe field with Rabi frequency g couples the transition $|2\rangle \leftrightarrow |1\rangle$. γ_{21} is the radiative decay rates from the excited state $|2\rangle$ to the ground state $|1\rangle$.

1.3 Two level atomic system

A two-level atomic system can be realized when only two atomic levels are resonant with the frequency of an incident em field, while all other levels are highly detuned. A typical two level atomic system consisting of excited state $|2\rangle$ and a ground state $|1\rangle$ is shown in Fig.1.1. The electric dipole allowed atomic transition $|1\rangle \leftrightarrow |2\rangle$ is coupled by a probe field ($\mathcal{E}_p$) with frequency ω_p. The electric field of the probe is defined as

$$\mathbf{E}_p(\mathbf{r},t) = \hat{\mathbf{e}}_p \mathcal{E}_p(\mathbf{r}) e^{i(\mathbf{k_p}\cdot\mathbf{r}-\omega_p t)} + c.c, \tag{1.54}$$

where $\mathcal{E}_p(\mathbf{r})$ is the slowly varying amplitude, $\hat{\mathbf{e}}_p$ and $\mathbf{k_p}$ are the polarization unit vector and the wave vector of the probe field, respectively. The total Hamiltonian of two level system interacting with probe field under electric dipole approximation is given by

$$H = H_0 + H_I, \tag{1.55}$$

where H_0 is the unperturbed Hamiltonian of the system and H_I the interaction Hamiltonian for the atom-field coupled system. The unperturbed Hamiltonian can be expressed as

$$H_0 = \hbar\omega_{21}|2\rangle\langle 2| \tag{1.56}$$

where $\hbar\omega_{21}$ is the energy of the excited state $|2\rangle$ relative to the ground state $|1\rangle$. The dipole interaction term between the two-level atom and the coherent field can be

TH-1819_11612116

expressed as:

$$H_I = -\mathbf{d} \cdot \mathbf{E}_p(\mathbf{r}, t). \tag{1.57}$$

where $\mathbf{d}$ is the induced dipole moment of the system in the presence of an optical field. Now, the above interaction term can be expanded into the following form

$$\begin{aligned} H_I = &- \left[\mathbf{d}_{21} \cdot \hat{\mathbf{e}}_p \mathcal{E}_p(\mathbf{r}) e^{i(\mathbf{k_p}\cdot\mathbf{r}-\omega_p t)} + \mathbf{d}_{21} \cdot \hat{\mathbf{e}}_p \mathcal{E}_p^*(\mathbf{r}) e^{-i(\mathbf{k_p}\cdot\mathbf{r}-\omega_p t)}\right] |2\rangle\langle 1| \\ &- \left[\mathbf{d}_{12} \cdot \hat{\mathbf{e}}_p \mathcal{E}_p(\mathbf{r}) e^{i(\mathbf{k_p}\cdot\mathbf{r}-\omega_p t)} + \mathbf{d}_{12} \cdot \hat{\mathbf{e}}_p \mathcal{E}_p^*(\mathbf{r}) e^{-i(\mathbf{k_p}\cdot\mathbf{r}-\omega_p t)}\right] |1\rangle\langle 2|, \end{aligned} \tag{1.58}$$

where $\boldsymbol{d}_{ij} = \langle i|\boldsymbol{d}|j\rangle$ are dipole moments corresponding to $|i\rangle \leftrightarrow |j\rangle$ transition. In the dipole approximation, the spatial phase factors appearing in the above interaction term are taken to be unity. Hence under this approximation, the interaction Hamiltonian reduces to

$$H_I = -\left[g e^{-i\omega_p t} + \tilde{g} e^{i\omega_p t}\right] |2\rangle\langle 1| - \left[g^* e^{i\omega_p t} + \tilde{g}^* e^{-i\omega_p t}\right] |1\rangle\langle 2|. \tag{1.59}$$

where $*$ represents the complex conjugate. The probe Rabi frequency is given as

$$g = \frac{\mathbf{d}_{21} \cdot \hat{\mathbf{e}}_p \mathcal{E}_p(\mathbf{r})}{\hbar}, \quad \text{and} \quad \tilde{g} = \frac{\mathbf{d}_{21} \cdot \hat{\mathbf{e}}_p \mathcal{E}_p^*(\mathbf{r})}{\hbar}. \tag{1.60}$$

The dynamics of the system can be studied by using the following Schrödinger equation.

$$i\hbar \frac{\partial}{\partial t} |\psi(r,t)\rangle = H|\psi(r,t)\rangle. \tag{1.61}$$

To avoid the complexity in our calculations due to the time dependent Hamiltonian, we apply the following unitary transformation to the state vector $|\psi(\mathbf{r},t)\rangle$

$$|\psi(\mathbf{r},t)\rangle = e^{-\frac{i}{\hbar}Ut} |\phi(\mathbf{r},t)\rangle \tag{1.62}$$

where

$$U = \hbar\omega_p |2\rangle\langle 2| \,. \tag{1.63}$$

The modified Schrödinger equation can be expressed as

$$i\hbar \frac{\partial}{\partial t} |\phi(r,t)\rangle = H_{eff} |\phi(r,t)\rangle. \tag{1.64}$$

TH-1819_11612116

where the effective Hamiltonian is given by the following expression

$$\frac{H_{eff}}{\hbar} = -\Delta_p|2\rangle\langle 2| - \left[g + \tilde{g}e^{2i\omega_p t}\right]|2\rangle\langle 1| - \left[g^* + \tilde{g}^* e^{-2i\omega_p t}\right]|1\rangle\langle 2|. \tag{1.65}$$

Here $\Delta_p = \omega_p - \omega_{21}$ is the probe detuning. The above effective Hamiltonian contains a highly oscillating term (oscillating at $2\omega_p$ frequency) related to $\tilde{g}$. The value of $\tilde{g}$ becomes important only when $\tilde{g} \approx 2\omega_p$. Therefore the term $\tilde{g}$ can be neglected at optical frequency domain where $\tilde{g} \ll 2\omega_p$. This approximation is known as rotating wave approximation. Under this approximation, the Hamiltonian takes the following form

$$\frac{H_{eff}}{\hbar} = -\Delta_p|2\rangle\langle 2| - g|2\rangle\langle 1| - g^*|1\rangle\langle 2|. \tag{1.66}$$

1.3.1 Dynamics of a two-level atomic system

The density operator ρ is defined as a projection operator onto the state vector and is expressed as

$$\rho = |\psi\rangle\langle\psi| \tag{1.67}$$

Here $|\psi\rangle$ is the state of the two level system and can be expressed as a linear combination of the two states $|1\rangle$ and $|2\rangle$ in the following way

$$|\psi\rangle = c_1|1\rangle + c_2|2\rangle, \tag{1.68}$$

The corresponding density operator can be expressed as

$$\begin{aligned}\rho = |\psi\rangle\langle\psi| &= (c_1|1\rangle + c_2|2\rangle)(c_1^*\langle 1| + c_2^*\langle 2|) \\ &= |c_1|^2|1\rangle\langle 1| + c_1c_2^*|1\rangle\langle 2| + c_1^*c_2|2\rangle\langle 1| + |c_2|^2|2\rangle\langle 2| \\ &= \rho_{11}|1\rangle\langle 1| + \rho_{12}|1\rangle\langle 2| + \rho_{21}|2\rangle\langle 1| + \rho_{22}|2\rangle\langle 2|. \end{aligned} \tag{1.69}$$

The density matrix elements ρ_{11} and ρ_{22} give the population of the ground state $|1\rangle$ and the excited state $|2\rangle$, respectively, while the matrix elements ρ_{21} and ρ_{12} give the induced coherence between the states $|1\rangle$ and $|2\rangle$. To study the evolution of the atomic populations and coherence, we use the following Liouville equation

$$\frac{\partial\rho}{\partial t} = -\frac{i}{\hbar}[\mathcal{H}_{eff}, \rho]\,. \tag{1.70}$$

TH-1819_11612116

Thus the equation of motion for atomic populations and coherence can be obtained as

$$\dot{\rho}_{11} = -\dot{\rho}_{22} = ig^*\rho_{21} - ig\rho_{12}\,, \tag{1.71a}$$

$$\dot{\rho}_{21} = \dot{\rho}^*_{12} = i\Delta_p\rho_{21} + ig(\rho_{11} - \rho_{22})\,. \tag{1.71b}$$

1.3.2 Rabi oscillations

The equations Eq. (1.71) are known as Optical Bloch equations as they have similar structure as the equations obtained by Bloch in the context of magnetic spin 1/2 system. We solve these equations by assuming that the atom is initially in the ground state $|1\rangle$, *i.e.*, $\rho_{11}(0) = 1$ at time $t = 0$. The solutions for atomic population $\rho_{22}(t)$

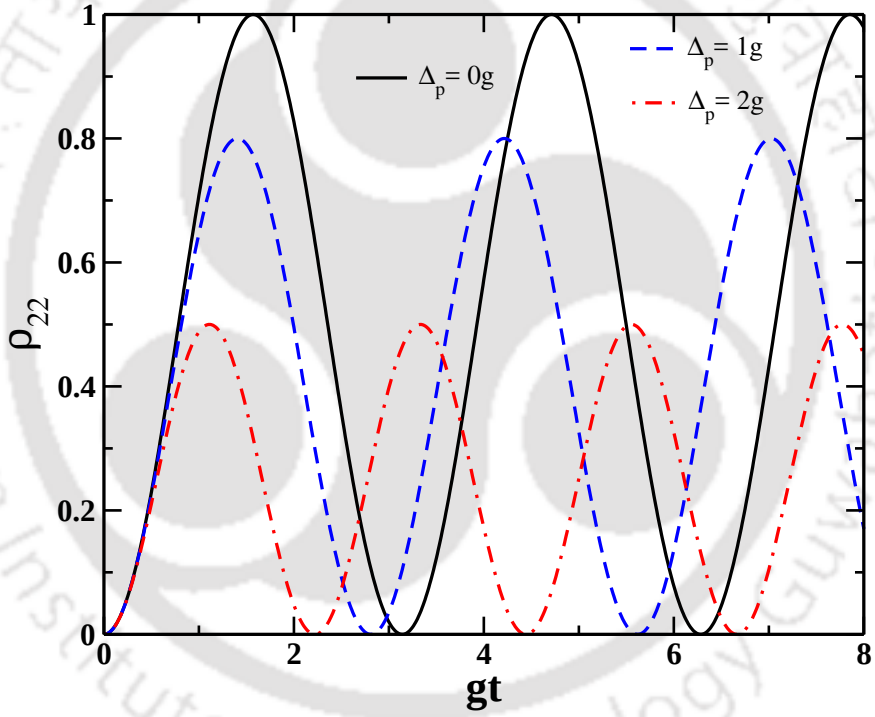

Fig. 1.2 Shows the excited state population ρ_{22} as a function of normalized time for three values of probe detuning.

and coherence $\rho_{21}(t)$ are then given by

$$\rho_{22}(t) = \frac{4|g|^2}{G^2}\sin^2\left(\frac{Gt}{2}\right), \tag{1.72}$$

$$\rho_{21}(t) = \frac{2|g|}{G^2}\sin\left(\frac{Gt}{2}\right)\left\{\Delta_p\sin\left(\frac{Gt}{2}\right) + iG\cos\left(\frac{Gt}{2}\right)\right\}, \tag{1.73}$$

where $G = \sqrt{\Delta_p^2 + 4|g|^2}$ is called the generalized Rabi frequency of the system. Figure.1.2, shows the variation of population of the upper level ρ_{22} with normalized time

TH-1819_11612116

for different values of Δ_p normalized with the input amplitude of the probe field. It can be seen in Fig.1.2 that the excited state population oscillates between its maximum and minimum values 0 and 1 at probe resonance $\Delta_p = 0$ with $2g$ frequency. This oscillatory behaviour of the population is known as Rabi oscillation or Rabi flopping and the frequency $2g$ is called Rabi frequency. It also evident from Fig.1.2 that with the increase in probe detuning, the frequency of Rabi oscillation increases but the amplitude decreases. This is due to the fact that both the amplitude and the frequency of oscillation are dependent on the probe detuning Δ_p as in Eq. (1.72). The first experimental observation of Rabi oscillation in rubidium vapors using nano-second pulse was reported by Gibbs [46]. In normal condition Rabi oscillations are very difficult to observe. It is due to the presence of various incoherent processes such as spontaneous emission, collisional induced decay, etc. These incoherent processes destroy the coherences of the system and hence curtail the phenomena of Rabi oscillation.

Effect of damping on the density matrix element

In normal conditions, an atom can change its state through several mechanisms, such as spontaneous emission and collision with other atoms. These processes not only affect the atomic population but can also affect the induced coherence of the system. To study the effect of these damping terms on the evolution of atomic populations and coherence, we use the following Liouville equation

$$\frac{\partial \rho}{\partial t} = -\frac{i}{\hbar}[\mathcal{H}_{eff}, \rho] + \mathcal{L}\rho\,. \tag{1.74}$$

The last term $\mathcal{L}\rho$ is Liouville operator which describes all the incoherent processes and is given by

$$\mathcal{L}\rho = -\frac{\gamma_{21}}{2}\left(|2\rangle\langle 2|\rho - 2|1\rangle\langle 1|\rho_{22} + \rho|1\rangle\langle 1|\right)\,, \tag{1.75}$$

where γ_{21} corresponds to radiative decay rates from excited states $|2\rangle$ to ground states $|1\rangle$. The equation of motion for atomic populations and coherence of the two level system can be described by the following density matrix equations:

$$\dot{\rho}_{11} = \gamma_{21}\rho_{22} + ig^*\rho_{21} - ig\rho_{12}\,, \tag{1.76a}$$

$$\dot{\rho}_{21} = -\left[\Gamma_{21} - i\Delta_p\right]\rho_{21} + ig(\rho_{11} - \rho_{22})\,, \tag{1.76b}$$

$$\dot{\rho}_{22} = -\dot{\rho}_{11}\,, \tag{1.76c}$$

$$\dot{\rho}_{ij} = \dot{\rho}^*_{ji}\,, \tag{1.76d}$$

where, the overdots stand for time derivatives and "*" denotes complex conjugate. We again solve these equations by assuming the field to be in resonance and that the

TH-1819_11612116

atom is initially in the ground state $|1\rangle$, *i.e.,* at time $t = 0$ and all other coherences to be zero. The solutions for atomic population ρ_{22} is then given by

$$\rho_{22} = \frac{g^2}{\gamma_{21}^2 + 2g^2}\left\{1 - \left[\cos(Gt) + \frac{3\gamma_{21}}{2G}\sin(Gt)\right]e^{(-3\gamma_{21}t/2)}\right\} \tag{1.77}$$

where $G = \sqrt{4g^2 - \frac{\gamma_{21}^2}{4}}$. Figure.1.3, shows the variation of population of upper level

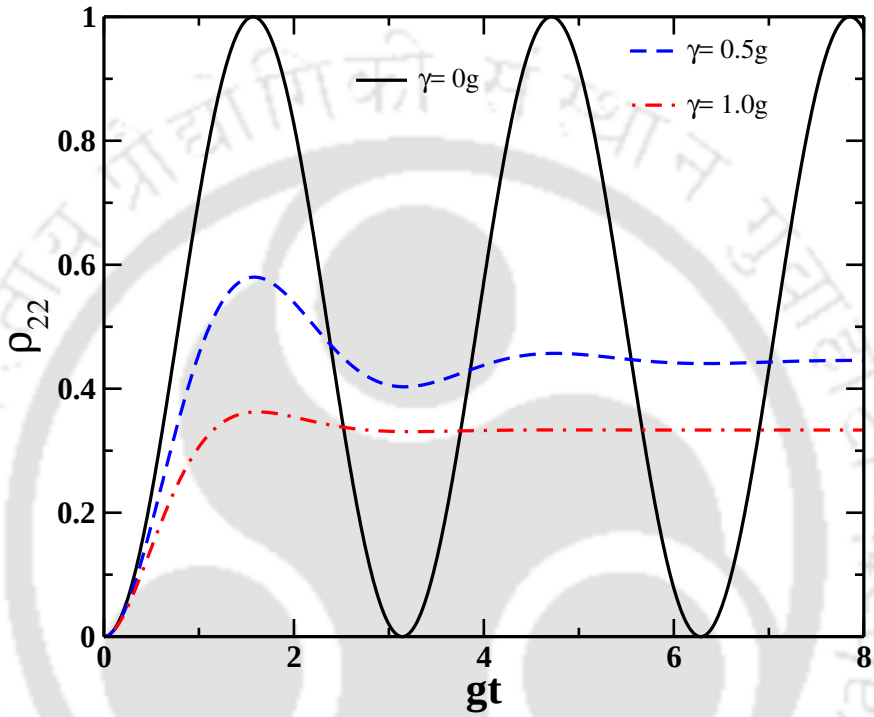

Fig. 1.3 Shows the effect of spontaneous decay rate on the excited state population ρ_{22}.

ρ_{22} with normalized time for different values of spontaneous decay. It can be seen from Fig.1.3 that in absence of damping constant γ_{21}, the population shows the usual Rabi oscillation as discussed earlier. In the presence of weak damping, the excited state population shows few oscillations before it reaches the constant value. However, for a strong damping case the excited state population doesn't show any oscillation and quickly saturates to a constant value of 0.33. In the strong damping limit, the value of the population can also be obtained from Eq. (1.77) and is given as

$$\rho_{22} \to \frac{g^2}{\gamma_{21}^2 + 2g^2} = 0.33, \quad for \quad \frac{\gamma}{g} = 1.0. \tag{1.78}$$

Hence it is evident from Fig.1.3 and Eq. (1.78) that in presence of damping, the system attains a steady state after a considerable interaction time $t \gg \gamma$. We now proceed further to evaluate the expression for the populations and coherence in the steady limit.

TH-1819_11612116

For this we set all the time derivatives of the populations and coherence in Eq. (1.76) to zero. We then solve these linear algebraic equations to obtain the expression of populations and coherence. The expression for the excited state population ρ_{22} and the coherence ρ_{21} is given by

$$\rho_{22} = \frac{|g|^2}{(\gamma_{21}^2 + \Delta_p^2) + 2|g|^2}, \tag{1.79}$$

$$\rho_{21} = \frac{ig(\gamma_{21} + i\Delta_p)}{(\gamma_{21}^2 + \Delta_p^2) + 2|g|^2}. \tag{1.80}$$

We can observe that the steady state population is exactly equal to the population value in the strong damping case given by Eq. (1.78). The induced polarization for

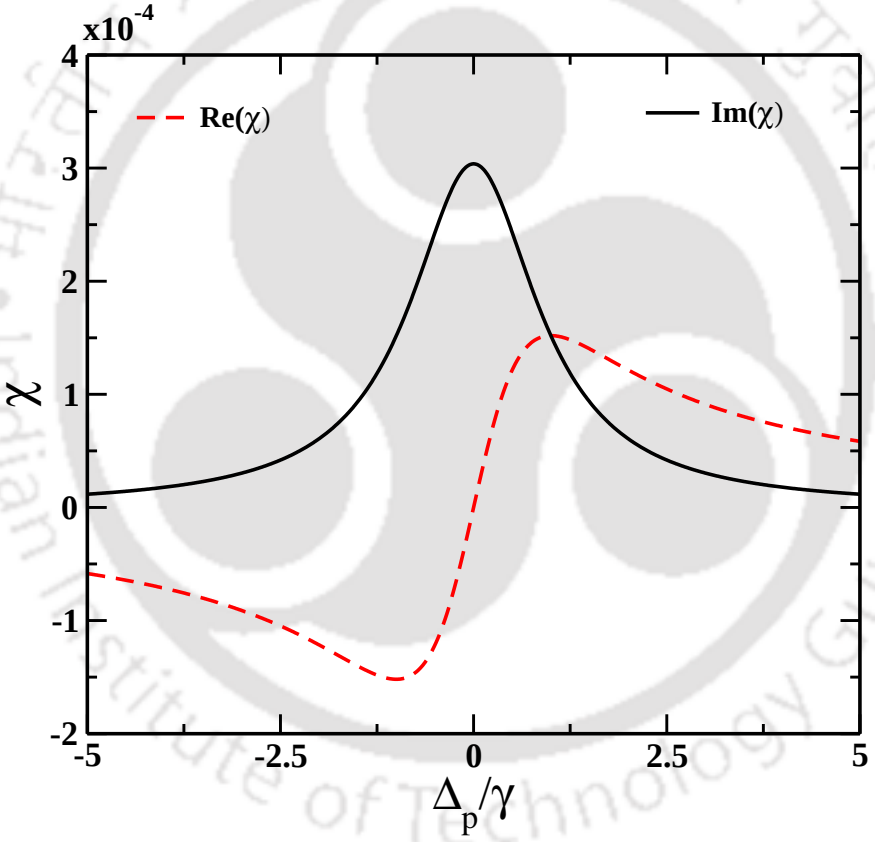

Fig. 1.4 Real and imaginary parts of the susceptibility plotted as a function of probe detuning for a weak probe case. Parameters are chosen as $\mathcal{N} = 10^{11}$ atoms/cm^3, $\gamma_{21} = 0.5\gamma$.

an ensemble of atoms with number density $\mathcal{N}$ and dipole moment $\mathbf{d}$ is defined as

$$\mathbf{P} = \mathcal{N}\langle\hat{\mathbf{d}}\rangle = \mathcal{N}Tr\{\rho\hat{\mathbf{d}}\} = \mathcal{N}(d_{12}\rho_{21} + h.c.). \tag{1.81}$$

The susceptibility of the medium is also related to the induced polarization by the relation $\mathcal{P} = \chi\mathcal{E}$. Hence, the expression for susceptibility of the medium can be

TH-1819_11612116

obtained using the above two definitions and is given by

$$\chi = \frac{\mathcal{N}\left|d_{21}\right|^2}{\hbar\gamma}\frac{i\gamma_{21}(\gamma_{21}+i\Delta_p)}{(\gamma_{21}^2+\Delta_p^2)+2|g|^2}. \tag{1.82}$$

It should be noted that the above susceptibility expression includes both linear and nonlinear parts due to the presence of probe Rabi frequency g in the denominator. For better understanding of the complex susceptibility, we separate the real and imaginary part of the susceptibility as given below

$$Re\left[\chi\right] = \frac{\mathcal{N}\left|d_{21}\right|^2}{\hbar\gamma}\frac{\gamma_{21}\Delta_p}{(\gamma_{21}^2+\Delta_p^2)+2|g|^2} \tag{1.83}$$

$$Im\left[\chi\right] = \frac{\mathcal{N}\left|d_{21}\right|^2}{\hbar\gamma}\frac{\gamma_{21}\gamma_{21}}{(\gamma_{21}^2+\Delta_p^2)+2|g|^2}\,. \tag{1.84}$$

The real part of the susceptibility contributes to the phase evolution of the field where as the imaginary part contributes to dissipation or absorption of the field. Figure.1.4 shows the variation of real and imaginary part of the susceptibility with the probe detuning Δ_p. It can be seen in Fig.1.4 that the absorption has a Lorentzian profile. In the weak field limit, the full width at half-maximum(FWHM) of the absorption profile can be estimated from Eq. (1.83) and is found to be $2\gamma_{21}$. Further, it is observed that the absorption attains a maximum value at probe resonance $\Delta_p = 0$. Hence the field suffers from high attenuation at resonance condition with the two level system. It is also evident from Fig.1.4 that the dispersion shows anomalous behaviour. It is found that $Re(\chi)$ vanishes at resonance condition $\Delta_p = 0$ while it has a maxima at $\Delta_p = +\gamma_{21}$. The refractive index n of the medium is associated with $Re(\chi)$ by the following relation

$$n = \sqrt{1+4\pi Re(\chi)}. \tag{1.85}$$

The above linear relation shows that the refractive index also attains a maximum value at $\Delta_p = +\gamma_{21}$. However, this high index cannot be utilized due to the presence of high absorption. Moreover increasing the intensity of the field minimizes the absorption. Figure.1.5 shows the effect of the probe intensity on the absorption profile. It is clear from Fig.1.5 that with the increase in the probe strength, absorption decreases. This is quite evident from the expression of the absorption in Eq.(1.83). The presence of g in the denominator shows that with increase in the value of g, the absorption will decrease. This reduction of the absorption with increasing intensity is known as saturation effect. Further, it is noticed that decrease in the absorption is accompanied by increase in the width of the absorption profile. This can again be explained using

TH-1819_11612116

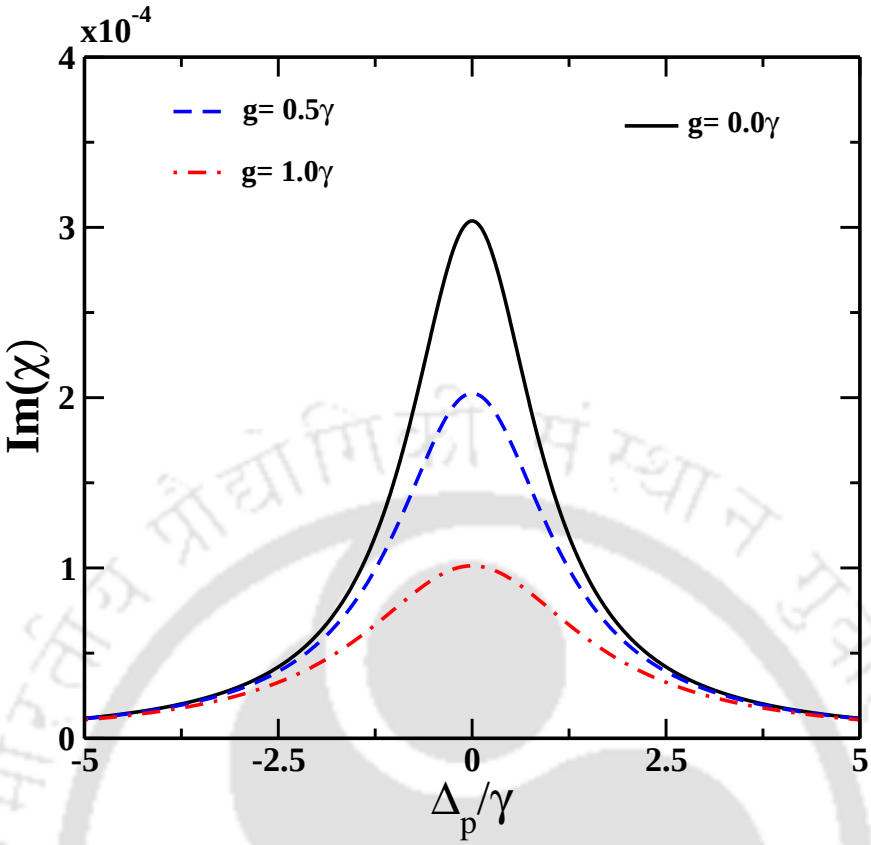

Fig. 1.5 Imaginary parts of the susceptibility plotted as a function of detuning for different probe intensities. Parameters are chosen as $\mathcal{N} = 10^{11}$ atoms/cm^3, $\gamma_{21} = 0.5\gamma$.

the expression of the absorption in Eq. (1.83). In the presence of a strong probe field, the FWHM gets modified by the intensity of the probe. The modified FWHM is expressed by

$$FWHM = \sqrt{\gamma_{21}^2 + 2g^2}. \tag{1.86}$$

Now it is quite evident from above expression that the width of the absorption increases with the increase in probe strength. This increase in the absorption width due to a strong field is known as power broadening. We have seen that the two level system shows very high absorption due to which it doesn't have any application in coherent control. However there are several techniques to control this high absorption. One of the technique is self-induced transparency [1]. In this technique a strong probe pulse propagating through a two-level system creates a transparency for itself. It was first demonstrated experimentally in a ruby crystal by McCall and Hahn in 1969. They demonstrated that a probe pulse with a certain profile (2π-pulse) can be transmitted even through this strongly absorbing two-level medium without any change in its shape and energy. This induced transparency is a result of Rabi oscillation in the

TH-1819_11612116

two-level system. Another well known technique to get rid of this high absorption is saturation absorption technique [10]. In this technique an extra strong field is applied which takes the medium into a saturation stage and protects the weak probe field from absorption. However both these techniques requires a very high intense field to observe the coherence effects due to which they have very low applicability.
Interestingly, the susceptibility of the two-level system can be manipulated by a strong field. The strong field not only suppresses the high absorption, but also gives rise to steep dispersion characteristics which can be utilized in many diverse areas of optics. These features will be discussed in detail in the subsequent sections.

1.4 Three level atomic system

In this section, we will extend the semiclassical theory from two level system to three level atomic system by introducing another coherent driving field which will couple two unpopulated states. As in our treatment of the two-level system, we will address all the coherent effects using the optical Bloch equations.

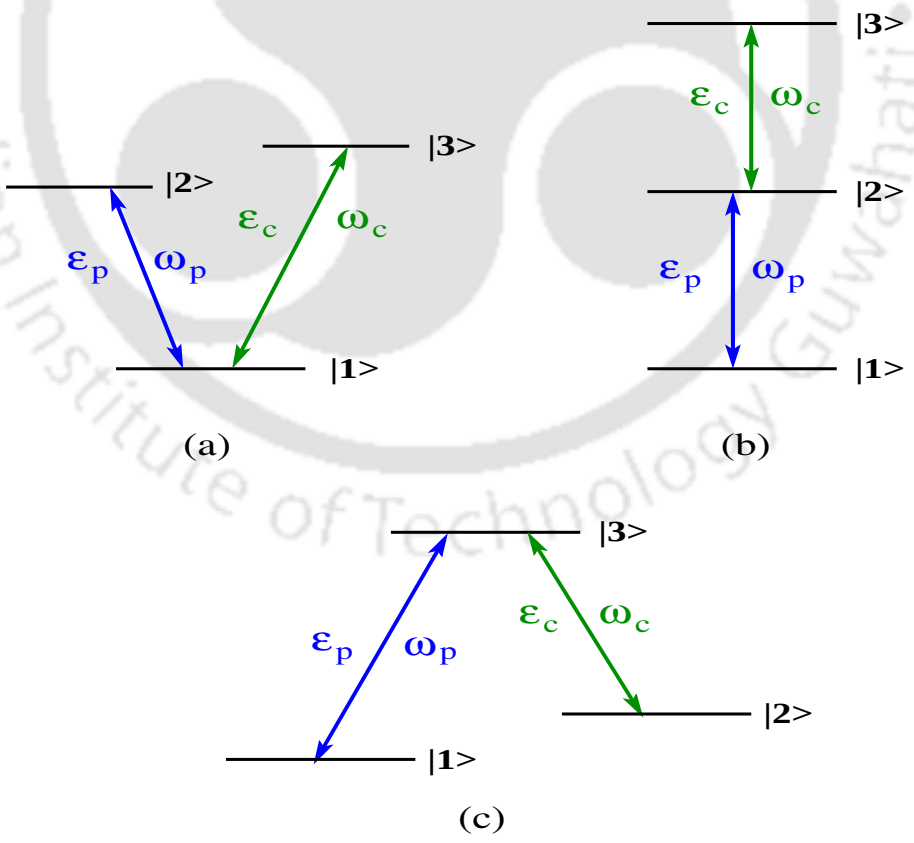

Fig. 1.6 Different level schemes (a) V, (b) ladder, and (c) Λ driven with two optical fields $\mathcal{E}_p$ and $\mathcal{E}_c$.

TH-1819_11612116

Formalism:

Unlike its two-level counterpart, the three-level system presents choices in the arrangement of the energy levels and driving fields. The geometrical configuration between level system and driving fields lead to various level schemes such as V, Ladder and Λ configurations as shown in Fig.1.6. Among the three different level structures, Λ

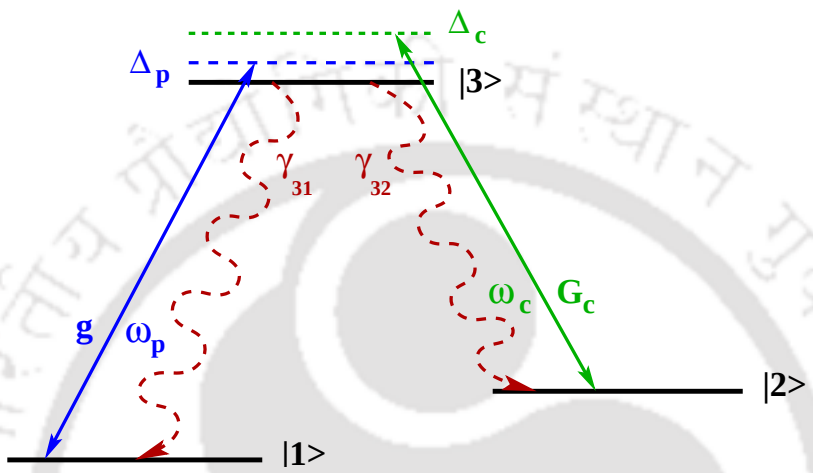

Fig. 1.7 (Color online) Shows a schematic diagram of the level system. A probe field with Rabi frequency g and a strong control with Rabi frequency G_c couples the transitions $|3\rangle \leftrightarrow |1\rangle$ and $|3\rangle \leftrightarrow |2\rangle$, respectively. γ_{3i}, $i \in \{1, 2\}$ are the radiative decay rates from the excited states $|3\rangle$ to the ground states $|1\rangle$ and $|2\rangle$.

system exhibits the greatest range of interesting physics due to its long living intermediate ground level that allows longer coherence between the levels. A typical three level Λ-type atomic system where a single excited state $|3\rangle$ is coupled with two closely spaced ground metastable states $|1\rangle$ and $|2\rangle$ by two optical fields is shown in Fig.1.7. The transitions $|1\rangle \leftrightarrow |3\rangle$ and $|3\rangle \leftrightarrow |2\rangle$ are electric dipole allowed whereas the transition $|1\rangle \leftrightarrow |2\rangle$ is electric dipole forbidden. A weak probe field ($\mathcal{E}_p$) with frequency ω_p couples the dipole allowed transition $|1\rangle \leftrightarrow |3\rangle$ while a strong control field ($\mathcal{E}_c$) with frequency ω_c drives the dipole allowed transition $|2\rangle \leftrightarrow |3\rangle$. The probe and control fields are expressed by

$$\mathbf{E}_p(\mathbf{r}, t) = \hat{\mathbf{e}}_p \mathcal{E}_p(\mathbf{r}) e^{i(\mathbf{k_p}\cdot\mathbf{r} - \omega_p t)} + c.c., \tag{1.87}$$

$$\mathbf{E}_c(\mathbf{r}, t) = \hat{\mathbf{e}}_c \mathcal{E}_c(\mathbf{r}) e^{i(\mathbf{k_c}\cdot\mathbf{r} - \omega_c t)} + c.c., \tag{1.88}$$

where $\mathcal{E}_p(\mathbf{r})$ and $\mathcal{E}_c(\mathbf{r})$ are slowly varying envelopes, $\hat{\mathbf{e}}_p$ and $\hat{\mathbf{e}}_c$ are the polarization unit vectors, $\mathbf{k_p}$ and $\mathbf{k_c}$ are the wave vectors of the probe and control field respectively. In presence of both probe and control fields, the total Hamiltonian for the three level

TH-1819_11612116

$\Lambda-$system under electric dipole approximation is given by

$$H = H_0 + H_I, \tag{1.89}$$

where H_0 is the unperturbed Hamiltonian and H_I the interaction Hamiltonian for the three level system. The unperturbed Hamiltonian is expressed as

$$H_0 = \hbar\omega_1|1\rangle\langle 1| + \hbar\omega_2|2\rangle\langle 2| + \hbar\omega_3|3\rangle\langle 3|. \tag{1.90}$$

where $\hbar\omega_1$, $\hbar\omega_2$ and $\hbar\omega_3$ are the energies of the states $|1\rangle$, $|2\rangle$ and $|3\rangle$, respectively. The interaction Hamiltonian between the atom and the coherent fields is given by

$$H_I = -\mathbf{d}\cdot\left[\mathbf{E}_p(\mathbf{r},t) + \mathbf{E}_c(\mathbf{r},t)\right]. \tag{1.91}$$

where $\mathbf{d}$ is the induced dipole moment of the system in the presence of the optical fields. The explicit form of interaction Hamiltonian including electric fields expressions can be rewritten as

$$\begin{aligned} H_I = &-\left[\mathbf{d}_{31}\cdot\hat{\mathbf{e}}_p\mathcal{E}_p(\mathbf{r})e^{i(\mathbf{k_p}\cdot\mathbf{r}-\omega_p t)} + \mathbf{d}_{31}\cdot\hat{\mathbf{e}}_p\mathcal{E}_p^*(\mathbf{r})e^{-i(\mathbf{k_p}\cdot\mathbf{r}-\omega_p t)}\right]|3\rangle\langle 1| \\ &-\left[\mathbf{d}_{13}\cdot\hat{\mathbf{e}}_p\mathcal{E}_p(\mathbf{r})e^{i(\mathbf{k_p}\cdot\mathbf{r}-\omega_p t)} + \mathbf{d}_{13}\cdot\hat{\mathbf{e}}_p\mathcal{E}_p^*(\mathbf{r})e^{-i(\mathbf{k_p}\cdot\mathbf{r}-\omega_p t)}\right]|1\rangle\langle 3| \\ &-\left[\mathbf{d}_{32}\cdot\hat{\mathbf{e}}_c\mathcal{E}_c(\mathbf{r})e^{i(\mathbf{k_c}\cdot\mathbf{r}-\omega_c t)} + \mathbf{d}_{32}\cdot\hat{\mathbf{e}}_c\mathcal{E}_c^*(\mathbf{r})e^{-i(\mathbf{k_c}\cdot\mathbf{r}-\omega_c t)}\right]|3\rangle\langle 2| \\ &-\left[\mathbf{d}_{23}\cdot\hat{\mathbf{e}}_c\mathcal{E}_c(\mathbf{r})e^{i(\mathbf{k_c}\cdot\mathbf{r}-\omega_c t)} + \mathbf{d}_{23}\cdot\hat{\mathbf{e}}_c\mathcal{E}_c^*(\mathbf{r})e^{-i(\mathbf{k_c}\cdot\mathbf{r}-\omega_c t)}\right]|2\rangle\langle 3|. \end{aligned} \tag{1.92}$$

where $\boldsymbol{d}_{ij} = \langle i|\boldsymbol{d}|j\rangle$ are dipole moments corresponding to $|i\rangle \leftrightarrow |j\rangle$ transition. We now define the Rabi frequencies for the probe and control field as

$$g = \frac{\mathbf{d}_{31}\cdot\hat{\mathbf{e}_p}\mathcal{E}_p(\mathbf{r})}{\hbar},\ \tilde{g} = \frac{\mathbf{d}_{31}\cdot\hat{\mathbf{e}_p}\mathcal{E}_p^*(\mathbf{r})}{\hbar}, \tag{1.93}$$

$$G_c = \frac{\mathbf{d}_{32}\cdot\hat{\mathbf{e}}_c\mathcal{E}_c(\mathbf{r})}{\hbar},\ \tilde{G}_c = \frac{\mathbf{d}_{32}\cdot\hat{\mathbf{e}}_c\mathcal{E}_c^*(\mathbf{r})}{\hbar}. \tag{1.94}$$

Using the above definition of the Rabi frequencies, the interaction Hamiltonian can be reduced to the following form

$$\begin{aligned} H_I = &-\left[ge^{-i\omega_p t} + \tilde{g}e^{i\omega_p t}\right]|3\rangle\langle 1| - \left[g^*e^{i\omega_p t} + \tilde{g}^*e^{-i\omega_p t}\right]|1\rangle\langle 3| \\ &-\left[G_c e^{-i\omega_c t} + \tilde{G}_c e^{i\omega_c t}\right]|3\rangle\langle 2| - \left[G_c^* e^{i\omega_c t} + \tilde{G}_c^* e^{-i\omega_c t}\right]|2\rangle\langle 3|. \end{aligned} \tag{1.95}$$

TH-1819_11612116

In order to make the above Hamiltonian time-independent we use the following unitary transformation

$$U = e^{-\frac{i}{\hbar}(\hbar\omega_p|3\rangle\langle 3|+\hbar(\omega_p-\omega_c)|2\rangle\langle 2|)t} \tag{1.96}$$

The effective Hamiltonian under this transformation is given as

$$\begin{aligned}\frac{H_{eff}}{\hbar} = UHU^\dagger = (\Delta_c-\Delta_p)|2\rangle\langle 2| - \Delta_p|3\rangle\langle 3| - \left[g+\tilde{g}e^{2i\omega_p t}\right]|3\rangle\langle 1| \\ - \left[g^*+\tilde{g}^*e^{-2i\omega_p t}\right]|1\rangle\langle 3| - \left[G_c+\tilde{G}_c e^{2i\omega_c t}\right]|3\rangle\langle 2| \\ - \left[G_c^*+\tilde{G}_c^* e^{-2i\omega_c t}\right]|2\rangle\langle 3|\,.\end{aligned} \tag{1.97}$$

here $\Delta_p = \omega_p - \omega_{31}$ and $\Delta_c = \omega_c - \omega_{32}$ are the detuning of the probe and control fields, respectively. We now use the rotating wave approximation to reduce the effective Hamiltonian to the following form

$$\begin{aligned}\frac{H_{eff}}{\hbar} = (\Delta_c-\Delta_p)|2\rangle\langle 2| - \Delta_p|3\rangle\langle 3| - g|3\rangle\langle 1| \\ - g^*|1\rangle\langle 3| - G_c|3\rangle\langle 2| - G_c^*|2\rangle\langle 3|\,.\end{aligned} \tag{1.98}$$

We further use this effective Hamiltonian in the Liouville equation to study the dynamics of the three level $\Lambda-$system.

Dynamics of three level $\Lambda-$system

We study the equation of motion for the density matrix elements by the Liouville Equation:

$$\frac{\partial\rho}{\partial t} = -\frac{i}{\hbar}[\mathcal{H}_{eff},\rho] + \mathcal{L}\rho\,. \tag{1.99}$$

where the term describing various incoherent processes is given by Liouvillean operator

$$\mathcal{L}\rho = -\sum_{i=3,j=1}^{2}\frac{\gamma_{ij}}{2}\left(|i\rangle\langle i|\rho - 2|j\rangle\langle j|\rho_{ii} + \rho|i\rangle\langle i|\right)\,. \tag{1.100}$$

where γ_{ij} corresponds to radiative decay rates from excited states $|i\rangle$ to ground states $|j\rangle$. The equation of motion for the density matrix elements are given by

$$\dot{\rho}_{11} = \gamma_{31}\rho_{33} + ig^*\rho_{31} - ig\rho_{13}\,, \tag{1.101a}$$

$$\dot{\rho}_{22} = \gamma_{32}\rho_{33} + iG_c^*\rho_{32} - iG_c\rho_{23}\,, \tag{1.101b}$$

$$\dot{\rho}_{21} = -\left[\gamma_c - i(\Delta_p-\Delta_c)\right]\rho_{21} - ig\rho_{23} + iG_c^*\rho_{31}\,, \tag{1.101c}$$

TH-1819_11612116

$$\dot{\rho}_{31} = -\left[\Gamma_{31} - i\Delta_p\right]\rho_{31} + iG_c\rho_{21} + ig(\rho_{11} - \rho_{33})\,, \tag{1.101d}$$

$$\dot{\rho}_{32} = -\left[\Gamma_{32} - i\Delta_c\right]\rho_{32} + ig\rho_{12} + iG_c(\rho_{22} - \rho_{33})\,, \tag{1.101e}$$

$$\dot{\rho}_{33} = -\dot{\rho}_{11} - \dot{\rho}_{22}\,, \tag{1.101f}$$

$$\dot{\rho}_{ij} = \dot{\rho}^*_{ji}\,. \tag{1.101g}$$

The excited state $|3\rangle$ decay to the ground states with equal rates, *i.e.*, $\gamma_{31} = \gamma_{32} = \gamma/2$, with γ is the spontaneous decay rate of excited state. The coherence decay rates $\Gamma_{31} = \Gamma_{32} = \gamma/2$.

1.4.1 Steady state solution of density matrix elements

In this section, we use a perturbative approach to solve the density matrix equations Eq. (1.101). We consider the probe field to be very weak and hence expand the density matrix to first order in probe as

$$\rho_{ij} = \rho^{(0)}_{ij} + \frac{g}{\gamma}\rho^{(+)}_{ij} + \frac{g^*}{\gamma}\rho^{(-)}_{ij}, \tag{1.102}$$

where $\rho^{(0)}_{ij}$ is the zeroth order solution determined in the absence of probe field. We assume all population to be in ground state $\rho^{(0)}_{11} = 1$ in the absence of the optical fields. The second and third term represent the first order solutions at positive and negative frequency of the probe field, respectively. We now substitute the above equation in Eq. (1.101) and equate the coefficients of g to obtain a set of 8 coupled equations. Next we solve these equations in the steady state limit to obtain the expression of the atomic coherence $\rho^{(+)}_{31}$. The linear susceptibility χ_{31} of the medium at frequency ω_p is expressed in terms of the atomic coherence $\rho^{(+)}_{31}$ by the following equation

$$\chi(\omega_p) = \frac{\mathcal{N}\left|d_{31}\right|^2}{\hbar\gamma}\rho^{(+)}_{31}\,, \tag{1.103}$$

where

$$\rho^{(+)}_{31} = \frac{2i\ \Gamma_{31}(\gamma_c + i\ (\Delta_c - \Delta_p))}{(\Gamma_{31} - i\Delta_p)(\gamma_c + i\ (\Delta_c - \Delta_p)) + \left|G_c\right|^2}\,. \tag{1.104}$$

The imaginary and real part of the susceptibility in Eq. (1.104) at $\Delta_c = 0$ are given by

$$\chi^{''} = \frac{\mathcal{N}\left|d_{31}\right|^2}{\hbar\gamma}\frac{\Gamma_{31}\gamma_c(\Gamma_{31}\gamma_c - 2\Delta_p^2 + G_c^2) + \Delta_p^2\Gamma_{31}^2}{(\Gamma_{31}\gamma_c - \Delta_p^2 + G_c^2)^2 + \Delta_p^2(\Gamma_{31} + \gamma_c)^2}\,, \tag{1.105a}$$

$$\chi^{'} = \frac{\mathcal{N}\left|d_{31}\right|^2}{\hbar\gamma}\frac{\Gamma_{31}\Delta_p(\gamma_c^2 - \Delta_p^2 + G_c^2) + 2\Delta_p\Gamma_{31}^2\gamma_c}{(\Gamma_{31}\gamma_c - \Delta_p^2 + G_c^2)^2 + \Delta_p^2(\Gamma_{31} + \gamma_c)^2}\,. \tag{1.105b}$$

TH-1819_11612116

The effect of the control field G_c on the medium susceptibility is displayed in Fig. 1.8. Figure 1.8 shows the variation of real and imaginary part of the medium susceptibility with probe detuning. It is observed that in absence of control field G_c, the susceptibility has qualitatively the same shape as for the two-level system. This is evident

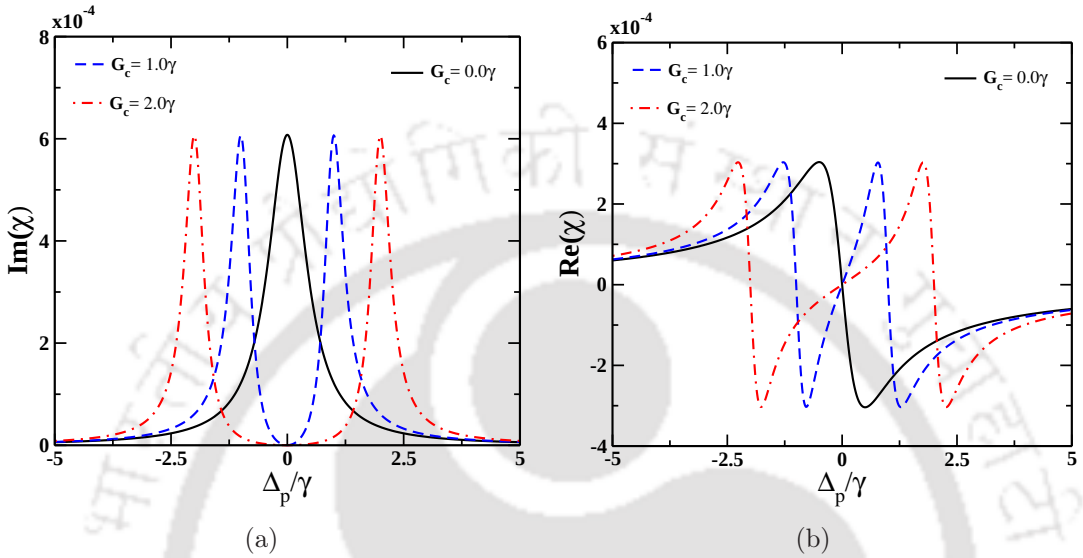

Fig. 1.8 Panel (a) and (b) shows the variation of imaginary and real parts of susceptibility as a function of probe detuning Δ_p for different control field intensities. Parameters are chosen as $\mathcal{N} = 10^{11}$ atoms/cm^3, $\Gamma_{31} = 0.5\gamma$, $\Delta_c = 0.0\gamma$, and $\gamma_c = 0.001\gamma$.

.

from the susceptibility expression Eq. (1.105a), which reduces to that of a two-level case in absence of a strong control field. However, in presence of G_c a dip appears in the absorption profile at probe resonance $\Delta_p = 0$. The value of the transmission at the line centre can be obtained from χ'' expression in Eq. (1.105a). At $\Delta_p = 0$, $\chi'' = \Gamma_{31}\gamma_c/(\gamma_c\Gamma_{31} + G_c^2) \rightarrow \Gamma_{31}\gamma_c/G_c^2$ in the limit $G_c \geq \gamma_c$. This shows that the absorption decreases with the increase in control field strength. The phenomena of cancellation of the absorption at the line centre in presence of a strong control field is known as *electromagnetically induced transparency (EIT)*. EIT was first coined by Harris *et al.* [13] where they discussed the enhancement of nonlinear effects in a three level system. The phenomenon of EIT was later experimentally observed by Boller *et al.* [14]. In their experiment using neutral Strontium atoms, they showed an improvement in the probe transmission from e^{-20} to e^{-1} in the presence of a strong control field. Later on there have been several studies on EIT using various atomic vapors [47, 48]. EIT technique has various application in slow light [49], fast light [50], stored light [51], etc.

TH-1819_11612116

1.4.2 Physical interpretation and analysis of EIT:

We have observed that the absorption vanishes at $\Delta_p = 0$ in the presence of a strong control field. The vanishing of absorption at the line center can be understood by using the quantum interference theory. The transition amplitudes of atomic states coupled via several possible alternative transition processes can interfere either constructively or destructively to give the total transition probability. It should be noted that the medium absorption is correlated to this total transition probability. For the case of lambda system, the atom in state $|1\rangle$ can be excited to the state $|3\rangle$ via two possible pathways. One is the direct path $|1\rangle \rightarrow |3\rangle$ and the other is indirect path $|1\rangle \rightarrow |3\rangle \rightarrow |2\rangle \rightarrow |3\rangle$. The transition amplitude corresponding to these two transition pathways can interfere destructively at two photon resonance condition resulting in vanishing of the absorption. The formation of the transparency window can also be explained using the dressed state picture.

Dressed state picture for three level Λ-system:

In the dressed state picture we first calculate the eigenvalues and eigenvectors of the effective Hamiltonian Eq. (1.98). In the absence of the coherent fields, the eigenvectors are the bare states $|1\rangle$, $|2\rangle$, and $|3\rangle$. However, in the presence of both control and probe field these bare states are no longer the basis vectors of the effective Hamiltonian. The effective Hamiltonian in the matrix form is represented as

$$H_{eff} = -\hbar \begin{pmatrix} 0 & 0 & g^* \\ 0 & -(\Delta_p - \Delta_c) & G_c^* \\ g & G_c & -\Delta_p \end{pmatrix}$$

For the case of simplicity, we will calculate the eigenvalues and eigenvectors at the two photon resonance condition $\Delta_p - \Delta_c = 0$. Eigenvectors and eigenvalues of the matrix is found in the usual way. The eigenvalues are given as

$$\epsilon_0 = 0, \tag{1.106}$$

$$\epsilon_+ = \frac{\hbar}{2}\left[\Delta_p + \sqrt{\Delta_p^2 + 4(|g|^2 + |G_c|^2)}\right], \tag{1.107}$$

$$\epsilon_- = \frac{\hbar}{2}\left[\Delta_p - \sqrt{\Delta_p^2 + 4(|g|^2 + |G_c|^2)}\right]. \tag{1.108}$$

The corresponding eigenvectors are given by

$$|0\rangle = \cos\theta\ |1\rangle - \sin\theta\ |2\rangle, \tag{1.109a}$$

$$|+\rangle = \sin\theta \sin\phi\ |1\rangle + \cos\theta \sin\phi\ |2\rangle + \cos\phi\ |3\rangle, \tag{1.109b}$$

TH-1819_11612116

$$|-\rangle = \sin\theta\cos\phi\ |1\rangle + \cos\theta\cos\phi\ |2\rangle - \sin\phi\ |3\rangle, \tag{1.109c}$$

where θ and ϕ are defined as

$$\tan\theta = \frac{g}{G_c},\ \ \tan(2\phi) = \frac{2\sqrt{|g|^2 + |G_c|^2}}{\Delta_p}. \tag{1.110}$$

Next we discuss the properties of the state $|0\rangle$. This state is a linear combination of the two ground states $|1\rangle$ and $|2\rangle$ and does not contain the excited state $|3\rangle$. The transition probability between $|0\rangle \leftrightarrow |3\rangle$ transition is zero which implies that the atom will remain in state $|0\rangle$ even in the presence of radiation. This state is known as a dark state. The vanishing transition probability also implies that if the system is prepared in the state $|0\rangle$ then the population cannot be excited to the upper level and the population remains trapped in this state. This phenomenon is known as *Coherent Population Trapping(CPT)*. It should be noted that in CPT phenomena both the fields are of comparable strength *i.e.*, $g \approx G_c$. CPT was first observed by Alzetta *et al.* [12] in sodium fluorescent cell. In their experiment on sodium atoms in Λ-configuration, no fluorescent emission from the excited state was observed. Rather a dark line appeared inside a bright fluorescent cell, hence the name dark resonance is associated with CPT phenomena. Later on Erimondo and Orriols have theoretically explained the CPT phenomenon using induced atomic coherence and interference effects [2]. CPT has important applications in coherent population transfer [52], lasing without inversion [53], metrology [54], atomic clocks [55], etc.

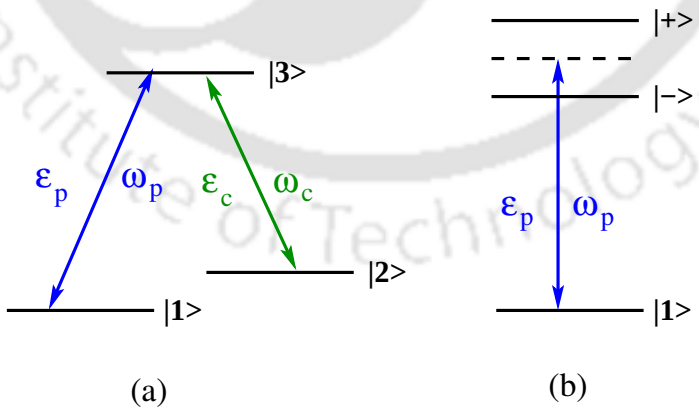

Fig. 1.9 Schematic diagram of the three level system (a) bare states and (b) dressed states.

We now consider a special case where the strength of the probe field is very small in comparison to the control field strength *i.e.*, $g \ll G_c$. The dressed states under this

TH-1819_11612116

weak probe approximation are given by

$$|0\rangle = |1\rangle, \tag{1.111}$$

$$|+\rangle = \frac{1}{\sqrt{2}}(|3\rangle + |2\rangle), \tag{1.112}$$

$$|-\rangle = \frac{1}{\sqrt{2}}(|3\rangle - |2\rangle). \tag{1.113}$$

In the weak probe field limit, the ground state $|1\rangle$ becomes a dark state. Hence atoms in this state cannot be excited to the state $|3\rangle$, resulting in a decrease in absorption at the two photon resonance. Moreover, a coherent dressing of the $|2\rangle \rightarrow |3\rangle$ transition by a strong control field results in two superposed states $|+\rangle$ and $|-\rangle$. Each of the states are equally spaced from the excited state $|3\rangle$ by a factor of $\pm G_c$. Hence transition from $|1\rangle$ to the dressed states $|+\rangle$ and $|-\rangle$ results in the formation of the two absorption peaks at $\Delta_p = \pm G_c$ as in Fig. 1.8(a). Also with the increase in control field strength, the spacing between the dressed state increases. This leads to the increase in the width of the transparency window as shown in Fig. 1.8(a). In earlier text we have only discussed about the formation of transparency window due to a strong control field. However, it is of utmost importance to study the dispersion of the three level system as well. The dispersion is related to the refractive index of the medium. Hence any modification of the dispersion can lead to a change in the refractive index of the medium. Figure. 1.8(b), shows the variation of dispersion with probe detuning. The EIT window is accompanied by a steep variation in the dispersion. This large dispersion near probe resonance is useful in changing the speed of the light. The group velocity of the light pulse propagating through a dispersive medium is given by

$$v_g = \frac{c}{Re\left[n(\omega)\right] + \omega Re\left[\frac{\partial n(\omega)}{\partial \omega}\right]}. \tag{1.114}$$

The above expression depicts that the group velocity is dependent on the slope of the dispersion $\partial n/\partial\omega$. Hence by increasing the slope of the dispersion group velocity can be greatly reduced. When $\partial n/\partial\omega > 0$, the medium is considered as normal dispersive medium. In these medium light propagates with subluminal velocity *i.e.,* light travels slower in the medium than in vacuum [16]. For the case of $\partial n/\partial\omega < 0$, the medium shows anomalous dispersion. Light propagates with superluminal velocity through this anomalous dispersive medium *i.e.,* light travels with velocity faster than in vacuum [50].

TH-1819_11612116

TH-1819_11612116

Chapter 2

Diffraction control via tunable optical waveguide based on atomic vapor

Optical diffraction is a physical phenomena due to which almost all beams propagating either through a medium or in free space spreads in the plane transverse to the propagation direction. However there exists some particular class of non-diffracting beams such as Airy [56, 57], Bessel [58, 59], Mathieu [60, 61], and parabolic beams [62]. Spreading of the beams due to diffraction causes loss of information carried by the beam and hence acts as a major obstacle in the generation, transfer, and processing of information. Therefore, controlling diffraction is a fundamental goal of image processing, high resolution imaging and optical lithography. In order to subdue the effect of diffraction, variety of techniques based on EIT [21, 20, 26–29], CPT [63–65, 116], and SAT [19] have been proposed. In most of these schemes, the salient feature is to manipulate the susceptibility of the medium along the transverse direction using a spatially dependent control field. A suitable spatially dependent control field can create an optical waveguide like structure inside the atomic medium. The generated optical waveguide protect the probe field from diffraction induced distortion during propagation through the medium. Moreover, the idea of manipulating the susceptibility of the medium along the transverse direction has been used for cloning of images, focusing, and self-imaging [68–73]. However in all the above cases the minimum feature size of the guided beam is $\sim 50\mu$m, which has a limitation for practical use in high resolution imaging, lithography, and image processing, due to its incapacity to process large density of information. Narrow feature size optical beams are essential to satisfy the above criterion. A high contrast waveguide is required to suppress or even eliminate diffraction of the narrow beam in the course of propagation. This waveguide may be realized by considering a medium with high optical density. Simultaneously, the high optical density also increases the gain or absorption of the medium, which limits it practical applicability.

TH-1819_11612116

In order to overcome these limitations, we look for a system where the refractive index can be enhanced without a significant change of absorption or gain. The main motivation for the present study derives from recent elegant experiments on photolithography by Scott *et al.* [74] and Andrew *et al.* [75]. In these experiments, they used photochromic molecules as a mask to imprint a nanoscale pattern on a target material. The mask shows very interesting behaviour while interacting with light. For a light with wavelength λ_1 (writing beam) the mask becomes transparent whereas for another light with wavelength λ_2 (inhibitor beam) it becomes opaque. Exploiting these properties of the mask, they created a nano-size pattern using Gaussian beam (writing-beam) and a Laguerre-Gaussian (LG) beam (inhibitor-beam). Such interesting ideas have also been used in Stimulated emission depletion (STED) microscopy to image nano size particles [76, 77]. A N-type four level system [78, 79] can be used as an atomic analog for the mask. The atomic system becomes transparent to the weak probe due to presence of a strong control field. However it becomes opaque in the presence of an additional Kerr field. The competition between control field induced EIT and Kerr field induced absorption along the transverse directions of the medium forms a narrow atomic waveguide. Also the Kerr field increases the variation of the refractive index between core and cladding which allows for distortionless propagation of narrow probe beam through several Rayleigh lengths.

In this chapter, we demonstrate how a high contrast tunable optical waveguide can be facilitated by using additional Kerr field. To achieve this, we use a four-level N-type atomic system driven by probe, control and Kerr fields. We first derive an analytical expression for the probe susceptibility in the steady state limit. We find that the control field induced probe transparency can be abolished by a Kerr field at probe resonance. This Kerr field assisted probe absorption plays an important role in the generation of tunable waveguide. Next, we investigate the spatial inhomogeneity of the medium caused by transverse variation of both control and Kerr fields. We find that a Gaussian control beam creates a wide waveguide structure with low refractive index variation between core and cladding, inside the atomic medium. The waveguide structure is sensitive to the control beam size, however, even a narrow control beam cannot create a narrow waveguide due to its inherent diffraction. Inevitably this wide waveguide fails to protect the propagation of the narrow probe beam without diffraction. To avoid this limitation, we consider a LG Kerr field to facilitate a high contrast narrow waveguide structure. In order to delineate the effect of the high contrast waveguide on probe beam dynamics, we numerically solve the Maxwell's wave equation at the paraxial limit. Finally, we show that Kerr field induced tunable optical atomic waveguide can guide different modes of the probe beam to several orders of Rayleigh length without any diffraction. This efficient guiding of narrow

TH-1819_11612116

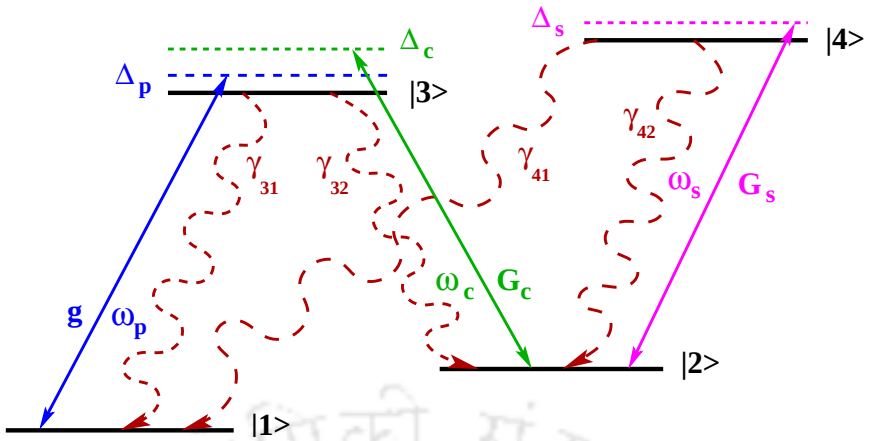

Fig. 2.1 (Color online) Shows a schematic diagram of the level system. A probe field with Rabi frequency g and a strong control with Rabi frequency G_c couples the transitions $|3\rangle \leftrightarrow |1\rangle$ and $|3\rangle \leftrightarrow |2\rangle$, respectively. The transition $|4\rangle \leftrightarrow |2\rangle$ is coupled by a strong Kerr field having Rabi frequency G_s. γ_{3i} and γ_{4i}, $i \in \{1, 2\}$ are the radiative decay rates from the excited states $|3\rangle$ and $|4\rangle$ to the ground states $|1\rangle$ and $|2\rangle$.

optical beam may have important applications in large density image processing and high resolution imaging.

2.1 Theoretical Formulations

2.1.1 Atomic model system

In this work, we consider a homogeneously broadened N-type atomic system consisting of excited states $|3\rangle$ and $|4\rangle$ and two metastable states $|1\rangle$ and $|2\rangle$, as shown in Fig.2.1. The proposed model system can be experimentally realized in ^{87}Rb, with $|1\rangle = |5S_{\frac{1}{2}}, F = 2\rangle$, $|2\rangle = |5S_{\frac{1}{2}}, F = 3\rangle$, $|3\rangle = |5P_{\frac{1}{2}}, F' = 2\rangle$ and $|4\rangle = |5P_{\frac{3}{2}}, F' = 4\rangle$. The atomic transition $|1\rangle \leftrightarrow |3\rangle$ is coupled by a weak probe field ($\mathcal{E}_p$) with frequency ω_p. A strong control field ($\mathcal{E}_c$) with frequency ω_c, and a strong Kerr field ($\mathcal{E}_s$) with frequency ω_s couple the transitions $|3\rangle \leftrightarrow |2\rangle$ and $|2\rangle \leftrightarrow |4\rangle$, respectively. The electric fields corresponding to the three coherent fields are defined as

$$\vec{E}_j(\vec{r}, t) = \hat{e}_j \mathcal{E}_j(\vec{r})\ e^{-i(\omega_j t - k_j z)} + c.c.\,, \tag{2.1}$$

where, $\mathcal{E}_j(\vec{r})$ is the slowly varying envelope, $\hat{e}_j$ is the unit polarization vector, ω_j is the laser field frequency and k_j is the wave number of the field, respectively. The index $j \in \{p, c, s\}$ denotes the probe, control and Kerr field, respectively. Under the electric dipole approximation, the time-dependent Hamiltonian of the system in the presence

TH-1819_11612116

of these three coherent fields can be written as

$$H = H_0 + H_I\,, \tag{2.2a}$$

$$H_0 = \hbar\omega_{12}|2\rangle\langle 2| + \hbar\omega_{13}|3\rangle\langle 3| + \hbar\omega_{14}|4\rangle\langle 4|\,, \tag{2.2b}$$

$$\begin{aligned} H_I = &-\left(|3\rangle\langle 1|\boldsymbol{d}_{31}\cdot\mathcal{E}_p e^{-i(\omega_p t - k_p z)} + |3\rangle\langle 2|\boldsymbol{d}_{32}\cdot\mathcal{E}_c e^{-i(\omega_c t - k_c z)}\right.\\ &\left. + |4\rangle\langle 2|\boldsymbol{d}_{42}\cdot\mathcal{E}_s e^{-i(\omega_s t - k_s z)} + \text{H.c.}\right), \end{aligned} \tag{2.2c}$$

where $\boldsymbol{d}_{ij} = \langle i|\boldsymbol{d}|j\rangle$ are dipole moments corresponding to $|i\rangle \leftrightarrow |j\rangle$ transition. To write the Hamiltonian in the time independent form, we use the following unitary transformation

$$W = e^{-\frac{i}{\hbar}Ut}\,, \tag{2.3a}$$

$$U = \hbar\omega_p|3\rangle\langle 3| + \hbar(\omega_p - \omega_c)|2\rangle\langle 2| + \hbar(\omega_p - \omega_c + \omega_s)|4\rangle\langle 4|\,. \tag{2.3b}$$

Under rotating wave approximation, the effective time independent Hamiltonian takes the following form

$$\begin{aligned} \frac{\mathcal{H}_I}{\hbar} = &(\Delta_c - \Delta_p)|2\rangle\langle 2| + (\Delta_c - \Delta_p - \Delta_s)|4\rangle\langle 4|\\ &- \Delta_p|3\rangle\langle 3| - g|3\rangle\langle 1| - G_c|3\rangle\langle 2| - G_s|4\rangle\langle 2| + \text{H.c.})\,, \end{aligned} \tag{2.4}$$

where the Rabi frequencies of the probe, control and the Kerr fields are defined as

$$g = \frac{\vec{d}_{31}\cdot\vec{\mathcal{E}}_{\rm p}}{\hbar}e^{ik_p z}, G_c = \frac{\vec{d}_{32}\cdot\vec{\mathcal{E}}_{\rm c}}{\hbar}e^{ik_c z}, G_s = \frac{\vec{d}_{42}\cdot\vec{\mathcal{E}}_{\rm s}}{\hbar}e^{ik_s z}.$$

The detuning of the probe, control and Kerr fields from the corresponding transition resonances are expressed as $\Delta_p = \omega_p - \omega_{31}$, $\Delta_c = \omega_c - \omega_{32}$, and $\Delta_s = \omega_s - \omega_{42}$, respectively.

2.1.2 Dynamical equations for density matrix elements

We use the following Liouville equation to study the dynamics of the atomic populations and coherences,

$$\frac{\partial\rho}{\partial t} = -\frac{i}{\hbar}[\mathcal{H}_I, \rho] + \mathcal{L}\rho\,. \tag{2.6}$$

TH-1819_11612116

The last term $\mathcal{L}\rho$ is Liouville operator which describes all the incoherent processes and is given by

$$\mathcal{L}\rho = -\sum_{i=3}^{4}\sum_{j=1}^{2}\frac{\gamma_{ij}}{2}\left(|i\rangle\langle i|\rho - 2|j\rangle\langle j|\rho_{ii} + \rho|i\rangle\langle i|\right) , \tag{2.7}$$

where γ_{ij} corresponds to radiative decay rates from excited states $|i\rangle$ to ground states $|j\rangle$. The equation of motion for atomic populations and coherences of the four level system can be described by the following density matrix equations:

$$\dot{\rho}_{11} = \gamma_{31}\rho_{33} + \gamma_{41}\rho_{44} + ig^*\rho_{31} - ig\rho_{13} , \tag{2.8a}$$
$$\dot{\rho}_{22} = \gamma_{32}\rho_{33} + \gamma_{42}\rho_{44} + iG_c^*\rho_{32} - iG_c\rho_{23} + iG_s^*\rho_{42} - iG_c\rho_{24} , \tag{2.8b}$$
$$\dot{\rho}_{33} = -(\gamma_{31} + \gamma_{32})\rho_{33} + ig\rho_{13} - ig^*\rho_{31} + iG_c\rho_{23} - iG_c^*\rho_{32} , \tag{2.8c}$$
$$\dot{\rho}_{21} = -\left[\gamma_c - i(\Delta_p - \Delta_c)\right]\rho_{21} - ig\rho_{23} + iG_c^*\rho_{31} + iG_s^*\rho_{41} , \tag{2.8d}$$
$$\dot{\rho}_{31} = -\left[\Gamma_{31} - i\Delta_p\right]\rho_{31} + iG_c\rho_{21} + ig(\rho_{11} - \rho_{33}) , \tag{2.8e}$$
$$\dot{\rho}_{32} = -\left[\Gamma_{32} - i\Delta_c\right]\rho_{32} + ig\rho_{12} + iG_c(\rho_{22} - \rho_{33}) - iG_s\rho_{34} , \tag{2.8f}$$
$$\dot{\rho}_{34} = -\left[\Gamma_{34} - i(\Delta_c - \Delta_s)\right]\rho_{34} + ig\rho_{14} + iG_c\rho_{24} - iG_s^*\rho_{32} , \tag{2.8g}$$
$$\dot{\rho}_{41} = -\left[\Gamma_{41} - i(\Delta_p - \Delta_c + \Delta_s)\right]\rho_{41} + iG_s\rho_{21} - ig\rho_{43} , \tag{2.8h}$$
$$\dot{\rho}_{42} = -\left[\Gamma_{42} - i\Delta_s\right]\rho_{42} + iG_s(\rho_{22} - \rho_{44}) - iG_c\rho_{43} , \tag{2.8i}$$
$$\dot{\rho}_{44} = -\dot{\rho}_{11} - \dot{\rho}_{22} - \dot{\rho}_{33} , \tag{2.8j}$$
$$\dot{\rho}_{ij} = \dot{\rho}_{ji}^* , \tag{2.8k}$$

where, the overdots stand for time derivatives and "*" denotes complex conjugate.

2.1.3 Solution of density matrix equations using perturbative approach

In this section, following perturbative calculations by Dey and Agarwal [78], we derive an analytical expression for the linear susceptibility of the medium at the steady state limit. We consider the probe to be very weak so that the density matrix can be expanded to first order in probe as

$$\rho_{ij} = \rho_{ij}^{(0)} + \frac{g}{\gamma}\rho_{ij}^{(+)} + \frac{g^*}{\gamma}\rho_{ij}^{(-)}, \tag{2.9}$$

where $\rho_{ij}^{(0)}$ is the zeroth order solution determined in the absence of probe field. The second and third term represent the first order solutions at positive and negative frequency of the probe field, respectively. We now substitute the above equation in

TH-1819_11612116

Eq. (2.8) and equate the coefficients of g to obtain a set of 15 coupled equations. Next we solve these equations in the steady state limit to obtain the expression of the atomic coherence $\rho_{31}^{(+)}$. The linear susceptibility χ_{31} of the medium at frequency ω_p is expressed in term of atomic coherence $\rho_{31}^{(+)}$ by the following equation

$$\chi(\omega_p) = \frac{\mathcal{N}\,|d_{31}|^2}{\hbar\gamma}\rho_{31}^{(+)}\,, \tag{2.10}$$

where

$$\rho_{31}^{(+)} = \frac{2i\ \Gamma_{31}\ A}{(\Gamma_{31} - i\Delta_p)\ A + B\ \ |G_c|^2}\,, \tag{2.11a}$$

$$B = \Gamma_{41} + i\ (\Delta_c - \Delta_p - \Delta_s)\,, \tag{2.11b}$$

$$A = (\gamma_c + i\ (\Delta_c - \Delta_p))\ B + |G_s|^2\ . \tag{2.11c}$$

Eq. (2.11a) shows the dependence of atomic coherence on intensities of the control and the Kerr fields, respectively. Subsequently the transverse spatial profiles of G_c and G_s play an important role in the manipulation of the medium susceptibility along the transverse directions. Hence the use of an appropriate transverse profile of Kerr field creates spatial modulation of the probe absorption which enables the formation of a high contrast tunable optical atomic waveguide.

2.1.4 Paraxial beam propagation equation

We use the Maxwell's wave equation under the paraxial approximation as in Eq. (1.20) to study the spatial evolution of the probe envelope propagating through the atomic medium. The propagation Eq. (1.20) can be transformed to the Rabi frequency of the probe beam as

$$\frac{\partial}{\partial z}g = \frac{i}{2k_p}\nabla_\perp^2\ g + 2i\pi k_p\chi\ g\,. \tag{2.12}$$

The first terms on the right hand side of Eq. (2.12) represents the transverse variation of the probe field and accounts for diffraction either in the medium or in free space. The second term on the right hand side of Eq. (2.12) lead to the dispersion and absorption of the probe beam. To study the effect of the transversely varying susceptibility on the probe propagation, we numerically solve Eq. (2.12) using Fourier split-step method [80] (see Appendix A). However, the paraxial approximation is valid only for the light beam with $\lambda/2\pi w_0 < 0.1$, where w_0 is the beam waist [81, 82]. Otherwise the non-paraxial term $(-i/2k_p)\partial_z^2 g$ needs to be incorporated in the left hand side of Eq. (2.12) [70]. We make use of the Angular Spectrum Representation Method (ASRM) [81] to confirm the validity of paraxial approximation for propagation of nar-

TH-1819_11612116

row waist beam. It should be borne in mind that the ASRM gives the exact solution of Maxwell's equation for a propagating beam either in free space or in a medium with spatial homogeneity. The transverse variation of narrow waist beam at any propagation distance z can be obtained by using ASRM, provided the spatial distribution of the beam at $z = 0$ is known. The spatial transverse profile of probe beam propagating in a isotropic homogeneous medium is given by

$$g(x, y, z) = \iint_{-\infty}^{\infty} g(k_x, k_y) e^{i[k_x x + k_y y + k_z z]} dk_x dk_y, , \tag{2.13}$$

where

$$g(k_x, k_y) = \frac{1}{4\pi^2} \iint_{-\infty}^{\infty} g(x, y; 0) e^{-i[k_x x + k_y y]} dx dy, . \tag{2.14}$$

Here $g(x, y; 0)$ is the initial probe profile, and k_x,k_y,k_z are the spatial frequencies of the probe. The wave vector k_z is defined as

$$k_z = \begin{cases} (k^2 - (k_x^2 + k_y^2))^{\frac{1}{2}}, & \text{if } k^2 > (k_x^2 + k_y^2) \\ i(k^2 - (k_x^2 + k_y^2))^{\frac{1}{2}}, & \text{if } k^2 < (k_x^2 + k_y^2) \end{cases} \tag{2.15}$$

where k corresponds to wave vector in the medium and is given as

$$k = k_0 n(\omega_p) , \tag{2.16}$$

$$n(\omega_p) = 1 + 2\pi\chi(\omega_p) , \tag{2.17}$$

$$k_0 = 2\pi/\lambda_p. \tag{2.18}$$

2.2 Results and discussion

2.2.1 Susceptibility with homogeneous fields

In this section, we study Eq. (2.10) to demonstrate the effect of the probe absorption in the presence of both cw control and Kerr fields. Fig. 2.2 shows the variation of probe absorption with probe detuning at different intensities of Kerr field. In the absence of Kerr field, the N-type system reduces to a three level Λ system wherein two arms are connected by weak probe and strong control fields, respectively. Hence the reduced model system exhibits a typical EIT-like feature accompanied with a transparency dip at resonance probe absorption. We adopt the dressed-state picture to explain the behaviour of the probe absorption [5]. The two absorption peaks

TH-1819_11612116

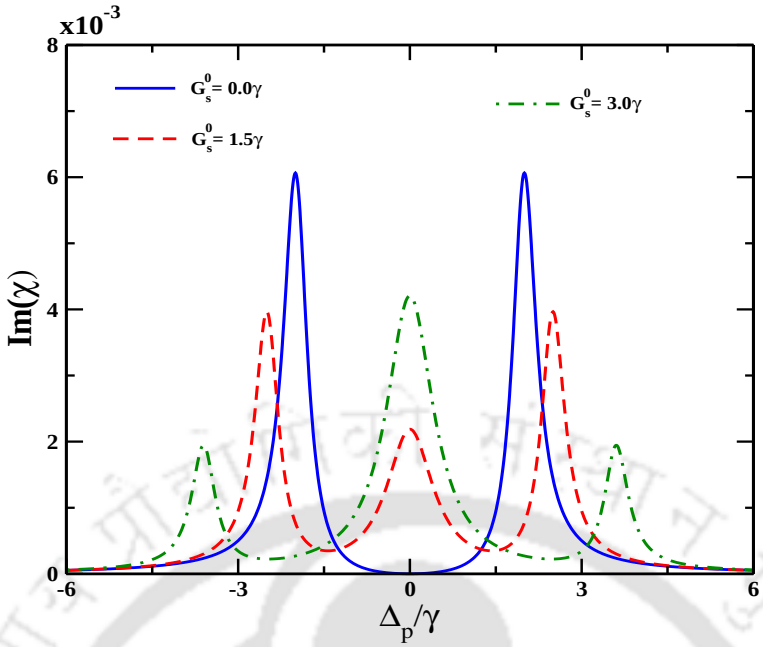

Fig. 2.2 (Color online) Shows variation of imaginary part of susceptibility with probe detuning Δ_p for different Kerr intensities. Parameters are chosen as $\mathcal{N} = 10^{12}$ atoms/cm^3, $\Gamma_{31} = 0.5\gamma$, $\Gamma_{41} = 0.5\gamma$, $\Delta_c = 0.0\gamma$, $\Delta_s = 0.0\gamma$, $G_c^0 = 2.0\gamma$ and $\gamma_c = 0.001\gamma$.

shown in Fig. 2.2 correspond to the transitions between bare state $|1\rangle$ to dressed states $|+\rangle = (|2\rangle + |3\rangle)/\sqrt{2}$ and $|-\rangle = (|2\rangle - |3\rangle)/\sqrt{2}$, respectively. Further, by an application of a strong Kerr field the probe transparency dip changes into an absorption peak around the resonance. As a result, the probe field experiences a huge absorption at the resonance. Hence, double transparency windows are formed in place of single transparency due to presence of peak absorption at the line center as shown in Fig. 2.2. Such modulation in the absorption of probe due to Kerr field is the key to confinement and guiding of light beam. Moreover, the formation of double transparency is generally due to Double-Dark resonance (DDR) effect, which can be well understood using the dressed state picture for the N-type system [79]. In the dressed state picture, the new eigenstates of the Hamiltonian in Eq. (2.4) are $|1\rangle$, $|0\rangle$, $|+'\rangle$, and $|-'\rangle$. The dressed states can be expressed in terms of the bare states $|2\rangle$, $|3\rangle$, and $|4\rangle$ as

$$|0\rangle = \frac{G_c}{\sqrt{G_c^2+G_s^2}}|3\rangle - \frac{G_s}{\sqrt{G_c^2+G_s^2}}|4\rangle\,, \tag{2.19}$$

$$|+'\rangle = \frac{1}{\sqrt{2}}\left(|2\rangle + \frac{G_c}{\sqrt{G_c^2+G_s^2}}|3\rangle + \frac{G_s}{\sqrt{G_c^2+G_s^2}}|4\rangle\right)\,, \tag{2.20}$$

$$|-'\rangle = \frac{1}{\sqrt{2}}\left(|2\rangle - \frac{G_c}{\sqrt{G_c^2+G_s^2}}|3\rangle + \frac{G_s}{\sqrt{G_c^2+G_s^2}}|4\rangle\right)\,. \tag{2.21}$$

TH-1819_11612116

The resonance absorption peak in Fig. 2.2 corresponds to the transition between $|1\rangle$ and $|0\rangle$. Whereas the left and right absorption peaks correspond to the transitions $|1\rangle \leftrightarrow |+'\rangle$ and $|1\rangle \leftrightarrow |-'\rangle$, respectively. Further, the energy separation between the dressed states $|+'\rangle$ and $|-'\rangle$ depend on both control and Kerr fields intensity and is given as $2\sqrt{G_c^2 + G_s^2}$. Hence, with the increase in Kerr field intensity the separation between the states $|+'\rangle$ and $|-'\rangle$ increases. Such modulation in probe absorption due to competition between transparency and absorption, induced by control and Kerr fields, can exactly mimic the behaviour shown by photopolymers and photochromic molecules used in photolithography experiments [74, 75]. Therefore, an N-level system which displays both EIT and DDR effects can have a potential application in optical lithography, image processing, etc. Further, the manipulation of the absorption and refractive index by the Kerr field holds the key to formation of high contrast tunable optical waveguide, which will be discussed in the next section.

2.2.2 Susceptibility with inhomogeneous control field

In this section, we explore the effect of spatially varying control field and Kerr field on the medium susceptibility. In this regard, we choose control field as a Gaussian beam (LG_0^0) and Kerr field to be a LG beam (LG_m^l), respectively. The spatial structure of the LG beam is expressed as

$$G_j(r,\phi,z) = G_j^0 \frac{w_j}{w_j(z)} \left(\frac{r\sqrt{2}}{w_j(z)}\right)^{|l|} L_m^l\left(\frac{2r^2}{w_j^2(z)}\right) e^{il\phi} e^{-\left(\frac{r^2}{w_j^2(z)}\right)} e^{\left(\frac{ikr^2}{2R_j(z)}\right)} e^{\left(-i(2m+l+1)\tan^{-1}\left(\frac{z}{z_{0_j}}\right)\right)}, \tag{2.22a}$$

$$r = \sqrt{x^2+y^2}\,, \tag{2.22b}$$

$$\phi = \tan^{-1}\left(\frac{y}{x}\right). \tag{2.22c}$$

where $R_j(z) = z + (z_{0j}^2/z)$, and $z_{0j} = \pi w_j^2/\lambda$ is the radius of curvature and the Rayleigh length of the beams, respectively. The spot size of the beams is $w_j(z) = w_j\sqrt{1+((z-q)/z_{0j})^2}$, where, w_j is the minimum beam waist and q is the focusing point. The index $j \in \{c, s\}$ denotes the control and Kerr beam, respectively. Fig. 2.3 depicts the variation of the absorption and the refractive index of the medium along the transverse direction x at $y = 0$ plane. The results are plotted for two different cases, (i) in the presence of only control beam and (ii) in the presence of both control and Kerr beams. In the first case, the variation of absorption and refractive index of the medium is solely dependent on the intensity and the spatial structure of the control beam. The central region of Gaussian profile of control beam permits a transparency

TH-1819_11612116

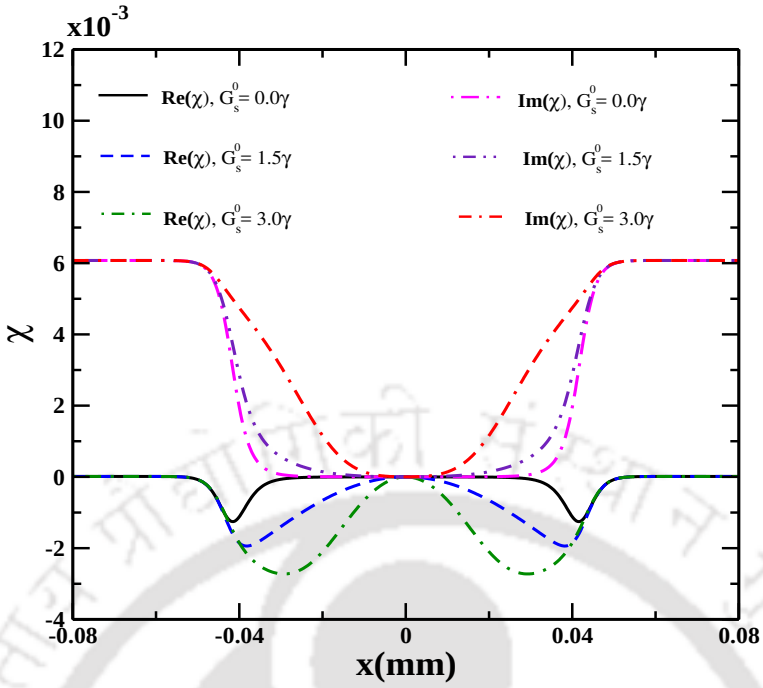

Fig. 2.3 (Color online) Panel displays transverse variation of both real and imaginary parts of susceptibility at $y = 0$ plane. Used parameters are same as in Fig.(2.2) except the control and Kerr beam parameters are $G_c^0 = 2.0\gamma$, $q = 1.0$ mm, $w_c = 20$ μm, and $w_s = 20$ μm, respectively. The probe detuning $\Delta_p = -0.001\gamma$.

window for the probe beam. However, a decrease in intensity of the control beam towards the wing region gives rise to a very high probe absorption, as shown in Fig. 2.3. Consequently, a spatially varying probe transparency window is formed inside the atomic medium. Interestingly, a similar behaviour of the refractive index of the medium is noticed. It is clear from Fig. 2.3, that the refractive index attains a maximum value at higher intensity region of the control beam which forms the core of the atomic waveguide. Simultaneously the cladding can be manifested by gradually decreasing intensity region towards the wing of the control beam. Note that probe field is red detuned. Figure 2.3 also shows that the induced waveguide structure consists of small refractive variation between core and cladding accompanied with a very wide core. Such a low contrast waveguide structure fails to guide narrow waist beam due to diffraction induced distortion. However, a suitable spatial profile of Kerr beam can significantly enhance the features of the induced waveguide. The intensity distribution of the LG_0^1 Kerr beam plays an important role in controlling the absorption and refractive index of the medium. The absorption of the medium remains unaffected at the nodal region where the intensity of the LG_0^1 Kerr beam vanishes. However, the non-zero intensity of the Kerr beam contributes sharply to the increase in medium absorption towards the outer region. As a result the transparency window gets narrow. Further, the region with higher intensity of the Kerr beam exhibits a

TH-1819_11612116

reduction in the refractive index between core and cladding. Hence, a sharply varying refractive index waveguide is constituted inside the atomic medium with a narrow core structure. We also notice from Fig. 2.3 that the width of the core can be further narrowed, and the refractive index sharply varied by using higher Kerr field intensity. Therefore, an intense spatial Kerr profile restricts the exposure of the control profile which forms a very narrow transparency window with a high contrast refractive index. Thus, the spatial structure of Kerr beam plays an important role in the generation of high contrast tunable waveguide.

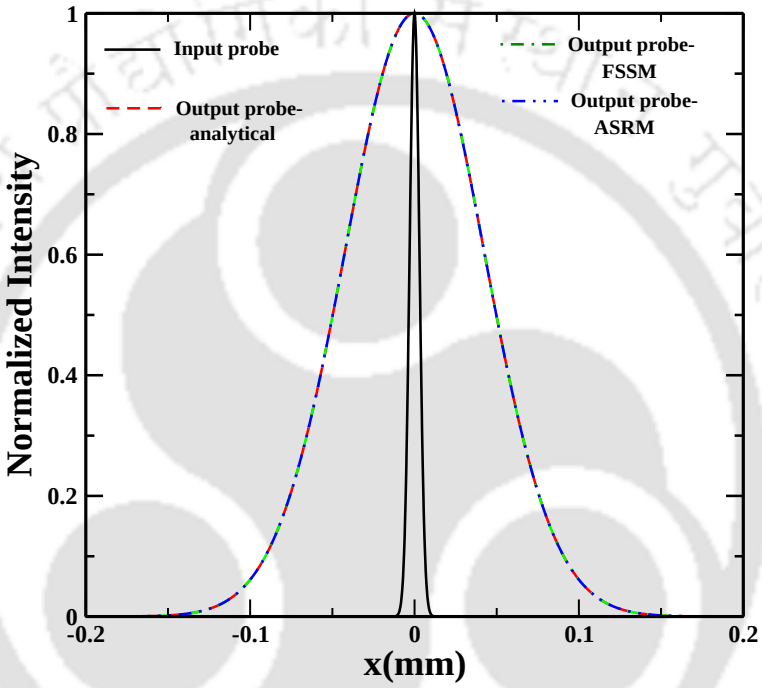

Fig. 2.4 (Color online) Normalized intensity variation of probe envelope along transverse direction x at $y = 0$ plane after traversing a distance of $z = 2$ mm through free space. The initial probe beam waist is $w_p = 6\mu$m.

2.2.3 Beam propagation dynamics

We now illustrate the effect of spatially varying absorption and refractive index on the probe beam propagation dynamics with different probe profiles. The spatial profile of the probe beam at medium entrance is given by

$$g(x, y, 0) = g_0 H_n\left(\frac{\sqrt{2}x}{w_p}\right) H_m\left(\frac{\sqrt{2}y}{w_p}\right) e^{-\frac{\left(x^2+y^2\right)^2}{w_p^2}}, \tag{2.23}$$

where H_n and H_m are the Hermite polynomials of order $\boldsymbol{n}$ and $\boldsymbol{m}$, respectively. Throughout our calculations, we consider probe beam width (w_p) to be 6 μm. We

TH-1819_11612116

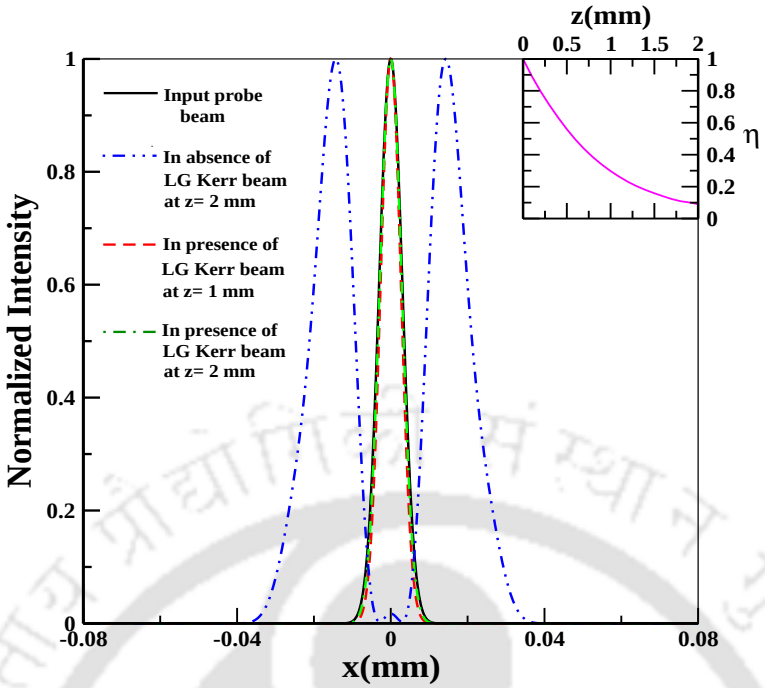

Fig. 2.5 (Color online) A comparison study of narrow probe beam propagation in the absence and presence of LG_0^1 Kerr beams at the output of the vapor cell. The variation of guiding efficiency (η) as a function of propagation distance z is shown in the inset. Other parameters are same as in Fig. 2.2.

consider the propagation of a Gaussian probe beam ($m = 0, n = 0$). We numerically solve Eq. (2.12) using Fourier split step method(FSSM) to study the propagation dynamics of probe beam having different Hermite-Gaussian modes. However, it is necessary to verify the validity of paraxial approximation for a beam having width of a few microns. For this purpose, we use ASRM as shown in Eq. (2.13) to confirm the validity of paraxial approximation. Fig. 2.4 compares the spatial distribution of probe beams, after propagating a distance of 2 mm in free space, which are determined by using FSSM, ASRM, and the analytical expression for paraxial Gaussian beam. It is clear from Fig. 2.4 that the results from FSSM matches exactly with ASRM. Hence, paraxial approximation holds good even for a beam with beam waist $\sim 6\ \mu m$. It is evident that the probe beam width increases to $4w_p$ after propagating a distance of 2 mm through free space. This width broadening of the probe beam can be understood by considering the probe as a superposition of different plane waves. Each plane wave acquires different phase shift during its propagation through space. Hence, the resultant superposition of all the plane waves give rise to the broadening of the beam, at a given distance. Moreover, the broadening of the probe beam can be controlled by manipulating spatially varying refractive index of the medium. Such transverse variation of refractive index can be generated using a suitable control beam as shown in Fig. 2.3 [71]. However, our numerical result shows that the Gaussian control beam

TH-1819_11612116

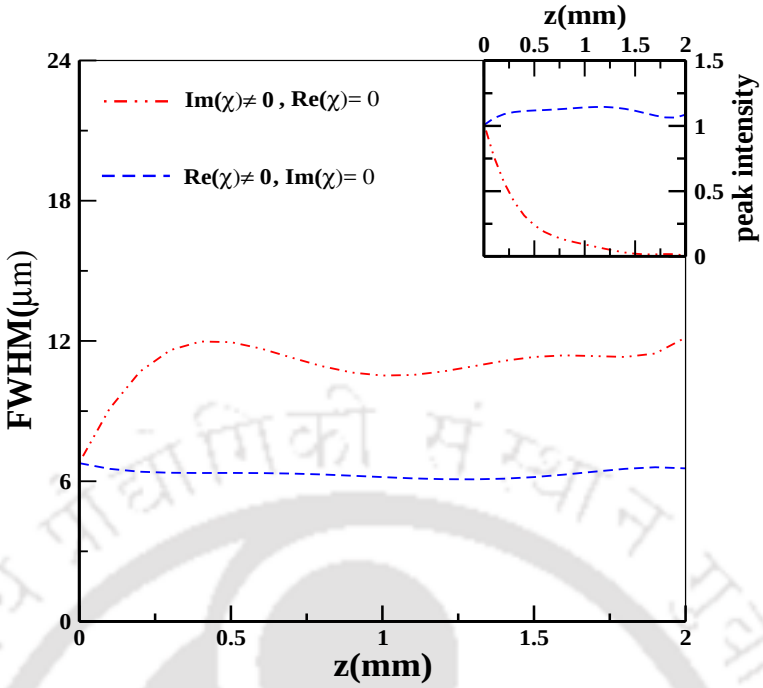

Fig. 2.6 (Color online) Calculated full width half maximum(FWHM) as a function of propagation distance z for two cases, (i) in the presence of transverse variation of only absorption (ii) in the presence of transverse variation of only refractive index. Inset of the above figure displays the propagation length dependent peak intensity. All parameters are same as in Fig. 2.5

is incapable of controlling the spreading of the narrow probe beam as seen in Fig. 2.5 and 2.7. The probe beam suffers severe shape distortion after propagating a distance of 2 mm through the medium due to the presence of low contrast waveguide. The characteristics of the probe beam propagation through the medium drastically changes in the presence of a LG Kerr beam. The shape preserving probe propagation is possible due to the presence of a high contrast waveguide. Now we define the guiding efficiency η as the ratio between output and input powers of the probe beam at a given propagation distance. In the inset of Fig. 2.5, we exhibit the behaviour of guiding efficiency η as a function of the propagation distance. We found the output transmission of the probe is 10% after propagating 2 mm (14 Z_r) through the medium. The main reason for low transmission of the probe beam is due to Kerr field induced absorption. A moderate transmission of narrow probe beam can be made possible by suitably choosing width and intensities of control and Kerr fields which can create a well suited spatial transparency window for probe beam. Note that the condition for minimum absorption of probe beam propagation requires the width of the probe beam to be well contained within the spatial transparency window of the medium.

Next we study the physical mechanism underlying the efficient guiding of narrow probe beam by exploring the individual effect of transverse variation of absorption

TH-1819_11612116

and refractive index on the probe beam propagation. It is evident from Fig. 2.6 that the spatially varying refractive index is able to control the diffraction of the narrow probe beam whereas transverse varying absorption fails to do it. The inset

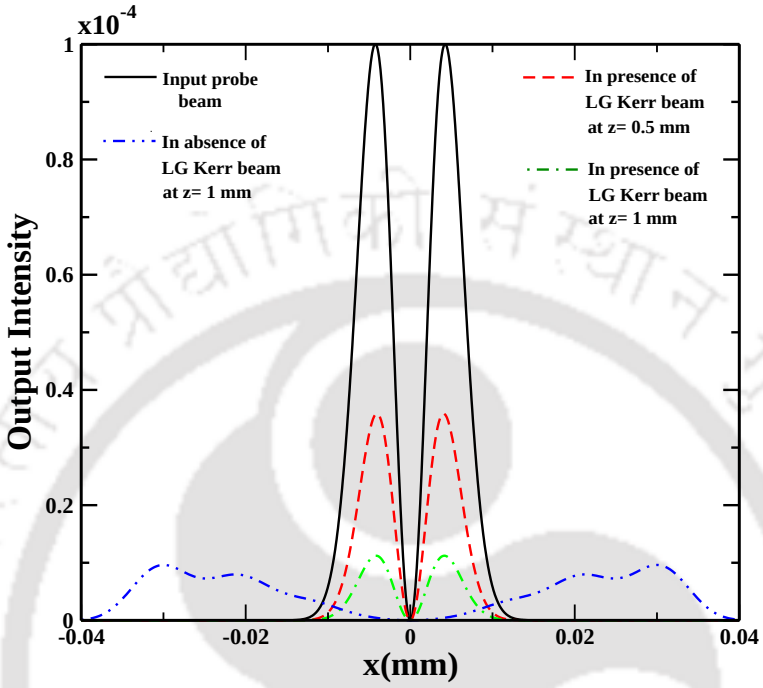

Fig. 2.7 (Color online) Shows the efficient guiding of HG_{10} probe in the presence of LG_0^1 Kerr beam. The output intensity of the probe beam in absence of LG Kerr beam is amplified by a factor of 5 in order to visualize with other three cases. Other parameters are same as in Fig. 2.3, except for $\mathcal{N} = 8 \times 10^{11} atoms/cm^3$, $q = 0.5$ mm, $w_c = 22$ μm, and $w_s = 22$ μm.

of Fig. 2.6 confirms unambiguously that focussing of probe beam is achieved due to spatially varying refractive index. It is clear that the transverse varying absorption is solely responsible for probe beam transmittivity. Therefore, the transverse variation in refractive index plays an important role in controlling the diffractive spreading of narrow probe beam.

Further, we also show diffraction-less propagation of arbitrary modes such as HG_{10} through the medium. Figure. 2.7 shows that HG_{10} mode can propagate upto 1 mm (7 Z_r) without any diffraction. The output transmission for the HG_{10} mode after traversing a propagation length of 1 mm is found to be 10%. We also perform numerical simulations for probe beam profile with other higher order modes of HG, and found shape preserving propagation. Hence, the spatial structure of Kerr beam plays an important role in guiding probe beams, with narrow width and arbitrary modes, to macroscopic propagation lengths.

TH-1819_11612116

2.3 Conclusion

We have demonstrated diffractionless propagation of narrow optical beam through tunable waveguide in a N-type four level system. We have shown how a suitably chosen spatial profile of control and Kerr beams enable us to form a high contrast atomic waveguide. We have also shown that contrast and tunability of the waveguide can be changed by varying the intensity of the LG Kerr beam. Our numerical results reveal a possibility of transferring arbitrary narrow probe image through homogeneously broadened atomic vapor to several Rayleigh lengths.

TH-1819_11612116

TH-1819_11612116

Chapter 3

Structured beam generation in a closed-loop four level atomic system

Laser beams with orbital angular momentum (OAM) have found many applications in quantum information processing [83, 84], atomic manipulation [85, 86], micromanipulation [87] and the biosciences [88]. One of the beams in this class is the Laguerre–Gaussian(LG) beams. Recently Laguerre–Gaussian beams have been used in creation of structured beams. Various techniques for the generation of such beams exists that uses conventional optical components like digital micro-mirror device(DMD) [89], laser resonator [90, 91], axially symmetric polarization element [92], porro-prism [93, 94] and spatial light modulator [95–97]. The key feature in the above techniques is to coherently superpose two LG beam modes with equal but opposite OAM, thus creating a structured beam profile.

Contrary to the above techniques, recently Radwell *et al.* have experimentally demonstrated structured beam generation using a atomic medium [44]. They have used a single phase structured light beam [98] and static magnetic field to form a closed-loop Hanle configuration [99] in a four level atomic system. The relative phase difference between the applied fields can drastically modify the Zeeman coherences of a closed-loop transition [100, 101]. The phase-dependent Zeeman coherence is a basic ingredient in the control of optical dispersion, absorption, and nonlinearity [102–109]. Manipulation of these coherences along the azimuthal plane is the main key behind spatially dependent electromagnetic transparency. Hence, an opaque medium becomes transparent at certain angular positions due to the presence of a phase structured beam. Thus controlling transparency in the transverse direction creates a new avenue for the generation of the structured beam. Radwell *et al.* [44]used a basic theoretical model based on Fermi-golden rule and provided an approximate expression for the periodic variation of the absorption profile to demonstrate how the structured beam can be produced. However to achieve good agreement with experiments, various transverse

TH-1819_11612116

and longitudinal relaxation effects must be incorporated in the propagation dynamics of the light beam with an azimuthally varying polarization and phase structure.
In this chapter, we provide a detailed theoretical explanation for the recent experiments on the generation of structured beams [44], based on full density matrix equations. To facilitate these structured beam generation, we use a homogeneously broadened four level atomic system driven by two orthogonal polarization components of probe beam as shown in Fig. 3.1. In order to create phase-dependent atomic coherences, we use a weak magnetic field to couple the ground states. We start by deriving an analytical expression for the probe susceptibility in the weak field regime. However, numerical solutions of density matrix equations at steady state limits is inevitable to obtain the response of the medium at strong probe field intensities. To illustrate the effect of phase dependent behaviour of the susceptibility on the probe beam propagation, we numerically study paraxial propagation equations. We find that the phase dependent absorption creates petal like structures on the probe beam. The contrast of the generated structured beam can be enhanced by increasing the coupling strength of the lower level magnetic field. Furthermore we study the refractive index profile of two orthogonal polarization components in the presence of strong probe field. A high contrast waveguide and anti-waveguide like structure is achieved unlike in the case of the weak field regime. We exploit these waveguide features to generate a diffraction controlled high contrast petal-like beam structure. Finally we show the rotation of the generated petal-like beam structure due to magneto optical rotation.

3.1 Theoretical Formulations

3.1.1 Model system

The system under consideration is shown in Fig. 3.1 where the electric dipole allowed transitions $|1\rangle \leftrightarrow |4\rangle$ and $|3\rangle \leftrightarrow |4\rangle$ are coupled by two orthogonal polarizations $\hat{\sigma}_+$ and $\hat{\sigma}_-$ of a linearly polarized probe field, respectively. Thus the electric field of x-polarized probe propagation along the z-axis, containing both orthogonal polarizations with carrier frequency ω_p, can be written as

$$\vec{E}(\vec{r},t) = \hat{x}\mathcal{E}(\vec{r})\ e^{-i(\omega_p t - k_p z)} + c.c.\,, \tag{3.1a}$$

$$= (\hat{\sigma}_+\mathcal{E}_+(\vec{r}) + \hat{\sigma}_-\mathcal{E}_-(\vec{r}))\ e^{-i(\omega_p t - k_p z)} + c.c.\,. \tag{3.1b}$$

where $\mathcal{E}_+(\vec{r})$ and $\mathcal{E}_-(\vec{r})$ are the slowly varying envelopes of right and left circularly polarized probe fields, respectively and are defined as $|\mathcal{E}_+(\vec{r})| = |\mathcal{E}_-(\vec{r})| = |\mathcal{E}(\vec{r})|/\sqrt{2}$. The wave number of probe field is denoted by k_p. An arbitrary magnetic field $\vec{B} =$

TH-1819_11612116

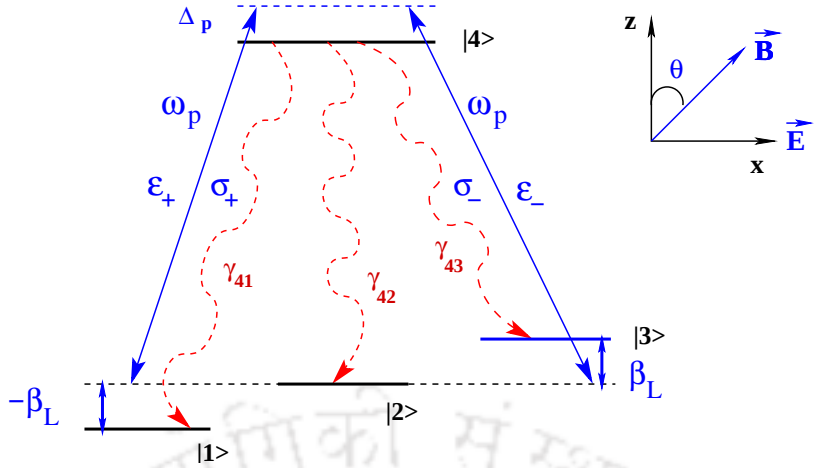

Fig. 3.1 (Color online) Schematic diagram of the four-level closed atomic system. The atomic transitions $|4\rangle \leftrightarrow |3\rangle$ and $|4\rangle \leftrightarrow |1\rangle$ are coupled by left($\hat{\sigma}_-$) and right($\hat{\sigma}_+$) circularly polarized components of the probe field, respectively. The Zeeman sublevels $|1\rangle$, $|2\rangle$, and $|3\rangle$ are coupled by a weak transverse magnetic field $Bsin\theta$ with $\theta << \pi/2$. The radiative decay rates γ_{4i} corresponds to decay from excited state $|4\rangle$ to ground states $|i\rangle$ where $i \in 1, 2, 3$. The direction of probe propagation and the quantization axis is taken along z-axis.

$B(\cos\theta\ \hat{\mathbf{z}} + \sin\theta\ \hat{\mathbf{x}})$ is used to form a closed loop system. Such a closed loop system exhibits interesting phase dependent behaviour of absorption and dispersion. The longitudinal component of the magnetic field $B\cos\theta$ induces the Zeeman shift between the states $|1\rangle$ and $|3\rangle$ whereas the transverse component $B\sin\theta$ redistributes the population among the ground states $|1\rangle$, $|2\rangle$, and $|3\rangle$. This level scheme has been realized experimentally in cold atomic ^{87}Rb vapour where the ground levels $|1\rangle = |5^2S_{1/2}, F = 1, m_F = -1\rangle$, $|2\rangle = |5^2S_{1/2}, F = 1, m_F = 0\rangle$, $|3\rangle = |5^2S_{1/2}, F = 1, m_F = 1\rangle$, and the excited level $|4\rangle = |5^2P_{3/2}, F' = 0, m'_F = 0\rangle$.

We consider the transverse component of the magnetic field to be weaker than the longitudinal component *i.e.*, $\theta << \pi/2$. This condition ensures that the probe polarization doesn't change in the presence of weak transverse magnetic field (TMF), $Bsin\theta$, and the quantization axis remains aligned along the z-axis [110]. Under these assumptions and in the approximations of electric dipole and rotating wave, the Hamiltonian of the system in the presence of probe and magnetic fields takes the following form

$$H = H_0 + H_I + H_B\,, \tag{3.2a}$$

$$H_0 = \hbar\omega_{42}|4\rangle\langle 4|\,, \tag{3.2b}$$

$$\begin{aligned} H_I &= -\hat{D}\cdot\hat{E} \\ &= -\hbar(|4\rangle\langle 1|g_1 e^{-i\omega_p t} + |4\rangle\langle 3|g_2 e^{-i\omega_p t} + \text{H.c.})\,, \end{aligned} \tag{3.2c}$$

$$H_B = g_F\mu_B\hat{F}\cdot\vec{B}$$

TH-1819_11612116

$$=\hbar\beta_L(|3\rangle\langle 3| - |1\rangle\langle 1|) + \hbar\beta_T(|1\rangle\langle 2| + |2\rangle\langle 3| \ + \text{H.c.}), \tag{3.2d}$$

where

$$g_1 = \frac{\vec{d}_+ \cdot \vec{\mathcal{E}}_+}{\hbar} e^{ik_p z} \ \text{ and } \ g_2 = \frac{\vec{d}_- \cdot \vec{\mathcal{E}}_-}{\hbar} e^{ik_p z},$$

are the Rabi frequencies of the probe fields corresponding to the left and right circular polarizations, respectively. The magnitude of Zeeman shift and the coupling strength between the ground levels are given by $\beta_L = \beta_0 \cos\theta$ and $\beta_T = \beta_0 \sin\theta/\sqrt{2}$, respectively. The parameter β_0 is defined as $\beta_0 = g_F \mu_B B/\hbar$ where g_F and μ_B are the Lande g-factor and Bohr magneton, respectively. We use following unitary transformation

$$W = e^{-\frac{i}{\hbar}Ut} \ \text{ where } \ U = \hbar\omega_p |4\rangle\langle 4|,$$

to express the Hamiltonian in the time independent form as given below

$$\begin{aligned} H_I &= WHW^\dagger = \hbar\Delta_p |4\rangle\langle 4| - \hbar\left(g_1 |4\rangle\langle 1| + g_2 |4\rangle\langle 3|\right) \\ &+\hbar\beta_L(|3\rangle\langle 3| - |1\rangle\langle 1|) + \hbar\beta_T(|1\rangle\langle 2| + |2\rangle\langle 3|) + \text{H.c.}, \end{aligned} \tag{3.3}$$

where $\Delta_p = \omega_p - \omega_{42}$ is the probe detuning.

3.1.2 Equations of motion for density matrix elements

We now present the full density matrix formalism to study the experimental work by Radwell *et al.* [44]. The closed loop tripod system possesses various radiative and non-radiative processes. To account for these incoherent decay, we use following the Liouville equation

$$\dot{\rho} = -\frac{i}{\hbar}\left[H_I, \rho\right] + \mathcal{L}\rho\,. \tag{3.4}$$

The second term in Eq.(3.4) represents radiative processes and non-radiative processes that can be determined by

$$\mathcal{L}\rho = \mathcal{L}_r\rho + \mathcal{L}_c\rho \tag{3.5}$$

with

$$\mathcal{L}_r\rho = -\sum_{i=1}^{3} \frac{\gamma_{4i}}{2}\left(|4\rangle\langle 4|\rho - 2|i\rangle\langle i|\rho_{44} + \rho|4\rangle\langle 4|\right),$$

$$\mathcal{L}_c\rho = -\sum_{j=1}^{3}\sum_{j\neq i=1}^{3} \frac{\gamma_c}{2}\left(|j\rangle\langle j|\rho - 2|i\rangle\langle i|\rho_{jj} + \rho|j\rangle\langle j|\right).$$

TH-1819_11612116

The first term of Eq.(3.5) represents radiative decay from excited state $|4\rangle$ to ground states $|i\rangle$, and are labeled by $\gamma_{4i}(i \in 1,2,3)$, whereas the second term represents pure dephasing for the coherence ρ_{ij} due to collision at a rate γ_c. The dynamics of the atomic population and coherences for the closed loop tripod system can be obtained by substituting the effective Hamiltonian (3.3) in the Liouville equation (3.4). Therefore, the following set of Bloch equations can be conveniently written

$$\dot{\rho}_{11} = \gamma_{41}\rho_{44} - i\beta_T\rho_{21} + i\beta_T\rho_{12} + ig_1^*\rho_{41} - ig_1\rho_{14} - 2\gamma_c\rho_{11} + \gamma_c\rho_{22} + \gamma_c\rho_{33}\,, \tag{3.7a}$$

$$\dot{\rho}_{12} = i\beta_L\rho_{12} - i\beta_T(\rho_{22} - \rho_{11}) + i\beta_T\rho_{13} + ig_1^*\rho_{42} - 2\gamma_c\rho_{12}\,, \tag{3.7b}$$

$$\dot{\rho}_{13} = 2i\beta_L\rho_{13} - i\beta_T(\rho_{23} - \rho_{12}) + ig_1^*\rho_{43} - ig_2\rho_{14} - 2\gamma_c\rho_{13}\,, \tag{3.7c}$$

$$\dot{\rho}_{14} = -i(\Delta_p - \beta_L)\rho_{14} - i\beta_T\rho_{24} + ig_1^*(\rho_{44} - \rho_{11}) - ig_2^*\rho_{13} - \Gamma_{41}\rho_{14}\,, \tag{3.7d}$$

$$\dot{\rho}_{22} = \gamma_{42}\rho_{44} - i\beta_T(\rho_{12} - \rho_{21}) - i\beta_T(\rho_{32} - \rho_{23}) + \gamma_c\rho_{11} - 2\gamma_c\rho_{22} + \gamma_c\rho_{33}\,, \tag{3.7e}$$

$$\dot{\rho}_{23} = i\beta_L\rho_{23} - i\beta_T\rho_{13} - i\beta_T(\rho_{33} - \rho_{22}) - ig_2\rho_{24} - 2\gamma_c\rho_{23}\,, \tag{3.7f}$$

$$\dot{\rho}_{24} = -i\Delta_p\rho_{24} - i\beta_T(\rho_{14} + \rho_{34}) - ig_1^*\rho_{21} - \Gamma_{42}\rho_{24} - ig_2^*\rho_{23}\,, \tag{3.7g}$$

$$\dot{\rho}_{33} = \gamma_{43}\rho_{44} - i\beta_T(\rho_{23} - \rho_{32}) + ig_2^*\rho_{43} - ig_2\rho_{34} + \gamma_c\rho_{11} + \gamma_c\rho_{22} - 2\gamma_c\rho_{33}\,, \tag{3.7h}$$

$$\dot{\rho}_{34} = -i(\Delta_p + \beta_L)\rho_{34} - i\beta_T\rho_{24} + ig_2^*(\rho_{44} - \rho_{33}) - ig_1^*\rho_{31} - \Gamma_{43}\rho_{34}\,. \tag{3.7i}$$

The remaining density matrix equations come from the population conservation law $\sum_{i=1}^{4}\rho_{ii} = 1$ and the complex conjugate expressions $\dot{\rho}_{ji} = \dot{\rho}_{ij}^*$. The coherence decay term $\Gamma_{4j}(j \in 1,2,3)$ are expressed as $\Gamma_{41} = \Gamma_{42} = \Gamma_{43} = \gamma_c + \sum_{i=1}^{3}\frac{\gamma_{4i}}{2}$. We assume that the excited state $|4\rangle$ decays to the ground state with equal rates i.e. $\gamma_{41} = \gamma_{42} = \gamma_{43} = \gamma/3$, where γ is the spontaneous decay rate of state $|4\rangle$. Further, we also assume collision rate γ_c of the metastable ground states to be very negligible.

3.1.3 Probe susceptibility of a homogeneous medium

In this section, we calculate the linear response of the probe field in a homogeneous medium. The probe field is to be weak enough to be treated as a perturbation to a system of linear order under steady-state condition. This assumption leads us to get a good agreement of the recent experiment results [44]. The perturbative expansion of the density matrix upto first order of probe field $g_i, (i \in 1,2)$ can be expressed as

$$\rho_{ij} = \rho_{ij}^{(0)} + \frac{g_1}{\gamma}\rho_{ij}^{(+)} + \frac{g_2}{\gamma}\rho_{ij}^{(+)}, \tag{3.8}$$

where, $\rho_{ij}^{(0)}$ is the solution obtained using the counterintuitive approach. The expression for the zeroth order populations and coherences are given in the appendix. The

TH-1819_11612116

second and third terms in Eq.(3.8) denote first-order solutions of the density matrix elements for both orthogonal polarizations at positive probe field frequency ω_p. We now substitute Eq. (3.8) in Eqs (3.7) and equate the coefficients of g_1 and g_2. As a result, we obtain two sets of 12 coupled linear equations. Next, we solve these algebraic equations to derive the atomic coherences $\rho_{41}^{(+)}$ and $\rho_{43}^{(+)}$. The off-diagonal density matrix elements $\rho_{41}^{(+)}$ and $\rho_{43}^{(+)}$ determine the linear susceptibility χ_{41} and χ_{43} of the medium at frequency ω_p respectively. Hence the medium polarization induced by the probe field can be expressed as

$$\chi_{41}(\Delta_p) = \frac{\mathcal{N}|d_+|^2}{\hbar\gamma}\rho_{41}^{(+)}\,, \tag{3.9a}$$

$$\chi_{43}(\Delta_p) = \frac{\mathcal{N}|d_-|^2}{\hbar\gamma}\rho_{43}^{(+)}, \tag{3.9b}$$

with

$$\rho_{41}^{(+)} = \frac{N_1}{D} + \beta_T^2\frac{N_2}{D}\frac{g_2}{g_1}\,, \tag{3.10}$$

$$\rho_{43}^{(+)} = \frac{N_3}{D} + \beta_T^2\frac{N_2}{D}\frac{g_1}{g_2}\,, \tag{3.11}$$

where

$$\begin{aligned} N_1 =&\beta_L^2(\Delta_p + i\Gamma_{41})(\Delta_p + i\Gamma_{41} + \beta_L)\rho_{11}^{(0)} + \beta_T^4(2\rho_{11}^{(0)} - \rho_{22}^{(0)}) - \beta_T^2(\rho_{11}^{(0)}(\Delta_p + i\Gamma_{41})^2 \\ &+ \beta_L\rho_{22}^{(0)}(\Delta_p + i\Gamma_{41} + \beta_L))\,, \end{aligned} \tag{3.12}$$

$$N_2 = (\Delta_p + i\Gamma_{41})^2(\rho_{11}^{(0)} - \rho_{22}^{(0)}) + \beta_L^2\rho_{22}^{(0)} - \beta_T^2(2\rho_{11}^{(0)} - \rho_{22}^{(0)})\,, \tag{3.13}$$

$$\begin{aligned} N_3 =&\beta_L^2(\Delta_p + i\Gamma_{41})(\Delta_p + i\Gamma_{41} - \beta_L)\rho_{11}^{(0)} + \beta_T^4(2\rho_{11}^{(0)} - \rho_{22}^{(0)}) - \beta_T^2(\rho_{11}^{(0)}(\Delta_p + i\Gamma_{41})^2 \\ &+ \beta_L\rho_{22}^{(0)}(\Delta_p + i\Gamma_{41} - \beta_L))\,, \end{aligned} \tag{3.14}$$

$$D = (\beta_L^2 - \beta_T^2)(\beta_L^2 + 2\beta_T^2 - (\Delta_p + i\Gamma_{41})^2)(\Delta_p + i\Gamma_{41})$$

$$\rho_{11}^{(0)} = (\frac{\beta_T}{\beta_L})^2\,, \tag{3.15}$$

$$\rho_{22}^{(0)} = 1 - 2(\frac{\beta_T}{\beta_L})^2\,. \tag{3.16}$$

Here $\mathcal{N}$ is the atomic density of the medium. The influence of transverse magnetic field on the steady state population in absence of the probe field is clearly seen from Eqs.(3.15) and (3.16). The phase dependent response of the medium can be explored by considering the spatial inhomogeneity of the probe field. Thus the spatial structure of the probe field for two orthogonal polarizations can be expressed as

$$g_1(\vec{r}) = g(r,z)e^{il\phi}\,, \tag{3.17}$$

TH-1819_11612116

$$g_2(\vec{r}) = g(r,z)e^{-il\phi}\,, \tag{3.18}$$

where l, ϕ and $g(r,z)$ represents OAM, phase and transverse variation of the probe beam at a given distance z, respectively. The phase dependent susceptibilities of the closed loop tripod system is given as

$$\chi_{41} = \frac{\mathcal{N}|d_+|^2}{\hbar\gamma}\left(\frac{N_1}{D} + \beta_T^2 e^{-2il\phi}\frac{N_2}{D}\right), \tag{3.19}$$

$$\chi_{43} = \frac{\mathcal{N}|d_-|^2}{\hbar\gamma}\left(\frac{N_3}{D} + \beta_T^2 e^{2il\phi}\frac{N_2}{D}\right). \tag{3.20}$$

The above analytical expressions of the susceptibilities for the transitions $|1\rangle \leftrightarrow |4\rangle$ and $|3\rangle \leftrightarrow |4\rangle$ display an insight on the physics behind the formation of structured beam profile. The transverse magnetic field β_T, OAM l and transverse phase ϕ plays a crucial role in the manipulation of the optical properties of closed loop tripod systems. We adopt Gauss-Jordan elimination method to solve linear algebraic Eq. (3.7) numerically at steady-state condition of the density matrix for a probe field at higher intensities limits.

3.1.4 Beam propagation equations

In order to investigate the effect of azimuthally varying susceptibilities on both left and right polarized components of the probe beam, we use Maxwell's wave equations under slowly varying envelope and paraxial wave approximations. The dynamics of the orthogonal polarization components with Rabi frequencies g_1 and g_2 propagating along the z-direction can be expressed in the following form:

$$\frac{\partial g_1}{\partial z} = \frac{i}{2k_p}\left(\frac{\partial^2}{\partial x^2} + \frac{\partial^2}{\partial y^2}\right) g_1 + 2i\pi k_p \chi_{41}\, g_1\,, \tag{3.21a}$$

$$\frac{\partial g_2}{\partial z} = \frac{i}{2k_p}\left(\frac{\partial^2}{\partial x^2} + \frac{\partial^2}{\partial y^2}\right) g_2 + 2i\pi k_p \chi_{43}\, g_2\,. \tag{3.21b}$$

The terms within the parentheses on the right hand side of Eq. (3.21a) and Eq. (3.21b) are account for transverse variation of the probe beam. These terms responsible for the diffraction either in the medium or in free space. The second terms on the right-hand side of Eq. (3.21a) and Eq. (3.21b) leads to the dispersion and absorption of the probe beam.

TH-1819_11612116

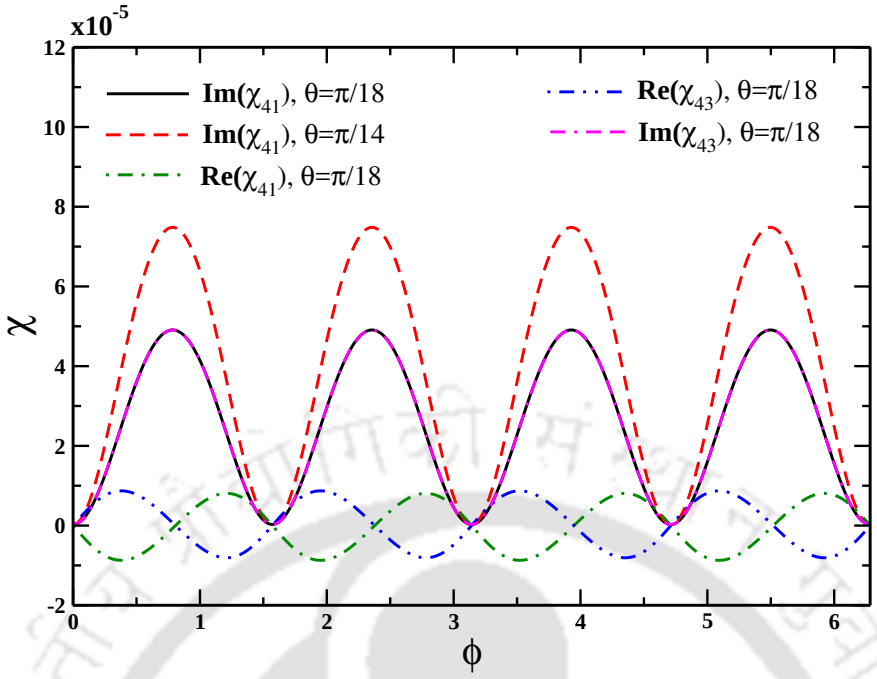

Fig. 3.2 (Color online) Real and imaginary parts of susceptibilities χ_{41} and χ_{43} as functions of phase for different θ are plotted. The parameters are chosen as $\mathcal{N} = 2 \times 10^{11} atoms/cm^3$, $\Gamma_{41} = 0.5\gamma$, $\Delta_p = 0$, $\beta_0 = 0.01\gamma$, $\gamma_c = 10^{-7}\gamma$, $g_0 = 0.01\gamma$ and $l = 2$.

3.2 Results and Discussions

3.2.1 Phase dependent susceptibility

We first study the effect of azimuthal phase on the absorption of two orthogonal polarization components $\hat{\sigma}_\pm$ of the probe field at weak intensity regime. The phase dependent susceptibilities χ_{41} and χ_{43} can be explored by considering the amplitude of both the polarization components to be continuous wave with $g_i(r, z = 0) = g_0 = 0.01\gamma, (i \in 1, 2)$. We assume the collisional decay term γ_c is very negligible to be consistent with the experimental results for the cold atomic system [44]. The absorption of right- and left-handed circular polarizations χ_{41} and χ_{43} are plotted against the azimuthal phase as shown in Fig. 3.2. Results are presented in Fig. 3.2 for two different intensities of magnetic field. From Fig. 3.2, we find that the absorption at the $\hat{\sigma}_+$ transition oscillates periodically. The periodic variation of this absorption can be well explained by considering the perturbative expression for the susceptibility as mentioned in Eq. (3.19). The term associated with the second fraction in the round bracket of Eq. (3.19) leads to phase dependent response of the medium. The $2l$ factor in the exponential term decides the number of transparency windows that can be formed within a period. It is clear from Fig. 3.2 that OAM $l = 2$ creates 4 transparency windows. The narrowing of the transparency window is a key mechanism to

TH-1819_11612116

generate the high contrast periodic absorption structures. It is evident from Fig. 3.2 that the sharp variation of transparency windows can be achieved by increasing θ value. The increment of θ returns the strength of TMF β_T at higher values that leads to an increase in the population of the ground states $|1\rangle$, and $|3\rangle$ as shown by the Eqs.(3.15) and (3.16). As a result, each polarization component suffer more absorp-

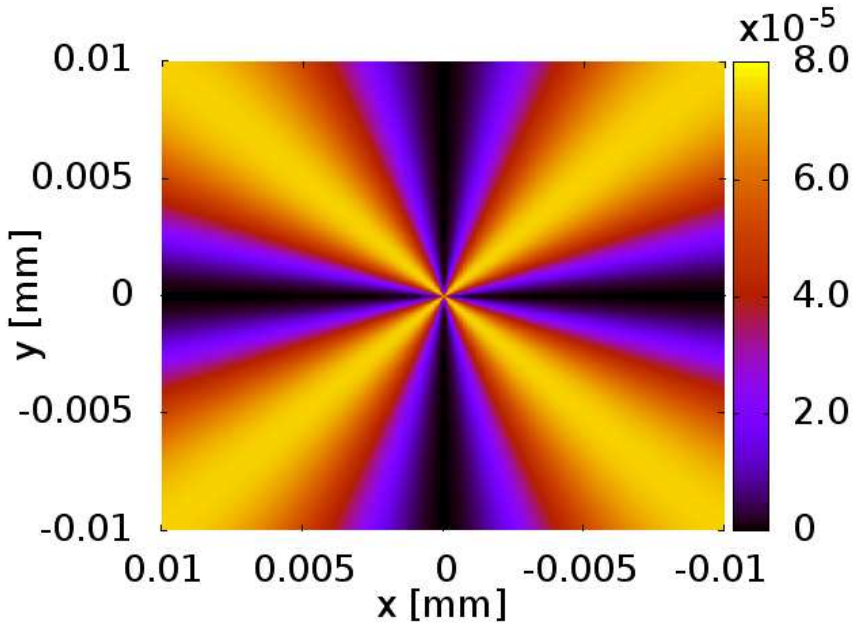

Fig. 3.3 (Color online) Absorption pattern of the $\hat{\sigma}_+$ polarization component is plotted against the two orthogonal axes x and y. Other parameters are same as in Fig. 3.2.

tion due to the narrowing of the transparency window. Hence the strength of TMF and the azimuthal phase plays an important role in creating a high contrast periodic absorption structure for the probe field. Note that the absorption of the left-handed polarization $\hat{\sigma}_-$ is identical to the absorption of the right-handed polarization $\hat{\sigma}_+$ at $\Delta_p = 0$ as shown in Fig. 3.2. The absorption of both circularly polarized components constitute the structure of the probe absorption. The phase dependent absorption structure is a result of the coupling among the degenerate ground states by a weak magnetic field. The degeneracy between the ground states $|i\rangle, (i \in 1, 2, 3)$ can be lifted in the presence of a longitudinal magnetic field β_L. The probe resonance condition $\Delta_p = 0$ facilitates the red and blue shifted detuning by an amount of β_L for each circularly polarized component. Thus the refractive index profile for $\hat{\sigma}_+$ component varies oppositely as the refractive index profile for $\hat{\sigma}_-$ component with a very small magnitude as shown in Fig. 3.2. This reverse nature of refractive index for both polarization components failed to resemble the wave-guided structure inside the medium. Hence the created structure of the probe beam suffers distortion due to diffraction. In Fig. 3.3, we show the surface plot of χ_{41} as a function of transverse directions x and y.

TH-1819_11612116

Two orthogonal axes x and y can be used to define azimuthal phase $\phi = \tan^{-1}(y/x)$. It can be seen from Fig. 3.3 that the medium becomes transparent at some specific angular positions for the right-handed polarization. These angular positions can be defined by $n\pi/l$ where n can change from 0 to l. As a result of angular dependency, the absorption profile for the right-handed polarization shows fourfold symmetry with OAM, $l = 2$. A similar periodic absorption pattern is exhibited by the left-handed circularly polarized component as mentioned in Eq. (3.20). Note that in absence of phase modulation, both polarization components suffer from high attenuation. Thus at weak field limits, in a closed loop tripod system, the phase information of each polarization component gets converted into the intensity information that renders transparent an otherwise opaque medium. We now discuss the response of the medium

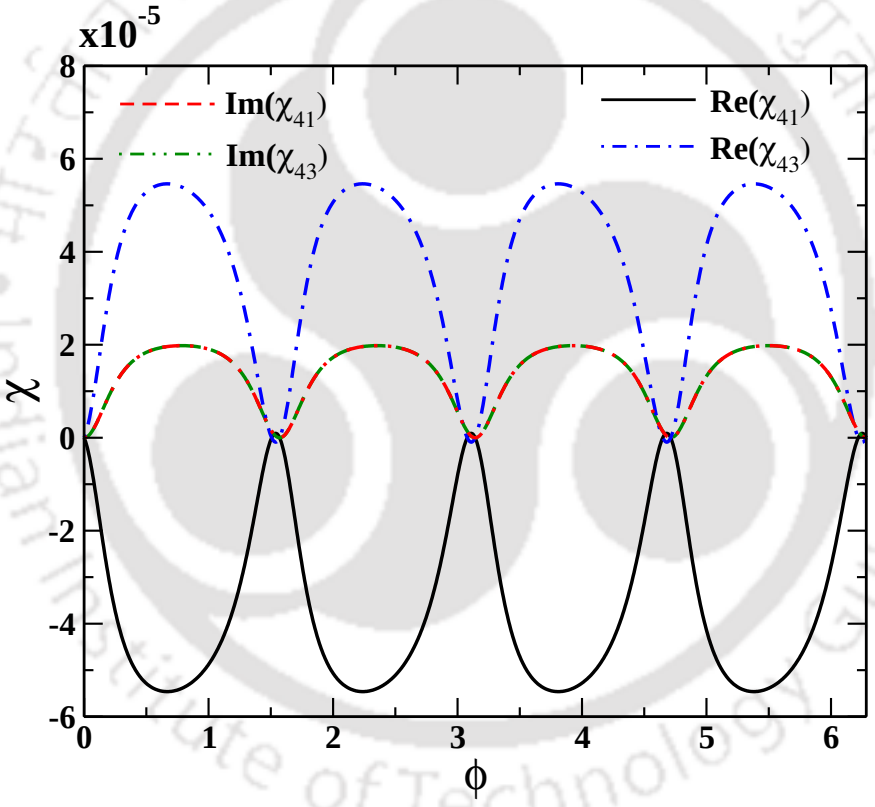

Fig. 3.4 (Color online) The variations of real and imaginary parts of susceptibilities χ_{41} and χ_{43} as functions of phase for relatively strong probe regime are plotted. The parameters are chosen as $\mathcal{N} = 2 \times 10^{11} atoms/cm^3$, $\Gamma_{41} = 0.5\gamma$, $\Delta_p = 0$, $\beta_0 = 0.01\gamma$, $\theta = \pi/14$, $\gamma_c = 10^{-7}\gamma$ and $l = 2$.

beyond the weak field limits as shown in Fig.(3.4). For a relatively strong probe field limit $g_0 = 0.1\gamma$, the numerical solutions of linear algebraic equations Eqs. (3.7) are inevitable to analyze the phase dependent susceptibility of the medium at steady state condition. The oscillating amplitude of polarization components reduces with increase in g_0. As a consequence the population in the ground states $|1\rangle$, and $|3\rangle$ gets depleted.

TH-1819_11612116

The depletion of population in these ground states is the cause of width-broadening of the transparency window. Surprisingly the refractive index profile of two orthogonal polarization components modify drastically as compared to the case in a weak field regime. It is evident from Fig. 3.4 that the gradient of refractive index is dependent on the detuning sign of polarization components. The slope of the refractive index attains its maximum around the transparency window and decreases gradually towards the wings for a red detuned right circular polarization component. A convex lens like refractive index is formed for the red shifted polarization component whereas concave lens like refractive index is experienced by the blue shifted polarization component. Thus by selecting detuning of two orthogonal polarizations $\hat{\sigma}_{\pm}$, leads to the formation of a waveguide [111] and an anti-waveguide [112] in the closed loop tripod system. Hence these waveguide/antiwaveguide structures can lead to focusing/defocusing of polarization components. These features are missing for the weak intensity limits as the susceptibilities are independent of polarization amplitude as shown in Eq. (3.19). Also the amplitude of the refractive index is stronger here than in the weak field limits. Hence a suitable choice of detuning of each polarization component at the strong field regime can lead to diffraction controlled petal like structured beam generation.

3.2.2 Formation of structured beam patterns

Next we illustrate how spatially dependent susceptibility enables us to generate the structured probe beam. For this purpose, the transverse spatial profile of both the polarization components is to be in the Laguerre-Gaussian mode that can be written as

$$\begin{aligned} g_j(r,\phi,z) =& g_0 \times \frac{w_p}{w(z)} \times \left(\frac{r\sqrt{2}}{w(z)}\right)^{|l|} L_m^l\left(\frac{2r^2}{w^2(z)}\right) \times e^{\pm il\phi} \\ & e^{-\left(\frac{r^2}{w^2(z)}\right)} e^{\left(\frac{ikr^2}{2R(z)}\right)} e^{-i(2m+l+1)\tan^{-1}\left(\frac{z}{z_0}\right)} \\ r =& \sqrt{x^2+y^2} \\ \phi =& \tan^{-1}\left(\frac{y}{x}\right). \end{aligned} \tag{3.22}$$

The indices m determine the shape of the probe field profile along the transverse directions. The radius of curvature and the Rayleigh length are defined as $R(z) = z+(z_0^2/z)$, and $z_0 = \pi w_p^2/\lambda$, respectively. The beam width is varied with propagation distance z as $w(z) = w_p\sqrt{1+(z/z_0)^2}$, where, w_p is the beam waist at $z = 0$ [113]. We adopt higher ordered split-step operator method to numerically study the beam propagation Eq. (3.21). Fig. 3.5 shows the output intensity pattern of the probe beam at a propagation distance of 0.5 mm. Since the left and right-handed polarization compo-

TH-1819_11612116

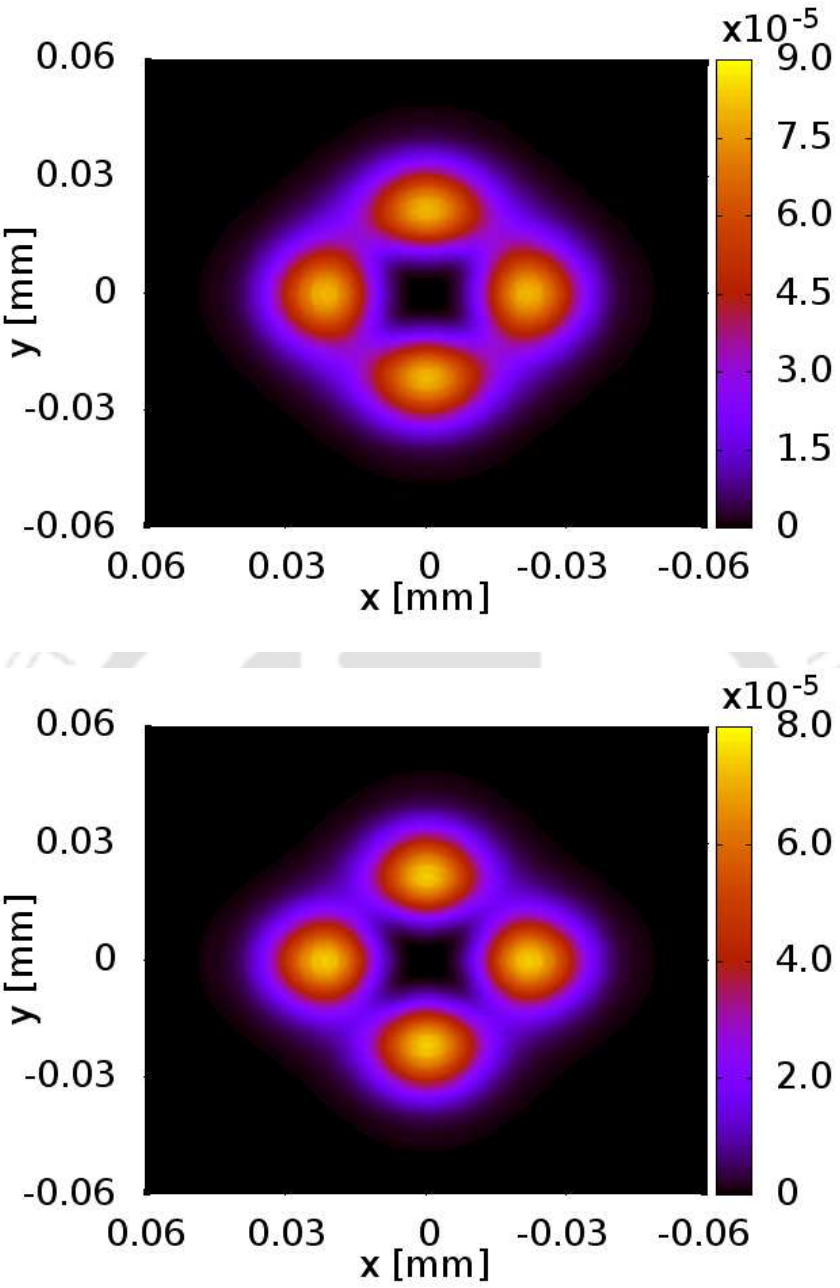

Fig. 3.5 (Color online) Panel (a) and (b) depict transmitted probe beam intensities in the transverse $(x-y)$ plane for $\theta = \pi/18$ and $\pi/14$, respectively. The intensity profiles of the probe beam is shown in panels (a) and (b) after the probe field components have traversed a distance of medium length 0.5 mm. The mode, OAM and waist of the Laguerre-Gaussian beam are $m = 0$, $l = 2$ and $w_p = 20$ μm, respectively at $z = 0$. Other parameters are same as in Fig. 3.2.

nents are orthogonal to each other, therefore the output intensity can be expressed as $I_{out} = |g_1|^2 + |g_2|^2$. It is evident from Fig. 3.5 that the fourfold symmetry which exists in the absorption profile of both the polarization components are mapped onto their transverse spatial profile. Also this spatial profile assures that each polariza-

TH-1819_11612116

tion component carries OAM with units of $\pm 2\hbar$. Thus the value of OAM dictates the formation of structured probe beam with desired shape. Hence manipulation of the absorption profile along the transverse direction forms the key idea behind the structured probe beam generation. We also find that the transmission for the probe beam at a propagation distance of 0.5 mm is 60% for $\theta = \pi/18$ and 49% for $\theta = \pi/14$ even at weak field limits. We further study how the magnetic field strength allows us to enhance the contrast of the structured beam. A higher strength β_T creates a high contrast periodic absorption profile as compared with a weak β_T as shown in Fig. 3.2. This sharp variation of absorption profile emulates a high contrast spatial probe beam profile as depicted in Fig. 3.5(b). On the other hand, Fig. 3.5(a) shows a low contrast spatial probe beam for the weak field regime at a propagation distance of $z = 0.5$ mm. Thus the contrast enhancement of the structured beam is possible by using a suitable magnetic field strength. We next study the effect of nonlinear susceptibility

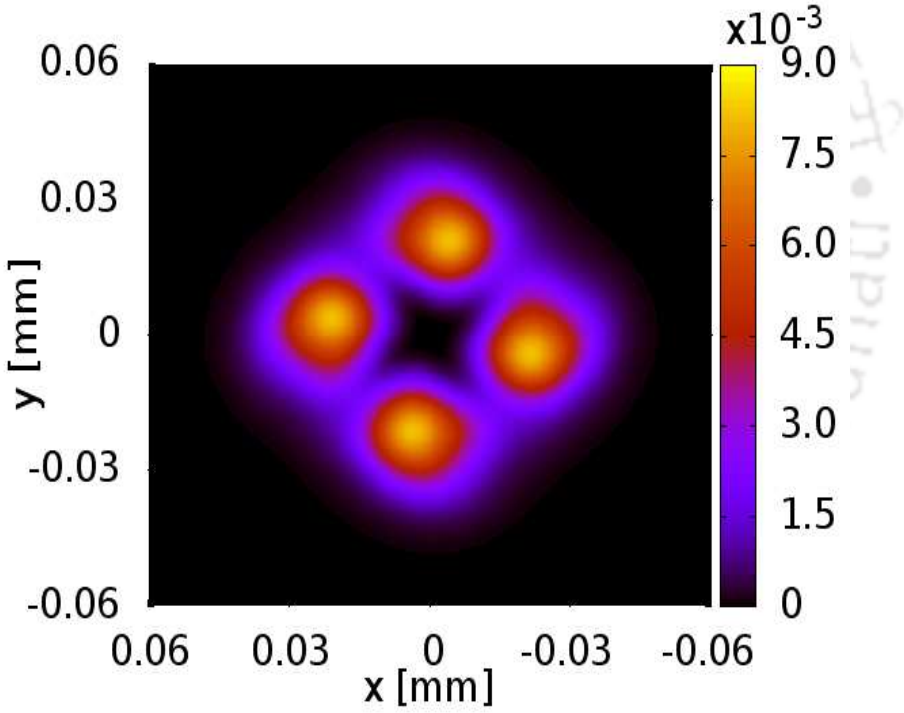

Fig. 3.6 (Color online) Intensity variation of the probe field in transverse $(x - y)$ plane, after a 0.5 mm length of propagation. The initial amplitude, mode, OAM and waist of the Laguerre-Gaussian beam are $g_0 = 0.1\gamma$, $m = 0$, $l = 2$ and $w_p = 20\mu$m, respectively. Other parameters are same as in Fig. 3.4.

on the spatial evolution of the probe beam envelope. As seen from Fig. 3.6, the output pattern of the probe intensity bears the same four-fold symmetric patterns as in the weak field case. However, the contrast and rotation of the patterns are changed significantly as compared to the later. Fig. 3.4 exhibits the waveguide and anti-waveguide

TH-1819_11612116

refractive index profile for the constituents of the probe beam at $\Delta_p = 0$, which enhances the contrast of the output pattern. The waveguide structure confine the σ_+ polarization component whereas the σ_- polarization component gets defocused due to the anti-waveguide structure. Moreover, the spreading of both the polarization components in the azimuthal plane is limited by the width of the spatial transparency window. Hence at the strong regime both absorption and dispersion profiles play important roles in improving the output beam pattern whereas the absorption profile is solely responsible in the weak field case. The transmission of the structured beam at a propagation distance of 0.5 mm. is found to be 55%. The increase in beam transmission is due to waveguide induced focusing of the probe beam in the azimuthal plane. We also notice from Fig. 3.6 that the generated structure beam is rotated by an angle of 10°. This rotation is attributed to strong field induced NMOR. The rotation of the structured beam can be enhanced by increasing the intensity of the probe and the magnetic field strengths [114]. Our approach opens up new possibilities for generating high contrast structured beam in other closed loop systems that display narrow EIT resonances. The steep variation of refractive index around the narrow transparency window is the main reason behind the formation of high contrast beams. Thus an atomic medium with buffer gas [115] and inhomogeneously broadened atomic system [116] may be suitable candidates for creating a diffraction controlled high contrast structured beam.

3.3 Conclusion

In conclusion, we have studied the generation of structured beam in a cold ^{87}Rb atomic vapor. For this purpose, a phase dependent transparency is prepared in a closed loop tripod system tailored with a phase structured probe beam and a TMF. In the presence of the TMF, the absorption of both weak and strong fields oscillates periodically in the azimuthal plane. However, a waveguide and anti-waveguide like refractive index features are formed for the later case. Such a periodic variation of medium absorption and refractive index are responsible for the creation of a high contrast structured beam. By numerically solving the propagation equations, we confirm the formation of petal like beam structure for both weak and strong field cases. Interestingly, the features of the generated structured beam is enhanced with high transmittivity at strong field limits. Further, increasing the amplitudes of the phase structured beam and TMF can lead rotation of the petal beam structure due to NMOR.

TH-1819_11612116

3.4 Appendix

In general, when external laser and magnetic fields are absent, the entire population is equally distributed among the ground states i.e., $\rho_{11}^{(0)} = \rho_{22}^{(0)} = \rho_{33}^{(0)} = 1/3$ under the thermal equilibrium condition [114]. However in the presence of external laser and magnetic fields, the population distribution among the ground states are very different from the above. In order to study the population distribution among the ground states of the closed-loop four-level system, we solve the density matrix Eq.(3.7) in transient domain as well as steady state limit. In transient domain, we study the behavior of atomic population and coherences by solving full density matrix Eq.(3.7) by using Runge Kutta method. We notice from Fig.3.7 that the population reaches a steady

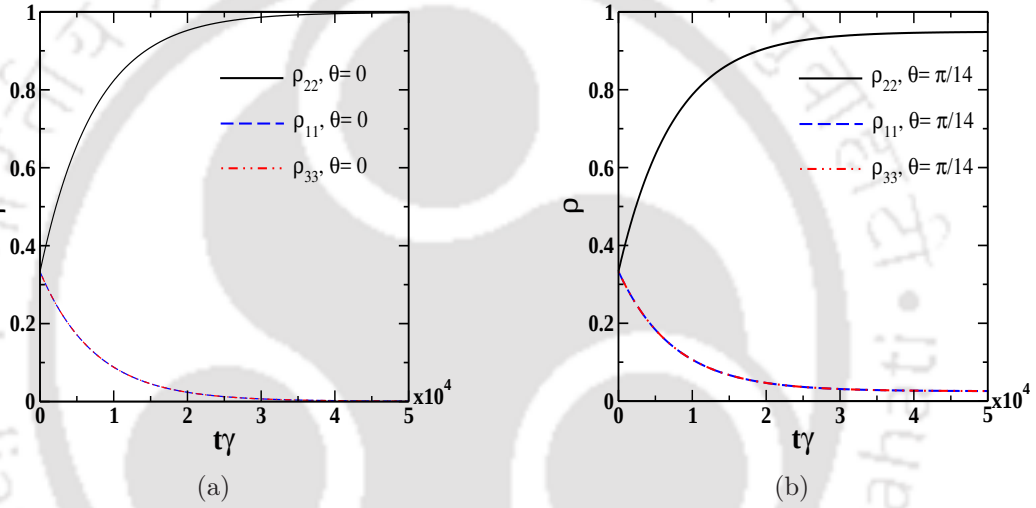

Fig. 3.7 Evolution of population with time (a) in absence of TMF, (b) in presence of TMF. The parameters are chosen as $\Gamma_{41} = 0.5\gamma$, $\Delta_p = 0$, $\beta_0 = 0.01\gamma$, $\gamma_c = 10^{-7}\gamma$, and $g_2 = g_1 = 0.01\gamma$.

Table 3.1 The value of the atomic populations in the long time interaction limit

	$\theta = 0$	$\theta = \pi/14$
ρ_{11}	0.0008	0.025
ρ_{22}	0.9984	0.95
ρ_{33}	0.0008	0.025

value after a certain time ($\gamma t >> 1$). In the absence of TMF, all the population is in state $|2\rangle$ and almost zero population are in state $|1\rangle$ and $|3\rangle$ as shown in Fig.3.7(a). With the application of TMF, the population gets transferred from state $|2\rangle$ to state $|1\rangle$ and $|3\rangle$ as in Fig.3.7(b). The numerical values of the population distribution in presence and absence of TMF are shown in Table 3.1.

Next we study exact response of the atomic population and coherences at the steady

TH-1819_11612116

state limit. Under steady state condition, the time derivative of density matrix is equal to zero, *i.e.,* $\dot{\rho}_{ij} = 0$. The exact response of the medium can be obtained by solving the linear algebraic Eq.(3.7) with use of Gauss-Jordan elimination method, both in presence and absence of TMF. We observe from Table 3.1 and 3.2 that the

Table 3.2 The value of the atomic populations in the steady state limit

	$\theta = 0$	$\theta = \pi/14$
ρ_{11}	0.0008	0.025
ρ_{22}	0.9984	0.95
ρ_{33}	0.0008	0.025

value of atomic population in both steady state limit and long time interaction limit are same. The population are redistributed among the ground states depending upon the strength of TMF as shown in Fig.3.7(a) and Fig.3.7(b).
It is well understood from Fig.3.7(a) that in the absence of TMF all the population are in state $|2\rangle$ *i.e.,* $\rho_{11} = \rho_{33} = 0, \rho_{22} = 1$ at resonant probe configuration. However we consider a model system where probe field and magnetic field are turned on in the counterintuitive sequence. Therefore this counterintuitive sequence leads to

Table 3.3 The value of the atomic populations estimated using the counterintuitive approach

	$\theta = 0$	$\theta = \pi/14$
ρ_{11}	0.0	0.026
ρ_{22}	1.0	0.948
ρ_{33}	0.0	0.026

redistributed the population among the ground states which can be estimated from Eq.(3.7) and are given as

$$\rho_{11}^{(0)} = \rho_{33}^{(0)} = (\frac{\beta_T}{\beta_L})^2 , \tag{3.23}$$

$$\rho_{22}^{(0)} = 1 - 2(\frac{\beta_T}{\beta_L})^2 , \tag{3.24}$$

$$\rho_{12}^{(0)} = \rho_{21}^{(0)} = \frac{\beta_L \beta_T (\rho_{22}^{(0)} - \rho_{11}^{(0)})}{\beta_L^2 - \beta_T^2} , \tag{3.25}$$

$$\rho_{13}^{(0)} = \rho_{31}^{(0)} = -\frac{\beta_T^2 (\rho_{22}^{(0)} - \rho_{11}^{(0)})}{\beta_L^2 - \beta_T^2} , \tag{3.26}$$

$$\rho_{23}^{(0)} = \rho_{32}^{(0)} = -\frac{\beta_L \beta_T (\rho_{22}^{(0)} - \rho_{11}^{(0)})}{\beta_L^2 - \beta_T^2} . \tag{3.27}$$

Now we treat these values of population and coherences as the zeroth order solutions and proceed further to find the first order solution of the probe field. We adopt

TH-1819_11612116

these perturbation approximation method in order to mimic the behaviour shown by the closed system in the steady state limit. We can see from Table 3.3 that all the populations are in state $|2\rangle$ in absence of TMF, which is consistent with the steady state and the transient solutions. Also we notice that for $\theta = \pi/14$, the population distribution is same for all the three cases i.e., the steady state limit, transient solution and the perturbative approach. Hence we can safely assume that our perturbative approach is correct and can be used to study the dynamics of the closed system.

TH-1819_11612116

TH-1819_11612116

Chapter 4

Control and manipulation of structured beam in atomic vapors

Generation of structured beams have gained a lot of momentum in recent years owing to their immense application in optical micromanipulation [117], quantum information processing [118], microtrapping and alignment [119–122], biosciences [123], etc. Recently Radwell *et al.* have experimentally demonstrated a new technique to create structured beam using an atomic medium [44]. In the experiment, they considered a cold rubidium system in closed-loop Hanle configuration, driven by a structured probe and a TMF. The presence of TMF along with a phase structured probe induces a phase dependent atomic coherences. Such phase dependent coherences(PDCs) are the key to creation of petal like beam structures. Later on Sharma and Dey [124] theoretically explained the formation of structured beam in this closed-loop Hanle configuration based on PDCs. They extensively showed that the PDCs induces periodic variation of absorption in the azimuthal plane. The periodic variation of absorption creates transparency window at various azimuthal position. Presence of such azimuthal transparency windows forms the key factor in generation of structured beams. Further, they also showed that by controlling the strength of both TMF and the probe the spatial characteristics of the structured beam can be modulated. Moreover, the absorption in the azimuthal plane can also be modified by a strong control field. Manipulation of medium absorption in the transverse direction using a spatial dependent control field have been used as a major tool in controlling diffraction [21, 20, 26, 19, 125], cloning of images [68, 69, 25], beam steering and splitting [23–25], atom localization [126–128], etc. Further, a spatial dependent control field allows transformation of information from selective spatial position onto probe beam [71–73]. Hence manipulating the PDCs using a spatial dependent control field can play a major role in controlling the spatial features of the structured beam.

TH-1819_11612116

In this chapter, we present an interesting method to create various structured beam patterns based on phase dependent atomic dynamics in closed-loop five level system as shown in Fig. 4.1. To facilitate this process, we employ a phase structured probe and a control field to drive the atomic system. Further, a transverse magnetic field is used to couple the ground states. We then derive an analytical expression for the medium susceptibility in the steady state limit for a weak probe field. In presence of phase structured probe and a TMF, the medium absorption oscillates periodically in the azimuthal plane. Such variation in the medium absorption is the key to formation of structured beams. Next, we investigate the effect of the spatially varying control field on the medium susceptibility. We find that the control field creates transparency window at specific spatial position depending on its spatial structure. Modulation of oscillating absorption by control induced transparency result in creation of phase dependent asymmetric absorption profile for the probe. To discern the effect of asymmetric phase dependent susceptibility on the probe beam propagation, we numerically solve the paraxial beam propagation equations. Our numerical results on beam propagation shows the dependence of the formed structured pattern on the control beam profile. Different control beam structures creates structured beam with different petal forms. Formation of various structured beam types have major application in trapping, manipulation and characterization of different biological cells [129].

4.1 Theoretical Formulations

4.1.1 Model

In this work, we consider an inverted Y-type five level atomic system consisting of two excited states $|5\rangle$ and $|4\rangle$ and three metastable states $|1\rangle$, $|2\rangle$, and $|3\rangle$ as shown in Fig.4.1. This level scheme can be experimentally realized in ^{87}Rb vapour where the ground levels $|1\rangle = |5^2S_{1/2}, F = 1, m_F = -1\rangle$, $|2\rangle = |5^2S_{1/2}, F = 1, m_F = 0\rangle$, $|3\rangle = |5^2S_{1/2}, F = 1, m_F = 1\rangle$, and the excited level $|4\rangle = |5^2P_{3/2}, F^{'} = 0, m_F^{'} = 0\rangle$, and $|5\rangle = |5^2D_{5/2}, F^{''} = 1, m_F^{''} = 0\rangle$. The atomic transition $|4\rangle \leftrightarrow |5\rangle$ is coupled by a strong control field, whereas the remaining transitions $|4\rangle \leftrightarrow |3\rangle$ and $|4\rangle \leftrightarrow |1\rangle$ are coupled by $\hat{\sigma}_-$ and $\hat{\sigma}_+$ polarized components of the probe field, respectively. The electric field expression corresponding to both probe and control fields propagating along the z-axis, can be written as

$$\vec{E}(\vec{r}, t) = \vec{E}_p(\vec{r}, t) + \vec{E}_c(\vec{r}, t) \tag{4.1}$$

TH-1819_11612116

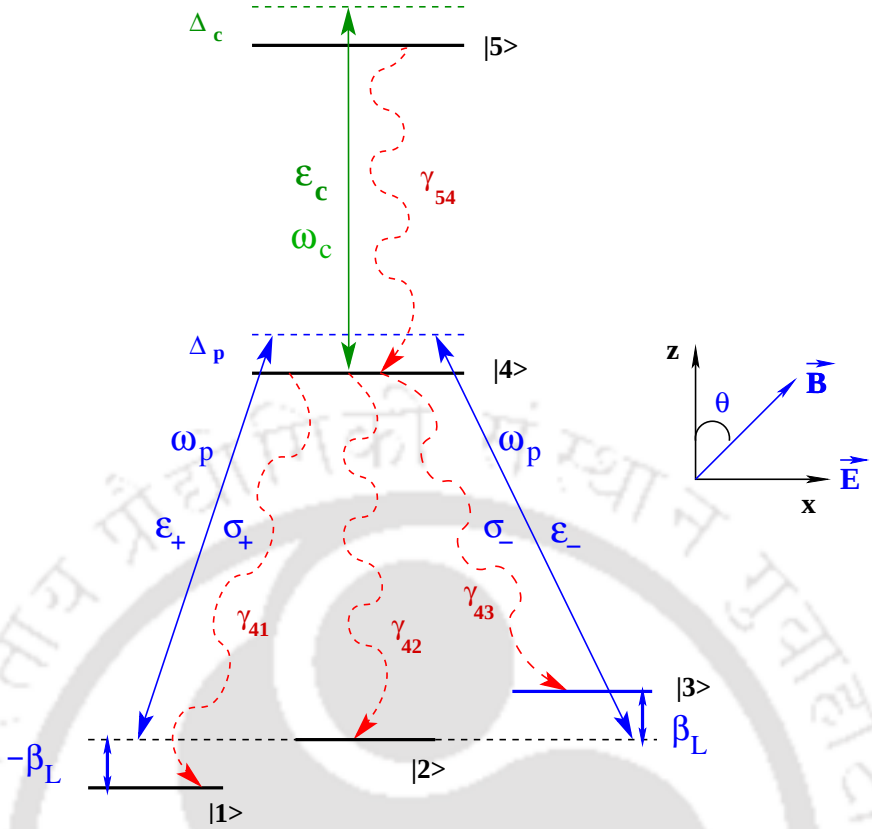

Fig. 4.1 (Color online) Schematic diagram of the proposed model system. A control field with frequency ω_c couples the atomic transitions $|4\rangle \leftrightarrow |5\rangle$ whereas the $\hat{\sigma}_+$ and $\hat{\sigma}_-$ components of the probe field with frequency ω_p couples the transitions $|4\rangle \leftrightarrow |3\rangle$ and $|4\rangle \leftrightarrow |1\rangle$, respectively. A weak transverse magnetic field $Bsin\theta$ with $\theta << \pi/2$ couples the ground level $|1\rangle$, $|2\rangle$, and $|3\rangle$. The quantization axis and the probe propagation direction is taken along z-axis.

with

$$\vec{E}_p(\vec{r},t) = \hat{x}\mathcal{E}_p(\vec{r})\ e^{-i(\omega_p t - k_p z)} + c.c.\,,$$
$$= (\hat{\sigma}_+\mathcal{E}_+(\vec{r}) + \hat{\sigma}_-\mathcal{E}_-(\vec{r}))\ e^{-i(\omega_p t - k_p z)} + c.c.\,, \tag{4.2a}$$
$$\vec{E}_c(\vec{r},t) = \hat{x}\mathcal{E}_c(\vec{r})\ e^{-i(\omega_c t - k_c z)} + c.c.\,. \tag{4.2b}$$

where $\mathcal{E}_+(\vec{r})$ and $\mathcal{E}_-(\vec{r})$ are the slowly varying envelopes of $\hat{\sigma}_-$ and $\hat{\sigma}_+$ polarized components of the probe fields, respectively and $\mathcal{E}_c(\vec{r})$ is the slowly varying envelope of linearly polarized control field. The wave number of probe and control field are denoted by k_p and k_c, respectively. To perceive phase dependent absorption behaviour, we employ an arbitrary magnetic field $\vec{B} = B(\cos\theta\ \hat{\mathbf{z}} + \sin\theta\ \hat{\mathbf{x}})$. The longitudinal component $B\cos\theta$ of the magnetic field is accountable for splitting between the Zeeman states $|1\rangle$ and $|3\rangle$, whereas the transverse component $B\sin\theta$ is the key factor in creation of phase dependent atomic coherence, as it couples the Zeeman sublevels to

TH-1819_11612116

form a closed loop system. Further, we work in the weak TMF regime i.e., $\theta << \pi/2$, where the probe polarization remains unaffected and the quantization axis remains aligned along z-axis [110]. In this limit, under the electric dipole approximation, the Hamiltonian of the system in presence of both control, probe fields and magnetic fields can be expressed as

$$\begin{aligned} H =& H_0 + H_I + H_B\,, && \text{(4.3a)}\\ H_0 =& \hbar\omega_{42}|4\rangle\langle 4| + \hbar\omega_{52}|5\rangle\langle 5|\,, && \text{(4.3b)}\\ H_I =& -\hat{D}\cdot\hat{E}\\ =& -\hbar(|4\rangle\langle 1|g_1 e^{-i\omega_p t} + |4\rangle\langle 3|g_2 e^{-i\omega_p t} + |5\rangle\langle 4|G\, e^{-i\omega_c t} + \text{H.c.})\,, && \text{(4.3c)}\\ H_B =& g_F\mu_B\hat{F}\cdot\vec{B}\\ =& \hbar\beta_L(|3\rangle\langle 3| - |1\rangle\langle 1|) + \hbar\beta_T(|1\rangle\langle 2| + |2\rangle\langle 3| + \text{H.c.}), && \text{(4.3d)} \end{aligned}$$

where the Rabi frequencies of left and right circular polarized components of probe are given by

$$g_1 = \frac{\vec{d}_+\cdot\vec{\mathcal{E}}_+}{\hbar}e^{ik_p z},\quad g_2 = \frac{\vec{d}_-\cdot\vec{\mathcal{E}}_-}{\hbar}e^{ik_p z}, \tag{4.4}$$

respectively and the Rabi frequency corresponding to the control field is given by

$$G = \frac{\vec{d}_{54}\cdot\vec{\mathcal{E}}_{\rm c}}{\hbar}e^{ik_c z}, \tag{4.5}$$

The coupling strength and the magnitude of Zeeman shift between the ground levels are given by $\beta_T = \beta_0\sin\theta/\sqrt{2}$ and $\beta_L = \beta_0\cos\theta$, respectively. The parameter β_0 is expressed as $\beta_0 = g_F\mu_B B/\hbar$, where μ_B and g_F are the Bohr magneton and Lande g-factor, respectively. In order to eliminate the time dependency of the Hamiltonian, we apply the following unitary transformation

$$W = e^{-\frac{i}{\hbar}Ut} \quad \text{where} \quad U = \hbar\omega_p|4\rangle\langle 4| + \hbar(\omega_p+\omega_c)|5\rangle\langle 5|, \tag{4.6}$$

We then make use of rotating wave approximation to write the Hamiltonian in the following time independent form

$$\begin{aligned} H_I =& \ \hbar\Delta_p|4\rangle\langle 4| + \hbar(\Delta_c+\Delta_p)|4\rangle\langle 4| - \hbar\,(g_1|4\rangle\langle 1| + g_2|4\rangle\langle 3| + G|5\rangle\langle 4|)\\ &+ \hbar\beta_L(|3\rangle\langle 3| - |1\rangle\langle 1|) + \hbar\beta_T(|1\rangle\langle 2| + |2\rangle\langle 3|) + \text{H.c.}, \end{aligned} \tag{4.7}$$

where $\Delta_p = \omega_p - \omega_{42}$ and $\Delta_c = \omega_c - \omega_{54}$ are the probe and control detuning, respectively.

TH-1819_11612116

4.1.2 Equation of motion

We use the following Liouville equation to study the evolution of atomic populations and coherences in the closed-loop inverted Y-level system

$$\dot{\rho} = -\frac{i}{\hbar}\left[H_I, \rho\right] + \mathcal{L}_r\rho + \mathcal{L}_c\rho\,. \tag{4.8}$$

The second and third term in Eq.(4.8) describes all incoherent processes and are given as

$$\begin{aligned}\mathcal{L}_r\rho = &-\sum_{i=1}^{3}\frac{\gamma_{4i}}{2}\left(|4\rangle\langle 4|\rho - 2|i\rangle\langle i|\rho_{44} + \rho|4\rangle\langle 4|\right)\\ &-\frac{\gamma_{54}}{2}\left(|5\rangle\langle 5|\rho - 2|4\rangle\langle 4|\rho_{55} + \rho|5\rangle\langle 5|\right)\,,\end{aligned} \tag{4.9}$$

$$\mathcal{L}_c\rho = -\sum_{j=1}^{3}\sum_{j\neq i=1}^{3}\frac{\gamma_c}{2}\left(|j\rangle\langle j|\rho - 2|i\rangle\langle i|\rho_{jj} + \rho|j\rangle\langle j|\right)\,. \tag{4.10}$$

where $\gamma_{4i}(i \in 1,2,3)$ are the radiative decay rate of excited state $|4\rangle$ and γ_{54} is the decay rate of excited state $|5\rangle$. The dephasing rate for the atomic coherence ρ_{ij} due to collision is given by γ_c. Substituting the effective Hamiltonian (4.7) in the Liouville equation (4.8), the equations for the evolution of atomic population and coherences can be written as

$$\dot{\rho}_{11} = \gamma_{41}\rho_{44} - i\beta_T\rho_{21} + i\beta_T\rho_{12} + ig_1^*\rho_{41} - ig_1\rho_{14} - 2\gamma_c\rho_{11} + \gamma_c\rho_{22} + \gamma_c\rho_{33}\,, \tag{4.11a}$$

$$\dot{\rho}_{12} = i\beta_L\rho_{12} - i\beta_T(\rho_{22} - \rho_{11}) + i\beta_T\rho_{13} + ig_1^*\rho_{42} - 2\gamma_c\rho_{12}\,, \tag{4.11b}$$

$$\dot{\rho}_{13} = 2i\beta_L\rho_{13} - i\beta_T(\rho_{23} - \rho_{12}) + ig_1^*\rho_{43} - ig_2\rho_{14} - 2\gamma_c\rho_{13}\,, \tag{4.11c}$$

$$\dot{\rho}_{14} = -i(\Delta_p - \beta_L)\rho_{14} - i\beta_T\rho_{24} + ig_1^*(\rho_{44} - \rho_{11}) - ig_2^*\rho_{13} - iG_c\rho_{15} - \Gamma_{41}\rho_{14}\,, \tag{4.11d}$$

$$\dot{\rho}_{15} = -i[(\Delta_c + \Delta_p) - \beta_L]\rho_{15} - i\beta_T\rho_{25} + ig_1^*\rho_{45} - iG_c^*\rho_{14} - \Gamma_{54}\rho_{15}\,, \tag{4.11e}$$

$$\dot{\rho}_{22} = \gamma_{42}\rho_{44} - i\beta_T(\rho_{12} - \rho_{21}) - i\beta_T(\rho_{32} - \rho_{23}) + \gamma_c\rho_{11} - 2\gamma_c\rho_{22} + \gamma_c\rho_{33}\,, \tag{4.11f}$$

$$\dot{\rho}_{23} = i\beta_L\rho_{23} - i\beta_T\rho_{13} - i\beta_T(\rho_{33} - \rho_{22}) - ig_2\rho_{24} - 2\gamma_c\rho_{23}\,, \tag{4.11g}$$

$$\dot{\rho}_{24} = -i\Delta_p\rho_{24} - i\beta_T(\rho_{14} + \rho_{34}) - ig_1^*\rho_{21} - ig_2^*\rho_{23} - iG_c\rho_{25} - \Gamma_{42}\rho_{24}\,, \tag{4.11h}$$

$$\dot{\rho}_{25} = -i(\Delta_c + \Delta_p) - i\beta_T(\rho_{15} + \rho_{35}) + iG_c^*\rho_{24} - \Gamma_{54}\rho_{25}\,, \tag{4.11i}$$

$$\dot{\rho}_{33} = \gamma_{43}\rho_{44} - i\beta_T(\rho_{23} - \rho_{32}) + ig_2^*\rho_{43} - ig_2\rho_{34} + \gamma_c\rho_{11} + \gamma_c\rho_{22} - 2\gamma_c\rho_{33}\,, \tag{4.11j}$$

$$\dot{\rho}_{34} = -i(\Delta_p + \beta_L)\rho_{34} - i\beta_T\rho_{24} + ig_2^*(\rho_{44} - \rho_{33}) - ig_1^*\rho_{31} - \Gamma_{43}\rho_{34}\,, \tag{4.11k}$$

$$\dot{\rho}_{35} = -i[(\Delta_c + \Delta_p) + \beta_L]\rho_{35} - i\beta_T\rho_{25} + ig_2^*\rho_{45} - iG_c^*\rho_{34} - \Gamma_{54}\rho_{35}\,, \tag{4.11l}$$

$$\dot{\rho}_{44} = ig_1\rho_{14} - ig_1^*\rho_{41} + ig_2\rho_{34} - ig_2^*\rho_{43} - iG_c\rho_{45} + iG_c^*\rho_{54} - \gamma\rho_{44} + \gamma_{54}\rho_{55}\,, \tag{4.11m}$$

$$\dot{\rho}_{45} = -i\Delta_c\rho_{45} + ig_1\rho_{15} + ig_2\rho_{35} + iG_c^*(\rho_{55} - \rho_{44}) - (\frac{\gamma}{2} + \Gamma_{54})\rho_{45}\,. \tag{4.11n}$$

TH-1819_11612116

The remaining equations for the density matrix elements can be obtained from the the complex conjugate expressions $\dot{\rho}_{ji} = \dot{\rho}^*_{ij}$ and the population conservation law $\sum_{i=1}^{5} \rho_{ii} = 1$. Under the assumption of equal decay rates from the excited state to the ground states, the population decay rates are expressed as $\gamma_{41} = \gamma_{42} = \gamma_{43} = \gamma/3$, where γ is the spontaneous decay rate of state $|4\rangle$. The population decay rate of the excited state $|5\rangle$ is expressed as $\gamma_{54} = 0.1\gamma$. The coherence decay rates $\Gamma_{4j}(j \in 1, 2, 3)$ and Γ_{54} are expressed as $\Gamma_{41} = \Gamma_{42} = \Gamma_{43} = \gamma_c + \sum_{i=1}^{3} \frac{\gamma_{4i}}{2}$ and $\Gamma_{54} = \frac{\gamma_{54}}{2}$, respectively. Further, we assume the collision rate γ_c of the metastable ground states to be very negligible in our calculations.

4.1.3 Probe susceptibility of a homogeneous medium

In this section, we adopt the perturbative approach used by Sharma and Dey [124] to evaluate an analytical expression for the medium susceptibility of closed-loop system. We assume probe field to be very weak, so that it can be treated as a perturbation to the system. In the weak probe field limit, the density matrix elements can be expanded upto first order in probe field $g_i, (i \in 1, 2)$ as

$$\rho_{ij} = \rho^{(0)}_{ij} + \frac{g_1}{\gamma}\rho^{(+)}_{ij} + \frac{g_2}{\gamma}\rho^{(+)}_{ij}, \tag{4.12}$$

where the first term $\rho^{(0)}_{ij}$ is the zeroth order solution and is evaluated using counter-intuitive approach as discussed in chapter 3. The second and third term in Eq.(4.12) represents the first-order solution of the density matrix elements for both right and left polarized components of probe at positive frequency ω_p. We now substitute the above expression in Eqs (4.11) and equate the coefficients of g_1 and g_2 to obtain two sets of 20 coupled equations. Next, we solve these linear equations to obtain the atomic coherences $\rho^{(+)}_{41}$ and $\rho^{(+)}_{43}$. The analytical expression for the zeroth and first order populations and coherences relevant to the calculations are given in the appendix. The linear susceptibility χ_{41} and χ_{43} of the medium at probe frequency ω_p can be expressed in terms of the atomic coherences $\rho^{(+)}_{41}$ and $\rho^{(+)}_{43}$, respectively by the following equations

$$\chi_{41}(\Delta_p) = \frac{\mathcal{N}|d_+|^2}{\hbar\gamma}\rho^{(+)}_{41}, \tag{4.13a}$$

$$\chi_{43}(\Delta_p) = \frac{\mathcal{N}|d_-|^2}{\hbar\gamma}\rho^{(+)}_{43}, \tag{4.13b}$$

TH-1819_11612116

where

$$\rho_{41}^{(+)} = \frac{N_1}{D} + \beta_T^2 \frac{N_2}{D}\frac{g_2}{g_1}\,, \tag{4.14}$$

$$\rho_{43}^{(+)} = \frac{N_3}{D} + \beta_T^2 \frac{N_2}{D}\frac{g_1}{g_2}\,, \tag{4.15}$$

Here $\mathcal{N}$ is the atomic density of the medium. The above Eqs.(4.13) clearly shows the coupling of both probe components due to the TMF β_T, which is necessary to observe phase dependent susceptibility. Further, the phase dependent characteristics of the medium can be well understood by considering spatial variations of the probe field components. The spatial structure of both the orthogonal components of the probe field are expressed as

$$g_1(\vec{r}) = g(r,z)e^{il\phi}\,, \tag{4.16a}$$

$$g_2(\vec{r}) = g(r,z)e^{-il\phi}\,, \tag{4.16b}$$

where $g(r,z)$ is the transverse profile of the probe beam and l, ϕ are the OAM and phase carried by probe beam, respectively. In presence of an inhomogeneous probe, the linear susceptibilities of the medium are expressed as

$$\chi_{41} = \frac{\mathcal{N}|d_+|^2}{\hbar\gamma}\left(\frac{N_1}{D} + \beta_T^2 e^{-2il\phi}\frac{N_2}{D}\right)\,, \tag{4.17}$$

$$\chi_{43} = \frac{\mathcal{N}|d_-|^2}{\hbar\gamma}\left(\frac{N_3}{D} + \beta_T^2 e^{2il\phi}\frac{N_2}{D}\right)\,. \tag{4.18}$$

The above analytical expressions show the dependence of medium susceptibilities on TMF strength β_T, OAM l, transverse phase ϕ and control field intensity. All these parameters plays a decisive role in creation and manipulation of the phase dependent medium susceptibility.

4.1.4 Paraxial beam propagation equations

We use Maxwell's wave equation to study the effect of azimuthally varying susceptibility on the profile of both right and left polarized components of the probe beam. The Maxwell's equations in terms of probe Rabi frequencies g_1 and g_2, under slowly varying envelope and paraxial wave approximation is given by

$$\frac{\partial g_1}{\partial z} = \frac{i}{2k_p}\left(\frac{\partial^2}{\partial x^2} + \frac{\partial^2}{\partial y^2}\right) g_1 + 2i\pi k_p \chi_{41}\, g_1\,, \tag{4.19a}$$

$$\frac{\partial g_2}{\partial z} = \frac{i}{2k_p}\left(\frac{\partial^2}{\partial x^2} + \frac{\partial^2}{\partial y^2}\right) g_2 + 2i\pi k_p \chi_{43}\, g_2\,. \tag{4.19b}$$

TH-1819_11612116

The terms on the right hand side of Eq. (4.19a) and Eq. (4.19b) account for diffraction of the probe beams either in free space or in the medium. The second terms on the right-hand side of Eq. (4.19a) and Eq. (4.19b) represents the effect of absorption and dispersion of the medium on probe beam.

4.2 Results and Discussions

4.2.1 Azimuthally varying susceptibility

In this section, we first study the creation of phase dependent absorption in the absence of control field. For this purpose, we consider the amplitude of both $\hat{\sigma}_+$ and $\hat{\sigma}_-$ component of the probe as in Eq. (4.16) to be continuous i.e. $g_i(r, z = 0) = g_0, (i \in 1, 2)$. We then numerically study the susceptibility expression for right circular polarization of probe χ_{41} given by Eq. (4.17). Result for the medium absorption of $\hat{\sigma}_+$ component of probe χ_{41} is plotted in the transverse $(x-y)$ plane as shown in Fig. 4.2. Figure 4.2 shows that the absorption varies periodically in the azimuthal plane. As a result, spatial transparency window is created at specific angular position in the azimuthal plane. The periodic formation of the transparency window is due to the TMF induced phase coupled term (exponential term) in the susceptibility expression of Eq. (4.17). The number of transparency window formed in the azimuthal plane can be determined by the $2l$ factor in the exponential term of Eq. (4.17). So for OAM $l = 4$, 8 transparency windows are created in the transverse plane as shown in Fig. 4.2. The position of minimum absorption is given by the angular value $n\pi/l$ where n varies from 0 to $2l$. A similar $2l-$fold symmetric absorption pattern is also displayed by the $\hat{\sigma}_-$ component of the probe at resonance $\Delta_p = 0$, as expressed by Eq. (4.18). Such phase dependent dynamics of the closed-loop tripod system is extensively in chapter 3. Phase dependent periodic variation in absorption forms the basis for generation of structured beams. We however are interested in the effect of control field on the medium absorption. A strong control field can significantly modify the medium optical properties [130]. So, in presence of a control field, the system in Fig. 4.1 can be decomposed as two ladder-type three level systems each for left and right polarized components of the probe field. Ladder systems are known to show EIT like line shape [130]. In these systems a strong control field induces a transparency for a weak probe at two photon resonance condition $\Delta_p = \Delta_c = 0$. We make use of this EIT induced transparency to create different structured absorption profiles. In this regard, we study the effect of different spatially varying control field structure on the phase dependent absorption. The spatial structure of the control field is given by

TH-1819_11612116

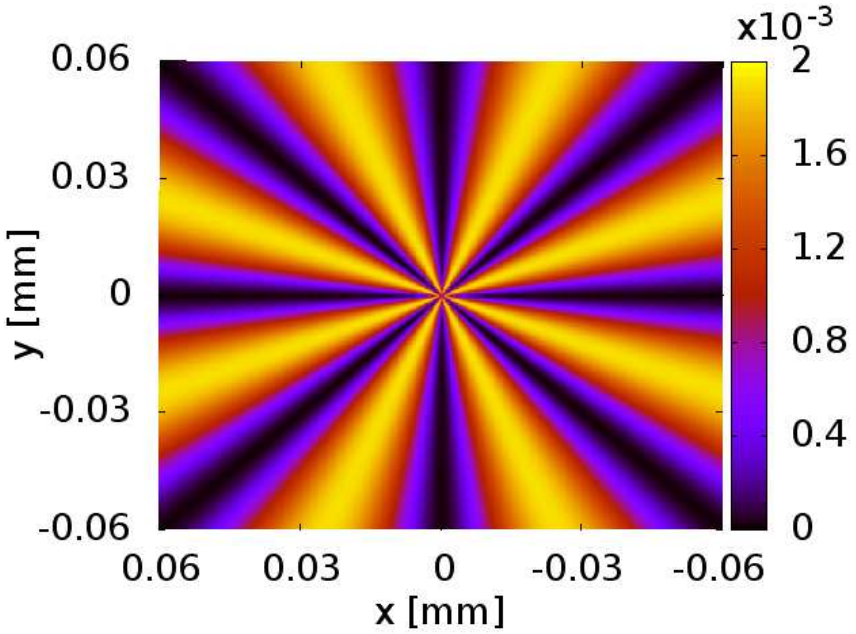

Fig. 4.2 (Color online) Imaginary part of susceptibility χ_{41} is plotted against the transverse axis x and y in absence of control field. The parameters are chosen as $\mathcal{N} = 4 \times 10^{12} atoms/cm^3$, $\Gamma_{41} = 0.5\gamma$, $\Gamma_{54} = 0.05\gamma$, $\Delta_p = 0$, $\Delta_c = 0$, $\beta_0 = 0.01\gamma$, $\gamma_c = 10^{-7}\gamma$, $\theta = \pi/14$, $G = 0\gamma$, and OAM of probe beam $l = 4$.

the following expression

$$G(x,y,z) = G_0 \times \frac{w_c}{w_c(z)} \times H_m\left(\frac{x\sqrt{2}}{w_c(z)}\right) H_n\left(\frac{y\sqrt{2}}{w_c(z)}\right) e^{-(x^2+y^2)/w_c^2(z)} e^{ik(x^2+y^2)/2R_c(z)} e^{i(kz-(m+n+1)\tan^{-1}(z/z_0))}. \tag{4.20}$$

where H_m and H_n are Hermite polynomials of order m and n, respectively. The initial beam waist, Rayleigh length, and radius of curvature of beam are defined as, w_c, $z_c = \pi w_c^2/\lambda$, and $R(z) = z + (z_c^2/z)$, respectively. $w_c(z)$ represents the beam waist after propagating a distance z through free space. We now study the effect of HG_{10} control beam on the phase dependent probe absorption. The intensity distribution of the control beam in the transverse plane shows two petal structure distributed symmetrically along the x-axis [113]. As control field induces transparency, the spatial position with maximum field intensity shows maximum transmission and with the decrease in field intensity the transmission decreases. As a result, two spatial transparency window are created in the azimuthal plane. The combination of phase induced transparency and control field transparency leads to creation of asymmetric absorption pattern in the azimuthal plane as shown in Fig. 4.3(a). Figure 4.3(a) also shows that the minimum of control induced transparency and phase induced trans-

TH-1819_11612116

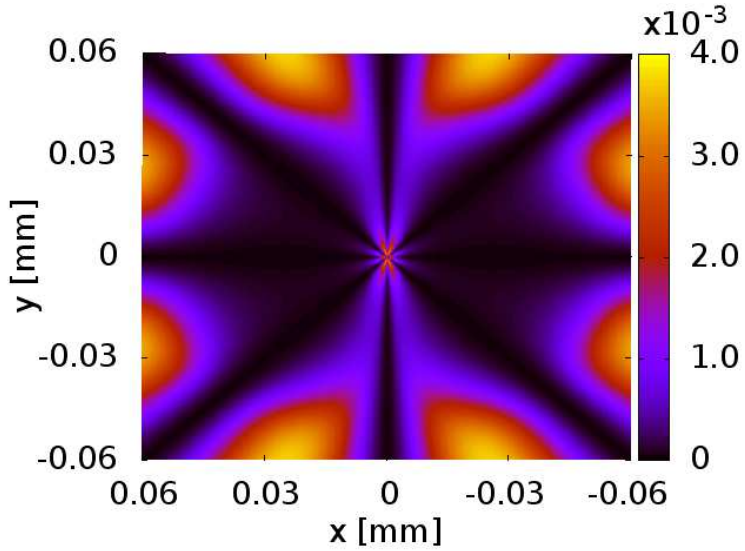

(a)

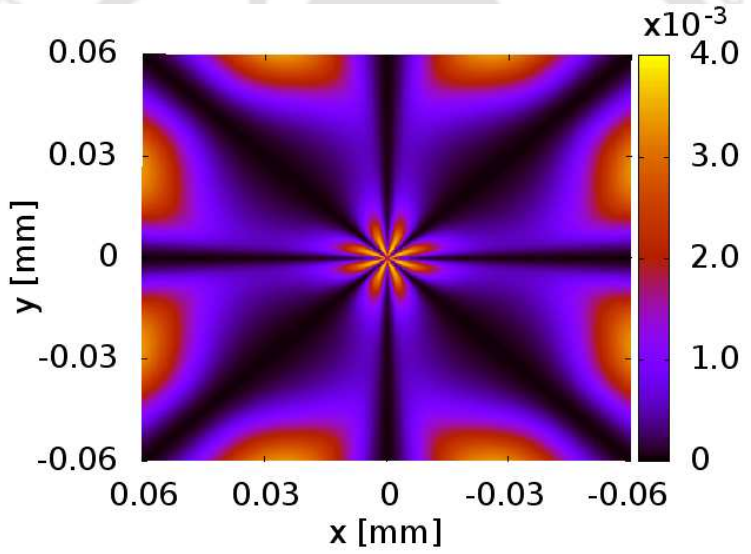

(b)

Fig. 4.3 (Color online)Panel (a) and (b) shows the variation of medium absorption in the transverse $(x-y)$ plane. Creation of structured absorption pattern by HG_{10} and HG_{11} control beam is shown in panel (a) and (b), respectively. The amplitude for HG_{10} mode is taken as $G_0 = 3.0\gamma$ and for HG_{11} mode is $G_0 = 4.0\gamma$. The width for both control beam modes is $w_c = 30$ μm. Other parameters are same as in Fig. 4.2.

parency coexist at same angular position represented as 0 and π. The co-existing transparencies forms the key to selective transfer and processing of phase information. To further establish the phase selective mechanism, we illustrate the modulation of probe absorption using HG_{11} mode control beam. The 4 petal structure of the control beam create transparencies at 4 azimuthal position denoted by $(2n+1)\pi/4$ with n varies from 0 to 3. The control field induced spatial transparencies along with the

TH-1819_11612116

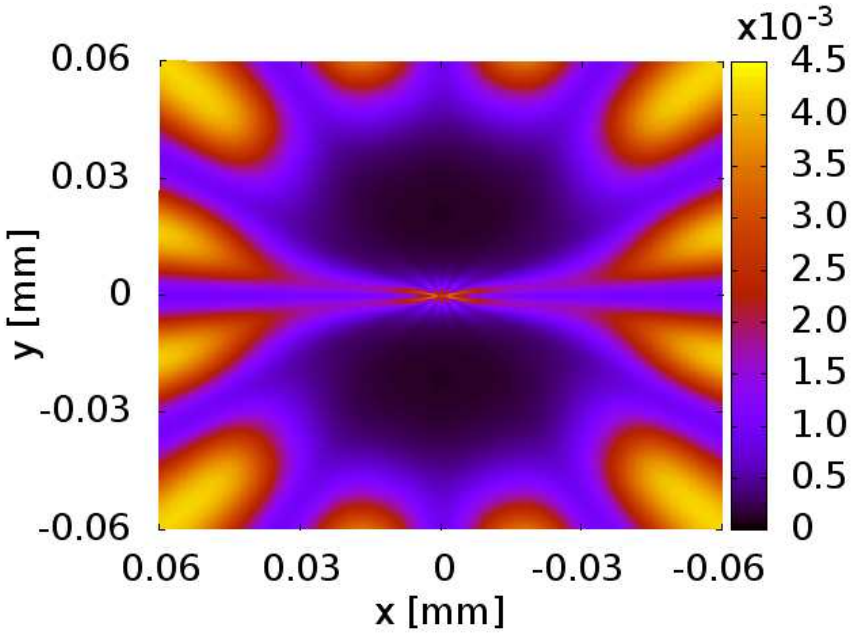

Fig. 4.4 (Color online) Shows the effect of OAM and HG_{01} mode control beam on structured absorption profile. The amplitude and the width of the HG_{01} mode control beam is taken as $G_0 = 3.0\gamma$ and $w_c = 30$ μm. The OAM of probe beam is $l = 6$. Other parameters are same as in Fig. 4.2.

phase induced transparencies in the azimuthal plane forms asymmetric absorption profile as shown in Fig. 4.3(b). Hence Spatial profile of the control beam plays a decisive role in creation of the asymmetric absorption pattern. Further the asymmetry in the absorption profile can be controlled by the intensity and the width of the control beam. A proper control and manipulation of the asymmetry in the absorption can be helpful in creation of high contrast structured beams.

Next we study the effect of OAM on the phase dependent medium susceptibility and its manipulation using a control field. As discussed above, the number of transparency windows formed in the azimuthal plane is determined by $2l$ with l being the OAM. Hence with the increase in l, the number of transparency windows increases. As a result, width of each transparencies present in the azimuthal plane decreases. Presence of narrow transparency window play a major role in creation of structured beam with petal features of the order of wavelength or can even surpass the diffraction limit. Manipulation of these phase induced narrow transparencies using a spatial dependent control field holds the key to formation of various structured beams with sub-wavelength petal feature. Hence to visualize the above fact, we create an asymmetric absorption profile by manipulating the phase induced absorption for OAM $l = 6$ using a HG_{01} control beam as shown in Fig. 4.4. Effect of these asymmetric

TH-1819_11612116

absorption pattern on the probe beam can be understood by studying the propagation dynamics of the beam.

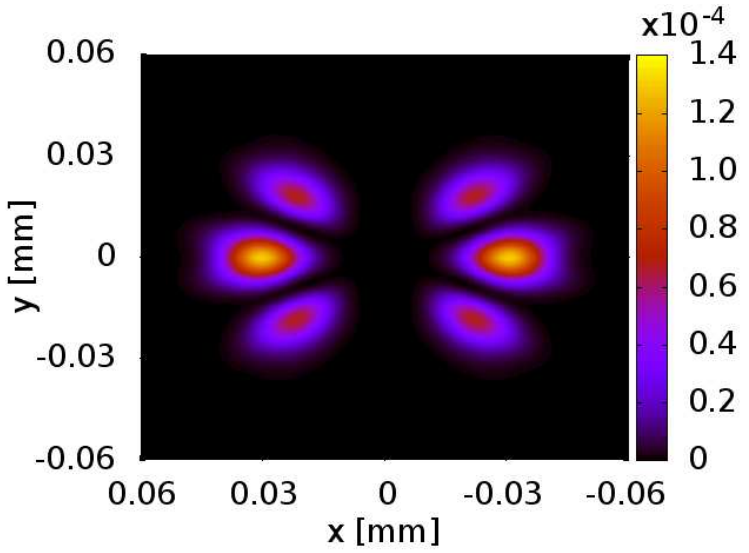

(a)

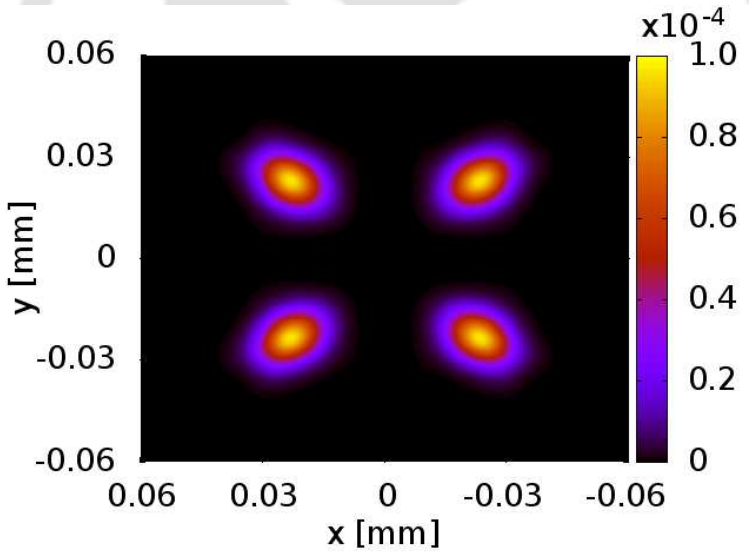

(b)

Fig. 4.5 (Color online) Panel (a) and (b) shows the variation of output probe beam intensity with transverse axis x and y in presence of HG_{10} and HG_{11} control beam, respectively. The transmitted intensity of the probe beam plotted in panels (a) and (b) are after a propagation length 0.8 mm. The parameters for the probe beam are $g_0 = 0.005\gamma$, $m = 0$, $l = 4$ and $w_p = 20$ μm. Other parameters are same as in Fig. 4.3.

4.2.2 Beam propagation dynamics

In this section we discuss the utility of asymmetric absorption profile on generation of structured beam with different petal forms. For this purpose, we consider the probe

TH-1819_11612116

beam components as Laguerre-Gaussian mode with equal but opposite OAM. The spatial profile of the probe components at the input of the medium is expressed as

$$\begin{aligned} g_j(r,\phi,z=0) =& g_0 \left(\frac{r\sqrt{2}}{w_p}\right)^{|l|} e^{-\left(\frac{r^2}{w_p^2}\right)} L_m^l \left(\frac{2r^2}{w_p^2}\right) e^{\pm il\phi} \\ r =& \sqrt{x^2+y^2} \\ \phi =& \tan^{-1}\left(\frac{y}{x}\right). \end{aligned} \tag{4.21}$$

To study the propagation dynamics of the probe beam components, we numerically solve the propagation Eq. (4.19a) and Eq. (4.19b) using Fourier split-step operator method. Figure 4.5 shows the output intensity pattern of the probe in the azimuthal plane after a propagation distance of 0.8 mm. The total output intensity is evaluated using the expression $I_{out} = |g_1|^2 + |g_2|^2$. The net output intensity is consequence of the orthogonality of the left and right polarization of the probe. It is evident from Fig. 4.5(a) that the HG_{10} control beam allows the phase information to be transferred from around two azimuthal position 0 and π on to the probe, thus resulting in a 2 petal structure. It can also be seen from Fig. 4.5(b) that HG_{11} control beam shows similar transfer of phase information from azimuthal position $(2n+1)\pi/4$ with n varies from 0 to 3 onto the probe beam. Hence a HG_{11} control beam creates a structured pattern consisting of 4 petals as shown in Fig. 4.5(b). The peak transmission for both the case is found to be 56%. Moreover it should be noted that in absence of control beam, for a probe beam carrying an OAM of 4, 8 petal structure is formed in its profile owing to the phase dependent absorption. So it is clearly evident form Fig. 4.5 that the control beam modes HG_{10} and HG_{11} manipulate the structured probe beam consisting of 8 petal-like structures to create 2 petal-like and 4-petal like structured probe respectively. Hence the control beam acts as a phase selective tool in controlling and manipulating the spatial features of the structured probe beam.

Next we demonstrate the manipulation of structured probe with OAM $l = 6$ using a HG_{01} mode control beam. Figure 4.6 shows the output intensity of probe beam at 0.8 mm length of propagation. As discussed above, the HG_{01} mode control beam acts as a phase selective tool and hence allows the transfer of phase information from around $\pi/2$ and $3\pi/2$ azimuthal position onto the probe beam. As a result a structured probe with 2 high intense petal-like structure accompanied by some low intense petal-like structure are formed as shown in Fig. 4.6. Moreover the low intense side lobes in the structured probe can be made negligible by choosing suitable width and the intensity of the control beam. Hence a spatial dependent control beam with suitable width and intensity can play a major role in creating high contrast structured probe beam. However it is necessary to understand the physical basis for this manipulation

TH-1819_11612116

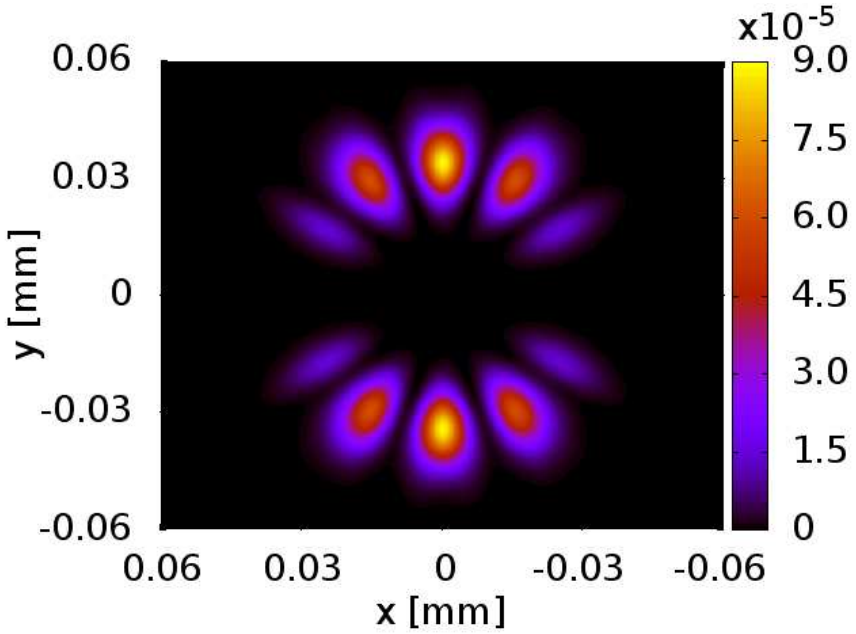

Fig. 4.6 (Color online) Intensity distribution of the transmitted probe beam in transverse $(x-y)$ plane, after a propagation length of 0.8 mm. The parameters for the probe beam are $g_0 = 0.001\gamma$, $m = 0$, $l = 6$ and $w_p = 20$ μm. Other parameters are same as in Fig. 4.4.

of structured probe with higher OAM using the control beam. In this regard, We study the variation of the petal width with OAM l. We assume that the bright and dark region in the structured beam are of equal width. So, for a probe with width w_p, the width of each bright or dark region is given by the ratio between the circumference of the beam and the total number of dark and bright regions. Hence the width of the bright region or spot is thus given as $\pi w_p/2l$. So for OAM $l = 4$, width of each spot is $\pi w_p/8$, whereas for OAM $l = 6$, width of each spot is $\pi w_p/12$. Hence with the increase in the OAM value the width of spot or petal decreases as can be seen from Fig. 4.5 and Fig. 4.6. Manipulation of structured beam possessing narrow petal features with a spatial dependent control beam is the key to formation of various asymmetric structured beam patterns. Asymmetric structured beams with narrow petal features have immense application in imaging, biosciences, and in manipulation and trapping of particles.

4.3 Conclusion

In conclusion, we have demonstrated a phase selective technique to generate structured beam with different petal forms using ^{87}Rb atomic vapor in inverted Y-level configuration. We have shown that a phase structured probe beam, in presence of a

TH-1819_11612116

TMF enables us to create a phase dependent medium absorption. Further, we utilized a suitable spatially dependent control beam to manipulate the phase varying absorption. An azimuthally varying control field creates transparency at different azimuthal position. This spatial transparency window allows us to transfer phase information from specific azimuthal position onto the probe beam. Our numerical results on probe propagation confirms the selective transfer of phase information to the probe profile, leading to formation of structured beam patterns with different petal forms. Our results can be utilized in realization of optical tweezers for controlled manipulation and trapping of particles, in high contrast imaging systems, and in micromachining.

4.4 Appendix

In appendix, we provide the relevant expressions for the zeroth order and first order atomic populations and coherences evaluated using counterintuitive approach as described in chapter 3. The zeroth order atomic populations and coherences are given as

$$\rho_{11}^{(0)} = \rho_{33}^{(0)} = (\frac{\beta_T}{\beta_L})^2\,, \tag{4.22}$$

$$\rho_{22}^{(0)} = 1 - 2(\frac{\beta_T}{\beta_L})^2\,, \tag{4.23}$$

$$\rho_{12}^{(0)} = \rho_{21}^{(0)} = \frac{\beta_L\beta_T(\rho_{22}^{(0)} - \rho_{11}^{(0)})}{\beta_L^2 - \beta_T^2}\,, \tag{4.24}$$

$$\rho_{13}^{(0)} = \rho_{31}^{(0)} = -\frac{\beta_T^2(\rho_{22}^{(0)} - \rho_{11}^{(0)})}{\beta_L^2 - \beta_T^2}\,, \tag{4.25}$$

$$\rho_{23}^{(0)} = \rho_{32}^{(0)} = -\frac{\beta_L\beta_T(\rho_{22}^{(0)} - \rho_{11}^{(0)})}{\beta_L^2 - \beta_T^2}\,. \tag{4.26}$$

The related first order coherences corresponding to both polarized components of the probe field, at two photon resonance condition $\Delta_p = \Delta_c = 0$ are expressed as

$$\rho_{41}^{(+)} = \frac{N_1}{D} + \beta_T^2\frac{N_2}{D}\frac{g_2}{g_1}\,, \tag{4.27}$$

$$\rho_{43}^{(+)} = \frac{N_3}{D} + \beta_T^2\frac{N_2}{D}\frac{g_1}{g_2}\,, \tag{4.28}$$

where

$$\begin{aligned} N_1 =& \beta_L^2 G_1\rho_{11}^{(0)} + \beta_L^3 G_1(G_2\rho_{11}^{(0)} + \beta_T^2(2\rho_{11}^{(0)} - \rho_{22}^{(0)})) - \beta_L\beta_T^2 G_1(2\beta_T^2 + G_2)\rho_{22}^{(0)} \\ &+ i\beta_L^4(G_1\Gamma_{41}\rho_{11}^{(0)} + \beta_T^2\Gamma_{54}\rho_{22}^{(0)}) - i\beta_L^2(-\Gamma_{54}G_1^2\rho_{11}^{(0)} + \beta_T^4\Gamma_{54}(2\rho_{11}^{(0)} - 3\rho_{22}^{(0)}) \\ &- \beta_T^2(\Gamma_{41}^2\Gamma_{54}\rho_{11}^{(0)} + \Gamma_{54}^3\rho_{22}^{(0)} + G^2(\Gamma_{41}(\rho_{11}^{(0)} - \rho_{22}^{(0)}) - 2\Gamma_{54}\rho_{22}^{(0)}))) - i\beta_T^2(\Gamma_{54}G_1^2\rho_{11}^{(0)} \end{aligned} \tag{4.29}$$

TH-1819_11612116

$$+\beta_T^4\Gamma_{54}(4\rho_{11}^{(0)}-2\rho_{22}^{(0)})+\beta_T^2(2\Gamma_{41}^2\Gamma_{54}\rho_{11}^{(0)}+\Gamma_{54}^3(2\rho_{11}^{(0)}-\rho_{22}^{(0)})+G^2(-2\Gamma_{54}(2\rho_{11}^{(0)}-\rho_{22}^{(0)})$$
$$+\Gamma_{41}\rho_{22}^{(0)}))),$$

$$N_2 =i(\beta_T^4\Gamma_{54}(4\rho_{11}^{(0)}-2\rho_{22}^{(0)})+\Gamma_{54}G_1^2(\rho_{11}^{(0)}-\rho_{22}^{(0)})-\beta_T^4\Gamma_{54}\rho_{22}^{(0)}-\beta_T^2(-\Gamma_{54}^3(2\rho_{11}^{(0)}-\rho_{22}^{(0)})$$
$$-\Gamma_{41}^2\Gamma_{54}(\rho_{11}^{(0)}-\rho_{22}^{(0)})+G^2(2\Gamma_{54}(2\rho_{11}^{(0)}-\rho_{22}^{(0)})+\Gamma_{41}\rho_{22}^{(0)}))+\beta_T^2(G^2(\Gamma_{41}\rho_{11}^{(0)}+2\Gamma_{54}\rho_{22}^{(0)})$$
$$-\Gamma_{54}(\Gamma_{54}^2\rho_{22}^{(0)}-\Gamma_{41}^2(\rho_{11}^{(0)}-\rho_{22}^{(0)})-\beta_T^2(2\rho_{11}^{(0)}-3\rho_{22}^{(0)})))),$$

$$N_3 =-\beta_L^2G_1\rho_{11}^{(0)}-\beta_L^3G_1(G_2\rho_{11}^{(0)}+\beta_T^2(2\rho_{11}^{(0)}-\rho_{22}^{(0)}))+\beta_L\beta_T^2G_1(2\beta_T^2+G_2)\rho_{22}^{(0)}+i\beta_L^4(G_1\Gamma_{41}\rho_{11}^{(0)}$$
$$+\beta_T^2\Gamma_{54}\rho_{22}^{(0)})-i\beta_L^2(-\Gamma_{54}G_1^2\rho_{11}^{(0)}+\beta_T^4\Gamma_{54}(2\rho_{11}^{(0)}-3\rho_{22}^{(0)})-\beta_T^2(\Gamma_{41}^2\Gamma_{54}\rho_{11}^{(0)}+\Gamma_{54}^3\rho_{22}^{(0)}$$
$$+G^2(\Gamma_{41}(\rho_{11}^{(0)}-\rho_{22}^{(0)})-2\Gamma_{54}\rho_{22}^{(0)})))-i\beta_T^2(\Gamma_{54}G_1^2\rho_{11}^{(0)}+\beta_T^4\Gamma_{54}(4\rho_{11}^{(0)}-2\rho_{22}^{(0)})$$
$$+\beta_T^2(2\Gamma_{41}^2\Gamma_{54}\rho_{11}^{(0)}+\Gamma_{54}^3(2\rho_{11}^{(0)}-\rho_{22}^{(0)})+G^2(-2\Gamma_{54}(2\rho_{11}^{(0)}-\rho_{22}^{(0)})+\Gamma_{41}\rho_{22}^{(0)}))),$$

$$D =(\beta_L^2-\beta_T^2)G_1(\beta_L^4+4\beta_T^4+G_1^2+2\beta_T^2(G_2+G_3)+\beta_L^2(4\beta_T^2+G_2+G_3)),$$

$$G_1 =G^2+\Gamma_{41}\Gamma_{54},$$

$$G_2 =-G^2+\Gamma_{54}^2, \tag{4.30}$$

$$G_3 =-G^2+\Gamma_{41}^2. \tag{4.31}$$

(4.32)

TH-1819_11612116

Chapter 5

Slow light in ultracold atom-molecule coupled system

Manipulation of dispersive properties of a medium with an external field is important for a variety of applications in optics, photonics, quantum information processing and related areas. In particular, propagation dynamics of a weak electromagnetic field can be controlled by tailoring the dispersive characteristics of the medium with a strong external field. One of the key physical effects underlying such control is electromagnetically induced transparency (EIT) [131, 132] by which a medium is rendered transparent to a weak (probe) field. This happens due to the manipulation of medium's optical properties by a strong (control) field. At a fundamental level, the optical response of a medium can be controlled by creating and manipulating coherent superpositions of quantum states of atoms or molecules of the medium with external fields. Thus, the basic mechanism to generate EIT stems from field induced atomic or molecular coherences.

EIT has been extensively studied in lambda-type three-level atoms where all the three levels are discrete; and applied in high precision spectroscopy [133, 134], atomic clocks [135, 136], slow light [137, 138], fast light [139, 140], *etc.* When EIT occurs, the dispersion profile shows a sharp variation over the spectral range of EIT window. A positive slope of the dispersion near this window leads to slow or subluminal light [141, 139], while a negative slope gives rise to fast or superluminal light [139]. The early experimental studies on subluminal light demonstrated a group velocity as low as 17 m s^{-1} [142] and 90 m s^{-1} [143] in atomic gases. Slow light is also possible in solid state systems [144, 145]. In order to make use of slow light for practical purposes, it is important to enhance delay-bandwidth product (DBP) [146] which is defined as the product of time-delay and the spectral width of transparency window (EIT window). Despite tremendous progress on the production of slow light over the years, applications of slow light is hindered due to the fact that, EIT width is found to

TH-1819_11612116

be very narrow so far. Although a narrow EIT width gives rise to a large time-delay which is desirable, but it occurs with a high absorption that degrades enormously the efficacy of slow light. On the other hand, a broad EIT width will lead to a very small time-delay though the absorption will be reduced. Therefore, Increasing DBP is found to be very difficult. How to increase DBP in various systems is an important pursuit in current slow light experiments [147, 148].

Here we theoretically show that it is possible to obtain slow light in an ultracold atom-molecule coupled system where DBP can be optimized and the transmission of probe field can be enhanced by narrowing a Feshbach resonance (FR). In general, it is difficult to generate slow light in a molecular system because of the complex level structure of the molecules unlike that in an atomic gas. Recent advances in the creation of ultracold diatomic molecules in a specific rovibrational level by associating ultracold atoms with photoassociation (PA) [149]-[151] or Feshbach resonances [152, 153] open up a new perspective in coherent control of light propagation. EIT-like features have been earlier observed in two-color PA [154]-[157]. However, to the best of our knowledge, slowing of light propagation through an atom-molecule coupled system has not been considered before. An atom-molecule coupled system provides a continuum-bound coupled medium where the continuum of atom-atom scattering states are coupled by photoassociating lasers to diatomic molecular bound states. Since at ultra low energy atom-atom interactions can be largely altered by changing the s-wave scattering length with an FR induced by an external magnetic or radio-frequency field, an FR can be used as a handle to control slow light propagation. Furthermore, one can optimize the EIT window with an FR to mitigate absorption. Thus, it is possible to achieve robust slow light production in an ultracold atom-molecule coupled medium.

In this chapter, we study light propagation through an atom-molecule resonantly interacting medium. We assume that the system is initially prepared in a specific molecular bound state in the electronically ground-state potential by Raman PA [155, 158] or by a magnetic FR (MFR) [159]. The system under consideration is schematically shown in Fig.1. The bound state $\mid 1\rangle$ in the ground-state potential is coupled to another bound state $\mid 2\rangle$ in the electronically excited potential by a weak probe, while $\mid 2\rangle$ is coupled to the continuum of atom-atom scattering states $\mid \epsilon\rangle$ (where ϵ denotes the collision energy) in the ground-state potential in the presence of a magnetic Feshbach resonance (MFR). Within the framework of two-channel model of Feshbach resonance, we assume the existence of a quasi-bound state $\mid a\rangle$ supported by a ground-state channel (closed-channel) whose threshold lies above the collision energy. We use well known method of Fano [160] to diagonalize the continuum-bound system and thereby to reduce the composite system of a bound state interacting with the continuum into

TH-1819_11612116

a single broadened discrete state. We find that with the decrease in the Feshbach resonance width, the width of the transparency window becomes very narrow and the absorption goes to zero. We exploit these features to reduce significantly the group velocity of the propagating weak pulse and to increase the output transmission efficiency.

5.1 Theoretical Formulations

5.1.1 Model

We consider a model consisting of 3 diatomic molecular bound states and the collisional continuum of two ground state atoms in a pump-probe Λ-type configuration as shown in Fig.5.1(b). There are two approaches to solve the problem of a continuum-bound coupled system, one is quasi-continuum [161]-[163] and the other is structured continuum approach [164]. The latter approach was introduced more than 50 years ago by Fano [160]. Structured continuum has been recently shown to arise in PA in the presence of magnetic Feshbach resonance (MFR) [165, 166].

Our model is schematically shown in Fig.1 with $|1\rangle$ and $|2\rangle$ being two molecular bound states, $|a\rangle$ representing a quasi-bound or predissociating state embedded in the continuum $|\varepsilon\rangle$ of scattering states of two ground state atoms. The excited rovibrational state $|2\rangle$ is coupled to the rovibrational state $|1\rangle$ in an electronic molecular ground state by a weak probe field with frequency ω_p and to the continuum $|\varepsilon\rangle$ by a strong control field with frequency ω_c, respectively. The two fields are given by

$$\vec{E}_j(z,t) = \hat{e}_j \mathcal{E}_j(z,t)\ e^{-i(\omega_j t - k_j z)} + c.c.\,, \tag{5.1}$$

where $\mathcal{E}_j(z,t)$ is the slowly varying electric field envelope, $\hat{e}_j$ is the unit polarization vector, ω_j is the laser field frequency and k_j is the wave number of the field. The index $j \in \{p, c\}$ denotes the probe (p) and control (c) field, respectively.

5.1.2 Theory

According to Fano theory, when the state $|a\rangle$ with energy E_a is embedded into the flat continuum $|\varepsilon\rangle$ via an interaction $V(\varepsilon)$(generally collisional interaction), a shift results in the energy of the state $|a\rangle$ leading to its dressing by the continuum. The flat continuum states $|\varepsilon\rangle$ also gets modified by the interaction $V(\varepsilon)$ to produce the dressed continuum states $|\epsilon\rangle$. The bound to dressed continuum dipole moment $d_{2\epsilon}$ is

TH-1819_11612116

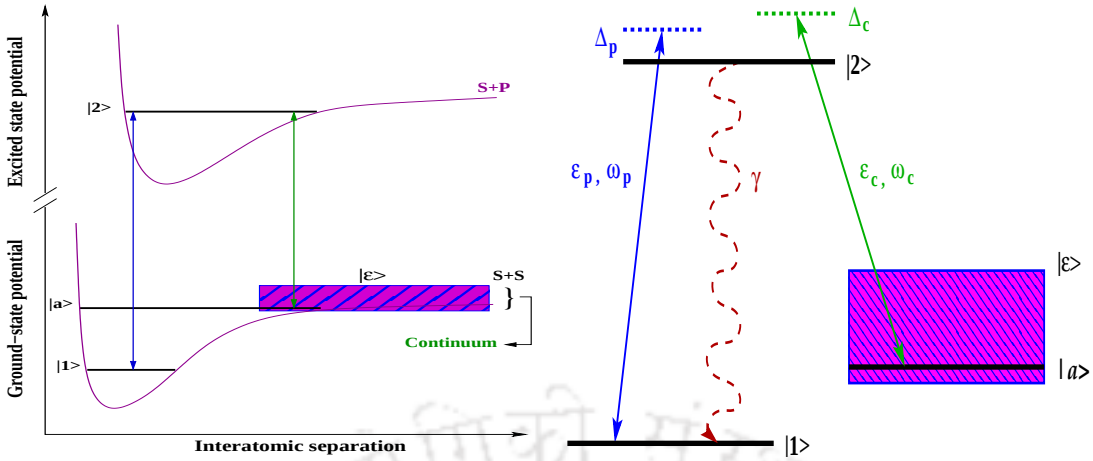

Fig. 5.1 (Color online) (a) A typical experimentally realizable molecular potential and level structure depicting the atom-molecule model system. (b) A simplified schematic diagram of (a) where the bound-state $|1\rangle$ is supported by an open-channel ground-state molecular potential that asymptotically corresponds to two separated ground state (S) atoms. $|1\rangle$ is coupled to the excited bound-state $|2\rangle$ via a probe field with frequency ω_p and the state $|2\rangle$ is coupled to the continuum $|\varepsilon\rangle$ of collisions between the two S atoms via a control field with frequency ω_c. The excited potential asymptotically corresponds to two free atom with one in P excited state and the other in S state. The quasi-bound state $|a\rangle$ supported by a closed channel (not shown in the figure) in the molecular ground-state manifold is coupled to $|\varepsilon\rangle$ via interaction $V(\varepsilon)$. The existence of $|a\rangle$ is assumed to model a Feshbach resonance. γ is the spontaneous linewidth for $|2\rangle \leftrightarrow |1\rangle$ transition. $\Gamma = 2\pi|V(\varepsilon)|^2/\hbar$.

related to bound to flat continuum dipole moment $d_{2\varepsilon}$ as

$$d_{2\epsilon} = \frac{\epsilon - E_a + q\Gamma}{\sqrt{(\epsilon - E_a)^2 + (\Gamma)^2}} d_{2\varepsilon}\,,$$
$$d_{2\varepsilon} = \frac{\sqrt{2}\bar{\boldsymbol{d}}}{q\sqrt{\pi\Gamma}}\,, \tag{5.2}$$

where $\bar{\boldsymbol{d}}$ is the matrix element of dipole moment between the ground and excited molecular electronic states, and q is the well-known Fano asymmetry parameter expressed as

$$q = \frac{\langle b|d|2\rangle}{\pi\langle 2|d|\varepsilon\rangle\langle\varepsilon|d|a\rangle}\,,$$
$$|b\rangle = |a\rangle + P\int \frac{V(\varepsilon)}{\epsilon - \varepsilon}|\varepsilon\rangle\, d\varepsilon\,, \tag{5.3}$$

and Γ is the half-width of the structure in the continuum $|\varepsilon\rangle$ due to the embedding of the discrete state $|a\rangle$. In the case of Feshbach resonance, 2Γ can be identified with

TH-1819_11612116

the width of the resonance. In the dressed continuum picture, the wave-function of the system is a coherent superposition of the two bound states $|1\rangle$, $|2\rangle$ and the dressed continuum $|\epsilon\rangle$ as given by

$$|\psi(t)\rangle = C_1(t)|1\rangle + C_2(t)|2\rangle + \int C_\epsilon(t)|\epsilon\rangle\, d\epsilon\,, \tag{5.4}$$

where C_1, C_2 and C_ϵ are the superposition coefficients. The corresponding density matrix is expressed as

$$\rho = |\psi(t)\rangle\langle\psi(t)|\,. \tag{5.5}$$

The time-dependent Hamiltonian of the system under the electric dipole approximation can be written as

$$\begin{aligned}
H =& H_0 + H_I\,, && \text{(5.6a)}\\
H_0 =& \hbar\omega_1|1\rangle\langle 1| + \hbar\omega_2|2\rangle\langle 2| + \int \epsilon|\epsilon\rangle\langle\epsilon|\, d\epsilon\,, && \text{(5.6b)}\\
H_I =& -|1\rangle\langle 2|\boldsymbol{d}_{12}[\mathcal{E}_p e^{-i\omega_p t} + c.c.]\\
&-|2\rangle\langle 1|\boldsymbol{d}_{21}[\mathcal{E}_p e^{-i\omega_p t} + c.c.]\\
&-\int |\epsilon\rangle\langle 2|\boldsymbol{d}_{\epsilon 2}[\mathcal{E}_c e^{-i\omega_c t} + c.c.]\, d\epsilon\\
&-\int |2\rangle\langle\epsilon|\boldsymbol{d}_{2\epsilon}[\mathcal{E}_c e^{-i\omega_c t} + c.c.]\, d\epsilon\,. && \text{(5.6c)}
\end{aligned}$$

where $\boldsymbol{d}_{ij} = \langle i|d.\hat{e}|j\rangle$ are dipole moments corresponding to $|i\rangle \leftrightarrow |j\rangle$ transition. The free-bound stimulated linewidth due to control field is given by $G_c = \frac{|\boldsymbol{d}_{\varepsilon 2}\mathcal{E}_c|^2}{\hbar}$. The dynamics of the atom-molecule coupled system is governed by the following master equation

$$\dot{\rho} = \frac{i}{\hbar}[H, \rho] - \mathcal{L}\rho\,. \tag{5.7}$$

The term $\mathcal{L}\rho$ is Liouville operator which represents all the incoherent processes and is given by

$$\mathcal{L}\rho = \gamma\left(\rho|2\rangle\langle 2| - 2\rho_{22}|1\rangle\langle 1| + |2\rangle\langle 2|\rho\right)\,. \tag{5.8}$$

where γ is the spontaneous decay rate of state $|2\rangle$ to $|1\rangle$. Note that, since the transition $|2\rangle \leftrightarrow |\epsilon\rangle$ is driven by a strong control field we have neglected bound to continuum spontaneous emission. In the weak probe field limit, the dynamics of atomic coher-

TH-1819_11612116

ences for the Λ system are governed by

$$\begin{aligned} i\hbar\dot{\rho}_{21} =& \hbar(\omega_2-\omega_1)\rho_{21} - \boldsymbol{d}_{21}[\mathcal{E}_p e^{-i\omega_p t} + c.c.] \\ & - \int \rho_{\epsilon 1}\boldsymbol{d}_{2\epsilon}[\mathcal{E}_c e^{-i\omega_c t} + c.c.]\, d\epsilon - i\hbar\gamma\rho_{21}\,. \\ i\hbar\dot{\rho}_{\epsilon 1} =& (\epsilon - \hbar\omega_1)\rho_{\epsilon 1} - \rho_{21}\boldsymbol{d}_{\epsilon 2}[\mathcal{E}_c e^{-i\omega_c t} + c.c.]\,. \end{aligned} \tag{5.9}$$

Under the unitary transformations $\sigma_{21} = \rho_{21}e^{i\omega_p t}$, $\sigma_{\epsilon 1} = \rho_{\epsilon 1}e^{i(\omega_p-\omega_c)t}$ and rotating wave approximation Eq. (5.9) reduce to

$$\begin{aligned} i\hbar\dot{\sigma}_{21} =& -(\hbar\Delta_p + i\hbar\gamma)\sigma_{21} - \boldsymbol{d}_{21}\mathcal{E}_p \\ & - \int \rho_{\epsilon 1}\boldsymbol{d}_{2\epsilon}\mathcal{E}_c\, d\epsilon\,. \\ i\hbar\dot{\sigma}_{\epsilon 1} =& (\epsilon - \hbar\omega_1 - \hbar\omega_p + \hbar\omega_c)\sigma_{\epsilon 1} - \sigma_{21}\boldsymbol{d}_{\epsilon 2}\mathcal{E}_c^*\,. \end{aligned} \tag{5.10}$$

Where $\Delta_p = (\omega_p - (\omega_2 - \omega_1))$, is the probe detuning.
In the next section we use these density matrix equation to find out the probe susceptibility in the steady state limit. We then study the dependency of probe susceptibility on G_c and resonance width Γ.

5.1.3 Susceptibility of the medium

Here we evaluate the probe susceptibility in the steady-state limit. Our assumption for steady-state analysis of the system may be justified for a magnetically induced narrow Feshbach resonance [153] whose linewidth $\Gamma \propto \Delta_B$ where Δ_B is the zero-crossing magnetic field. Furthermore, in the limit $\epsilon \to 0$ we have $\Gamma \propto \sqrt{\epsilon}$. The lifetime of the resonance is $\tau \sim 1/\Gamma$. We assume that the lifetime of the resonance would be in the millisecond regime which is long enough compared to the lifetime of the excited state (typically in the microsecond regime).
In the steady state limit, the probe susceptibility χ of the medium at frequency ω_p can be determined by the atomic coherence σ_{21}. From Eq. (5.10) we have

$$\begin{aligned} \sigma_{21} =& \frac{-\boldsymbol{d}_{21}\mathcal{E}_p}{\hbar\Delta_p + i\hbar\gamma + \mathcal{E}_c^2\beta}\,, \\ \beta =& \int \frac{\boldsymbol{d}_{2\epsilon}\boldsymbol{d}_{\epsilon 2}}{\epsilon + \hbar\omega_c - \hbar\omega_1 - \hbar\omega_p}\, d\epsilon\,. \end{aligned} \tag{5.11}$$

The polarization of the medium in terms of atomic coherence is given by

$$P(\omega_p) = \mathcal{N}\boldsymbol{d}_{12}\sigma_{21}\,. \tag{5.12}$$

TH-1819_11612116

where $\mathcal{N}$ is the density of molecular medium. Also polarization can be expressed in terms of medium susceptibility $\chi(\omega_p)$ as

$$P(\omega_p) = \epsilon_0 \chi(\omega_p) \mathcal{E}_p \,. \tag{5.13}$$

Both the above Eqs. (5.12) and (5.13) leads to the probe susceptibility as

$$\chi(\omega_p) = -\frac{\mathcal{N}}{\epsilon_0} \frac{|\boldsymbol{d}_{12}|^2}{(\hbar\Delta_p + i\hbar\gamma + \mathcal{E}_c^2\beta)} \,. \tag{5.14}$$

$$\beta = \lim_{\zeta \to 0} \int_{\epsilon_{th}}^{\infty} \frac{\boldsymbol{d}_{2\epsilon} \boldsymbol{d}_{\epsilon 2}}{\epsilon + \hbar\omega_c - \hbar\omega_1 - \hbar\omega_p - i\zeta} \, d\epsilon \,. \tag{5.15}$$

In order to get an analytical expression of the probe susceptibility as in Eq. (5.14), we proceed by expressing bound to the dressed continuum dipole moment $\boldsymbol{d}_{2\epsilon}$ in terms of bound to bare continuum dipole moment $\boldsymbol{d}_{2\varepsilon}$ using Eq. (5.2) and then substituting it in the Eq. (5.15). Next we extend ϵ_{th} to $-\infty$ as $\boldsymbol{d}_{2\varepsilon}$ is a slowly varying function of energy near resonance, and tends to zero at large energies *i.e.*, very far from the resonance. Hence $\boldsymbol{d}_{2\varepsilon}$ can safely be taken as constant in energy. This approach has been used earlier for solving bound-continuum coupled problems [164, 168]. Further, we use Cauchy's residue method to solve the integral in Eq. (5.15) and arrive at

$$\beta = \pi |\boldsymbol{d}_{2\varepsilon}|^2 \left(\frac{(q-i)^2 \Gamma}{(\hbar\Delta_c - \hbar\Delta_p) - i\Gamma} + i \right) \,. \tag{5.16}$$

Where $\Delta_c = (\omega_c - (\omega_2 - \omega_a))$, is the control detuning.

5.1.4 Pulse propagation equation

In order to see the effect of optical response on the pulse propagation dynamics, we consider a Gaussian probe pulse propagation [167] through Λ-type atom-molecule medium of length L. The envelope form of the input probe field is given by

$$\mathcal{E}_p(z=0,\tau) = \mathcal{E}_0 e^{-\frac{(\tau^2 - \tau_p^2)}{\sigma_p^2}} \,. \tag{5.17}$$

where $\mathcal{E}_0$ is the amplitude and σ_p is the width of the input pulse. After traveling a distance L through a medium, the output probe field has the form

$$\mathcal{E}_p(z=L,\tau) = \int_{-\infty}^{\infty} \mathcal{E}_p(z=0,\omega) e^{(-i(\omega t - \frac{\omega}{c} n(\omega) L)} \, d\omega \tag{5.18}$$

TH-1819_11612116

where $n(\omega) = 1 + 2\pi\chi(\omega)$. The Fourier transform of initial input pulse $\mathcal{E}_p(z = 0, \tau)$ and is given by

$$\mathcal{E}_p(z = 0, \omega) = \frac{\mathcal{E}_0}{\sqrt{\pi\sigma^2}} e^{-\frac{(\omega^2 - \omega_p^2)}{\sigma^2}} . \tag{5.19}$$

If we assume that the refractive index varies slowly around $\omega = \omega_p$ then

$$\begin{aligned} \omega n(\omega) = \omega_p n(\omega_p) + (\omega - \omega_p) \frac{\partial(\omega n(\omega))}{\partial\omega}|_{\omega=\omega_p} \\ + \frac{(\omega - \omega_p)^2}{2} \frac{\partial^2(\omega n(\omega))}{\partial\omega^2}|_{\omega=\omega_p} . \end{aligned} \tag{5.20}$$

substituting Eq. (5.20) and Eq. (5.21) in Eq. (5.18), we arrive at

$$\begin{aligned} \mathcal{E}_p(z = L, \tau) = \frac{\mathcal{E}_0}{\sqrt{1 - iL\kappa}} e^{(-i(\omega_p t - \frac{\omega_p}{c} n(\omega_p) L)} \\ e^{-\frac{\sigma^2}{4} \frac{(t - L/v_g)^2}{1 - iL\kappa}} . \end{aligned} \tag{5.21}$$

where v_g is the group velocity of the pulse and is given by

$$v_g = \frac{c}{1 + 2\pi Re(\chi(\omega_p)) + 2\pi\omega_p \frac{\partial Re(\chi(\omega_p))}{\partial\omega_p}} = \frac{c}{n_g} . \tag{5.22}$$

and the group velocity dispersion (GVD) is denoted by κ and is defined as

$$\kappa = \frac{\sigma^2}{2c} \frac{\partial^2(\omega n(\omega))}{\partial\omega^2}|_{\omega=\omega_p} . \tag{5.23}$$

For a positive v_g, the group delay is τ_g and is expressed as

$$\tau_g = \left(\frac{L}{v_g} - \frac{L}{c} \right) . \tag{5.24}$$

5.2 Results and discussion

Here we present the results of our investigations. First, we discuss the general features of the dressed states and then discuss our numerical results for model systems. Given the current experimental progress on production of ultracold molecules, Cs_2 and KRb molecular systems seem to be promising candidates for realization of our model. Recently, the production of ultracold Cs_2 molecular gas has been experimentally demonstrated [169]. The singlet electronic ground state $X^1\Sigma_g^+$ of Cs_2 with the rovibrational level $|v = 73, J = 2\rangle$ may be regarded as as $|1\rangle$. The electronic excited state $(A^1\Sigma_u^+ - b^3\pi_u)0_u^+$ with the vibrational level $v' = 225$ is assumed to be $|2\rangle$ which

TH-1819_11612116

is coupled to $|1\rangle$ and $|\varepsilon\rangle$ by two coherent fields, namely a weak probe field with wavelength 1006 nm and a control field with wavelength 1126 nm, respectively. For KRb

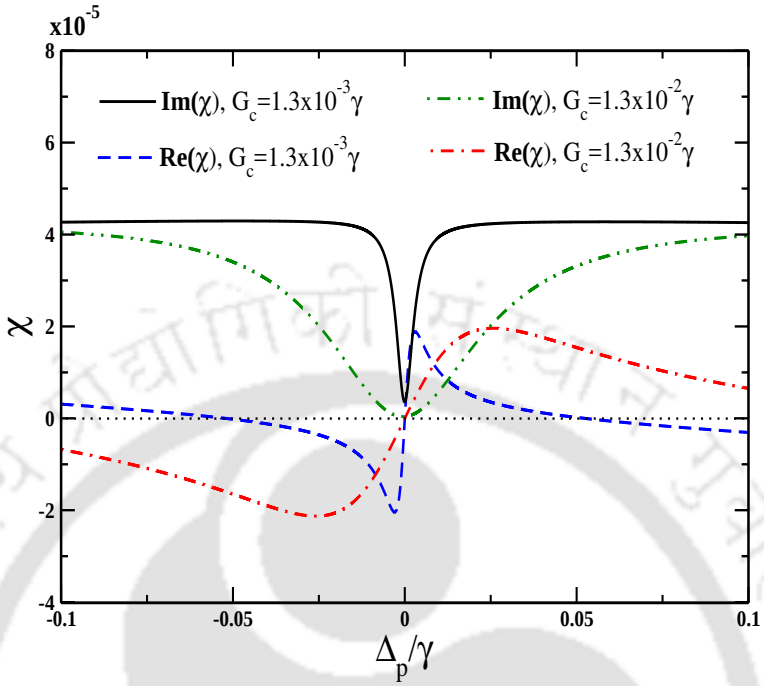

Fig. 5.2 (Color online) The variation of the real and imaginary parts of the susceptibility are plotted as a function of Δ_p (in unit of γ) for control field intensities G_c= $1.3\times10^{-3}\gamma$, and G_c= $1.3\times10^{-2}\gamma$. Other parameters used are $q = 50$, $N = 10^{14}$ molecules/c.c., $\Gamma = 4\times10^{-5}\gamma$, $d_{12} = 0.011ea_0$, $\gamma = 25$ MHz.

system, one may take the singlet electronic ground state $X^1\Sigma$ with the vibrational level $v = 0$ as $|1\rangle$. The electronic excited state $2^3\Sigma$ with the vibrational level $v' = 23$ may be assumed to be $|2\rangle$. The probe and control fields should have wavelength 690 nm and wavelength 970 nm, respectively. The existence of a quasi-bound state $|a\rangle$ embedded in (Cs + Cs) or (K + Rb) collisional continuum is assumed to model a narrow FR. The eigenstates or dressed states of the Hamiltonian of Eq. (5.6a) namely $|1\rangle$, $|+\rangle$, and $|-\rangle$ as discussed in section 1.4 of chapter 1. The dressed states $|+\rangle$, and $|-\rangle$ are separated by G_c. The right and left absorption peaks of Fig.5.2 are basically due to the transitions from the ground state $|1\rangle$ to the two dressed states $|+\rangle$ and $|-\rangle$, respectively. However in the absence of control field, the probe field will be highly absorbed when the probe frequency ω_p is closely tuned to $|1\rangle \leftrightarrow |2\rangle$ transition. Since the spacing between the state $|+\rangle$ and state $|-\rangle$ is proportional to G_c, as G_c increases the spacing between the state $|+\rangle$ and state $|-\rangle$ increases. Hence, the transparency window increases with the increase of G_c as can be seen from Fig.5.2. It is well known that any change in the absorption profile leads to considerable changes in the dispersion of the system [4]. As G_c increases, there is a broadening in the transparency window leading to a decrease in the slope of the dispersion as shown in Fig.5.2. So, by

TH-1819_11612116

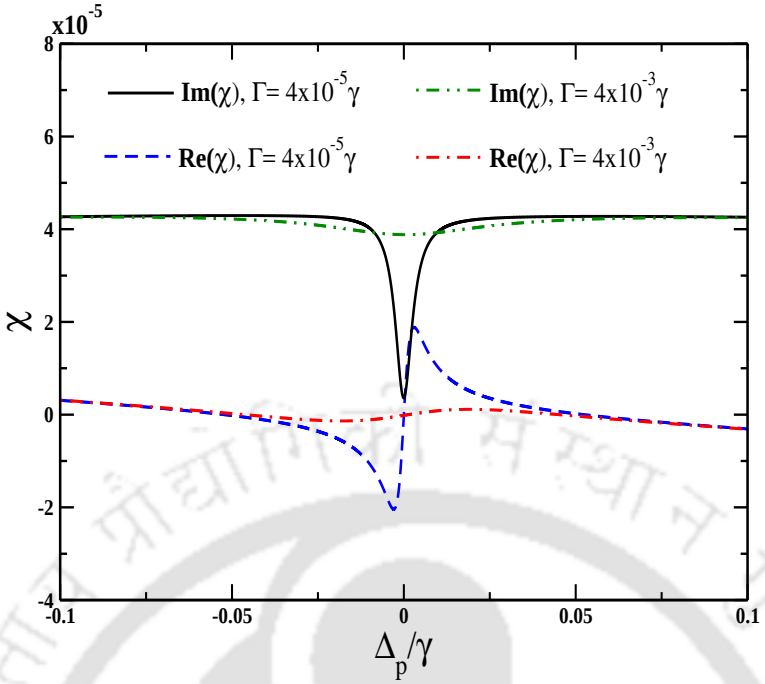

Fig. 5.3 (Color online) The variation of the real and imaginary parts of the susceptibility are plotted as a function of Δ_p (in unit of γ) for Feshbach resonance widths $\Gamma = 4\times10^{-5}\gamma$, and $\Gamma = 4\times10^{-3}\gamma$. Other parameters remain same as in Fig.5.2 with $G_c = 1.3\times10^{-3}\gamma$.

controlling the slope of the dispersion one can control the group velocity of the probe field [4]. Next, we investigate probe susceptibility for different resonance widths Γ while keeping G_c fixed. The aim here is to get a very narrow EIT window along with very less absorption as it leads to interesting application in high sensitive magnetometers, interferometry, high precision spectroscopy, ultra slow light etc., because of the sharp variation of the index inside the window.

We find that the absorptive and dispersive properties of the medium depend on the width of FR. The width Γ of FR for collision between Cs and Cs and between K and Rb at low energy can be calculated from the parameters given in Refs. [153, 171, 172] and is estimated to be about $4\times10^{-5}\gamma$ and 0.2γ respectively. We notice from Fig.5.3 that for $\Gamma = 4\times10^{-5}\gamma$, the transparency window becomes very narrow and the absorption goes to almost zero. However, with the increase in Γ, the width of the absorption profile increases, because the probability of transitions from ground state $|1\rangle$ to the two dressed states $|+\rangle$ and $|-\rangle$ increases. This increase in the width of the absorption profile leads to a decrease in the width of the transparency window along with an increase in the absorption. Hence, (Cs+Cs) system is much more suitable for slow light effect as it has narrower Feshbach resonance width than that of (K+Rb) one. Thus, our model will be realizable for ultracold diatomic systems having very narrow Feshbach resonance line width [173]-[176].

TH-1819_11612116

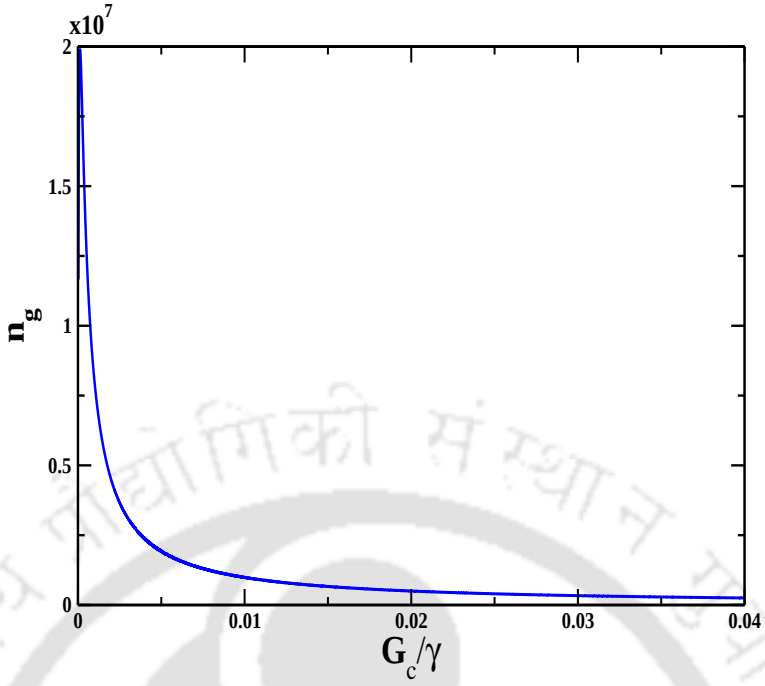

Fig. 5.4 (Color online) The variation of group index n_g is plotted as a function of G_c (in unit of γ). Other parameters remain same as in Fig.5.2.

The asymmetric shape in the EIT spectrum can be explained by the Fano parameter q. A small Fano parameter q results in when $|2\rangle$ is equally bound to both the states $|a\rangle$ and the bare continuum $|\varepsilon\rangle$ *i.e.*, the transition corresponding to $|2\rangle \leftrightarrow |a\rangle$ and $|2\rangle \leftrightarrow |\varepsilon\rangle$ are of equal strength. Hence the EIT line shape is determined by both these transitions, resulting in an asymmetric profile. However, this asymmetry can be removed by taking a very large Fano parameter q for which, the transition $|2\rangle \leftrightarrow |a\rangle$ is very strong compared to the transition $|2\rangle \leftrightarrow |\varepsilon\rangle$. In this case, the line shape is solely determined by $|2\rangle \leftrightarrow |a\rangle$ transition which has Lorentzian profile and EIT spectrum tends to become symmetric. The group index n_g decreases with increase of G_c as shown in Fig.5.4. One can see from the denominator of Eq. (5.22) that group index n_g depends upon the slope of the dispersion. The slope of the dispersion can be manipulated by changing G_c. It is evident from Eq. (5.21) that real and imaginary parts of both the refractive index $n(\omega)$ and GVD play an important role to modify the amplitude and width of the incident probe pulse. Therefore the amplitude reduction and spreading of the pulse width leads to shape distortion along the length of the propagation. The main aim here is to obtain pulse propagation free from any distortion and absorption but with large group delay. This can be achieved by tailoring the dispersion of the medium using coherent control field. For this purpose we study the propagation of probe pulse with two different shapes namely, a Gaussian pulse and a hyperbolic secant pulse in this medium. Fig.5.5 shows pulse envelope

TH-1819_11612116

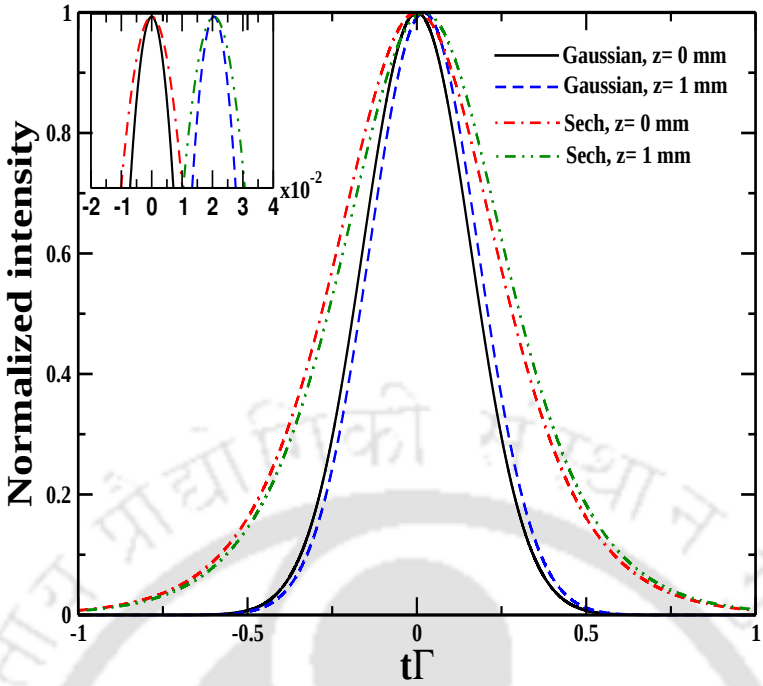

Fig. 5.5 (Color online) Propagation of both Gaussian pulse and hyperbolic secant pulse is shown for a spectral width of 20 KHz for different medium length. The time delay at 1 mm was 20 μs and the transmission of the probe is 74.0%. Other parameters remain same as in Fig.5.2 with G_c= $1.3\times10^{-3}\gamma$.

for both the Gaussian and hyperbolic secant pulse at different propagation distances. From Fig.5.5, we notice a considerable slowing down of the probe pulse. For the parameters of Cs_2 molecules, we find that both the Gaussian and hyperbolic secant pulses have a pulse delay of 20 μs for a maximum of 1 mm length of propagation in case of ultracold gases. The group velocity v_g calculated from the pulse delay as in Eq. (5.24) and that from Eq. (5.22) are in good agreement, and is about 50 m s^{-1}. The transmissions through 1 mm are found to be 74.0% for both the Gaussian and the hyperbolic secant pulses. Further one has to note that the distortion inflicted to the pulse can be minimized by keeping the spectral width of the pulse well inside the transparency window.

We next discuss DBP. Figure 5.6(a) shows the variation of DBP and transmission as a function of G_c. From this figure we see that as G_c increases, DBP decreases. This is because of the fact that the rate of decrease in the time-delay of pulse is very high in comparison to the rate of increase of the transparency width. Therefore, the product of time-delay and the spectral width of the transparency window *i.e.*, DBP decreases with the increase in G_c. We can also notice from Fig.5.6(a) that the transmission increases with the increase of G_c. The increase in transmission is due to the increase in the transparency window caused by increasing G_c. Generally, in a slow light experiment, a very low time delay corresponds to a high bandwidth, where

TH-1819_11612116

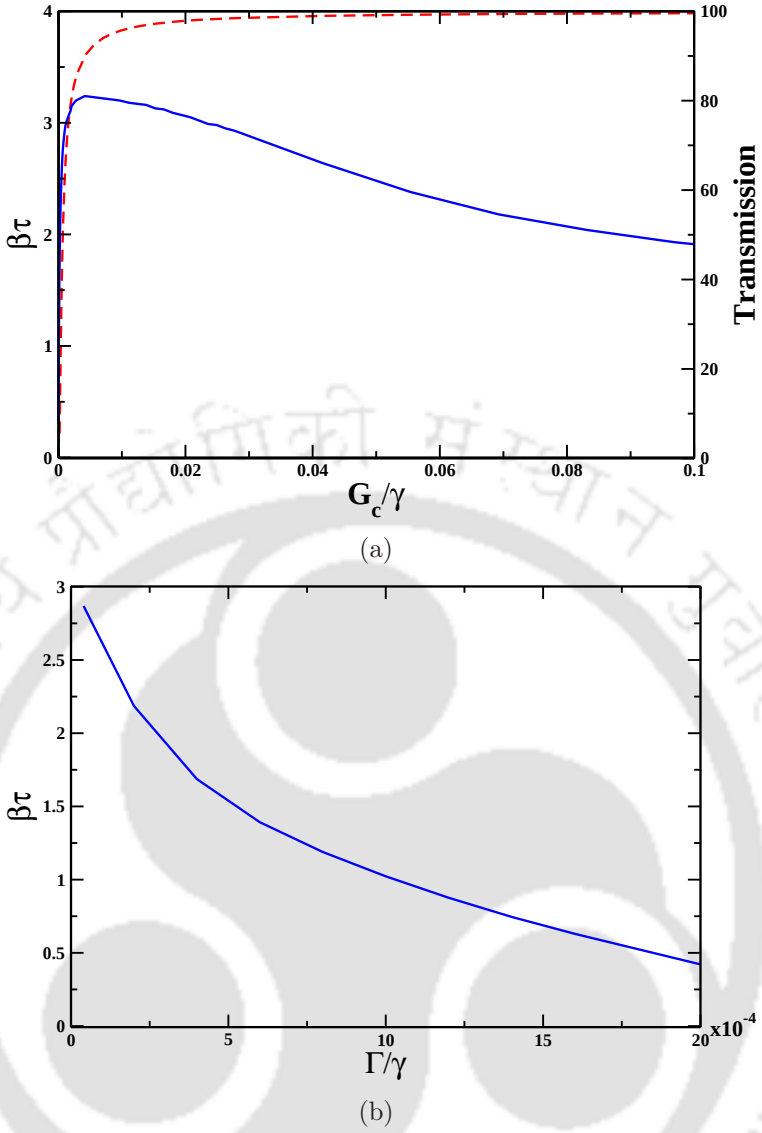

Fig. 5.6 (Color online) Panel (a) shows Delay-Bandwidth product (solid blue line) and Transmission (red long dashed line) as a function of G_c (in unit of γ) and (b) shows Delay-Bandwidth product as a function of Feshbach resonance width Γ (in unit of γ).Other parameters remain same as in Fig.5.2.

as a very high time delay corresponds to a low bandwidth. Therefore, one needs to optimize DBP to create a balance between time delay and the bandwidth for efficient slow light applications. The optimum DBP in our system is estimated to be around 3, which corresponds to G_c of $2\times10^{-3}\gamma$, a pulse delay of 15 μs and a transmission of 77.8% for a Gaussian pulse with a spectral width of 20 KHz. Furthermore, we notice from Fig.5.6(b) that as Γ increases DBP decreases. This is because with the increase in Γ the bandwidth increases, however the rate of decrease in the time-delay of pulse is very high in comparison to the rate of increase of the bandwidth width. Therefore,

TH-1819_11612116

the product of time-delay and the bandwidth of the transparency window *i.e.*, DBP decreases with the increase in Γ.

5.3 Conclusion

In conclusion, we have investigated light pulse propagation in atom-molecule coupled model systems. We have shown that the transparency window can be achieved in a medium where a molecular state is coupled with the continuum of atom-atom collisional states with a control field. We have found that the width of the transparency window can be controlled by both the stimulated line-width due to control field as well as Feshbach resonance width. We have demonstrated that controllable group velocity can be obtained by narrowing Feshbach resonance width Γ. We have also shown that dispersion-less pulse propagation is possible when pulse width is well contained within the transparency window. Furthermore, we have optimized DBP for Cs_2 atom-molecule coupled model system for a pulse with spectral width of 20 KHz, and optimum DBP for this system is found to be 3. Hence our model can be applied to those ultracold homo- or hetero-nuclear molecules for which the constituents atoms should exhibit narrow Feshbach resonance in ground-state collisions. Furthermore, these results may stimulate further studies into the effects such as optical switching, storage of pulses, information processing *etc.* using ultracold atom-molecule coupled systems.

TH-1819_11612116

Chapter 6

Conclusions and Future outlook

In conclusion, we show that the properties of optical medium can be manipulated by using quantum interference effects induced by coherent atom-light interaction. Variation of a medium's optical properties both in time and space domains is the key to control the properties of light in these optical systems. The important findings on coherent control of light in different optical systems are as follows:

In chapter 2, we have demonstrated diffractionless propagation of narrow optical beam through tunable waveguide in a N-type four level system. For this purpose, we have used a suitable spatially varying control and Kerr beams to manipulate medium susceptibility in transverse direction. We found that the competition between control beam induced transparency and Kerr beam induced absorption along the transverse directions of the medium forms a narrow atomic waveguide. Further, the contrast and tunability of the waveguide can also be changed by varying the intensity of the Kerr beam. By numerically solving the propagation equation of probe, we found that arbitrary narrow probe structures can be transferred through homogeneously broadened atomic vapor to several orders of Rayleigh lengths without any distortion.

In chapter 3, we set out to explain the experimental results of Radwell *et al.* [Phys. Rev. Lett. 114, 123603 (2015)] on generation of structured beam in a closed loop tripod system. We have shown that in the presence of a phase structured probe and a TMF, the absorption for both weak and strong probe field cases oscillates periodically in the azimuthal plane. Our numerical results on beam propagation exhibit the formation of petal like beam structure for both weak and strong field cases due to the azimuthally varying medium absorption. We found that the contrast of the structured beam can be controlled by changing the strength of both probe and TMF. Further, the formed structure can be rotated by controlling the probe strength owing to NMOR.

In chapter 4, we presented a new scheme based on PDEIT to generate structured beams in a closed loop inverted Y-type system. We have considered a phase struc-

TH-1819_11612116

tured probe and a TMF to create a phase-dependent medium absorption. Further, we utilized a spatially dependent control beam to manipulate the phase-dependent medium absorption. We have shown that different control beam structures create different phase structured absorption profiles. By studying the propagation equation, we have shown that various phase structured absorption profiles create structured beams with different spatial patterns.

In chapter 5, we have demonstrated slowing down of light pulse in an atom-molecule coupled system. We have shown how an EIT like feature can be created even in a medium where a molecular state is coupled with the continuum of atom-atom collisional states with a control field. We found that the EIT can be manipulated by changing the strength of the control field as well as the width of the Feshbach resonance. Further a narrow Feshbach resonance can result in ultra slow group velocity and also can lead to very high delay-bandwidth product (DBP).

Future outlook

Coherent control of optical fields using coherent optical media and vice versa have been carried out extensively in recent years. As discussed in this thesis, coherent control of optical fields have many applications in diffraction management, structured beam generation, slow light, etc. The future scope of the present thesis is not only limited to the propagation of optical fields in an atomic medium but also can be extended to other coherent media such as molecular or solid state medium.

In chapter 2, we have discussed about the diffraction control of narrow optical beams in four level system via tunable waveguide. However the induced waveguide has very low efficiency because of large absorption. This high absorption can be made negligible by using atomic medium in closed-loop configuration. These closed atomic systems show zero absorption with high refractive index. Hence creating a waveguide in these media may result in diffraction control of optical beams with high efficiency.

Closed-loop atomic systems show very interesting features where the properties of the medium can be modified by the phase of the interacting optical fields. These techniques have been used in the generation of structured beams and is discussed in chapters 3 and 4 of this thesis. It is observed that the formed structured beams have very low contrast due to the presence of weak optical fields and TMF. The contrast of the structured beams may be increased by using other closed loop systems, where both the phase and the strength of the optical fields play a major role in manipulating the optical properties of the medium.

Our work on propagation of light pulse in ultra-cold atom-molecule system has shown promising results on controlling the group velocity of light and hence can be extended

TH-1819_11612116

to other applications such as storage of light, optical switching, molecular localization, etc.

TH-1819_11612116

TH-1819_11612116

Appendix A

Fourier Split Step Method

In this appendix, we discuss the Fourier split-step method (FSSM), which is used to solve nonlinear differential equations. In general, it is difficult to get an analytical solution to Eq. (2.12). Hence, we use the split-step method to get a numerical solution to this propagation equation. In this regard, we write the propagation equation Eq. (2.12) in the following operator form:

$$\frac{\partial}{\partial z} g = (\hat{D} + \hat{S})\ g\,. \tag{A.1}$$

where $\hat{D} = \frac{i}{2k}(\partial^2/\partial x^2 + \partial^2/\partial y^2)$ is the differential operator and accounts for diffraction either in the medium or in free space. The operator $\hat{S} = 2\pi i K \chi$ is the nonlinear operator and is attributed to the dispersion and absorption of the probe beam. A general solution to Eq. (A.1) for a small propagation distance Δz is of the following form:

$$g(x, y; z + \Delta z) = exp[(\hat{D} + \hat{S})\Delta z]\ g(x, y; z). \tag{A.2}$$

Since $\hat{D}$ and $\hat{S}$, we make use of Baker-Campbell-Hausdorff formula to expand the exponential as

$$exp[(\hat{D} + \hat{S})\Delta z] = exp[\hat{D}\Delta z + \hat{S}\Delta z + \frac{1}{2}[\hat{D}, \hat{S}]\Delta z^2 + ...]. \tag{A.3}$$

If we consider the step size Δz to be very small, then the above equation reduces to

$$exp[(\hat{D} + \hat{S})\Delta z] = exp[\hat{D}\Delta z]\ exp[\hat{S}\Delta z]. \tag{A.4}$$

TH-1819_11612116

Substituting the above equation in Eq. (A.2), we get the following solution to the propagation equation

$$g(x, y; z + \Delta z) = exp[\hat{D}\Delta z]\ exp[\hat{S}\Delta z]\ g(x, y; z). \tag{A.5}$$

The exponential containing $\hat{S}$ can be computed directly in the real space domain using the initial field value $g(x, y; z)$, but to compute $\hat{D}$, we use use the fact that in frequency space, the partial derivatives $\partial/\partial x$ and $\partial/\partial y$ by ik_x and ik_y, respectively, where k_x, k_y are spatial frequencies. Hence, the exponential involving the operator $\hat{D}$ can be written in the fourier space as

$$exp[\hat{D}\Delta z] = exp\left[\frac{-i(k_x^2 + k_y^2)\Delta z}{2k}\right]. \tag{A.6}$$

We then use the above expression to find the product of exponential involving $\hat{D}$ and $\hat{N}$ in the frequency domain as below

$$exp\left[\frac{-i(k_x^2 + k_y^2)\Delta z}{2k}\right] \mathcal{F}[exp[2\pi i K\chi\Delta z]\ g(x, y; z)] \tag{A.7}$$

where $\mathcal{F}$ is the Fourier transform. Next, we use the inverse Fourier transform to write the above expression in the real space, which gives the final solution to the propagation equation as

$$g(x, y; z + \Delta z) = \mathcal{F}^{-1}\left[exp\left[\frac{-i(k_x^2 + k_y^2)\Delta z}{2k}\right] \mathcal{F}[exp[2\pi i K\chi\Delta z]\ g(x, y; z)]\right]. \tag{A.8}$$

TH-1819_11612116

References

[1] S. L. McCall and E. L. Hahn, Phys. Rev. **183**, 457 (1969).

[2] E. Arimondo, Progress in Optics, **35**, 257 (1996).

[3] M. O. Scully and M. S. Zubairy, Quantum Optics, (Cambridge University Press, Cambridge, England, 1997).

[4] S. E. Harris, Phys. Today **50(7)**, 36 (1997).

[5] M. Fleischhauer, and A. Imamoglu, and J. P. Marangos, Rev. Mod. Phys. **77**, 663 (2005).

[6] S. E. Harris, Phys. Rev. Lett. **62**, 1033 (1989).

[7] M. O. Scully, S. Y. Zhu, and A. Gavrielides, Phys. Rev. Lett. **62**, 2813 (1989).

[8] A. Imamolu, J. E. Field, and S. E. Harris, Phys. Rev. Lett. **66**, 1154 (1991).

[9] O. Kocharovskaya, Phys. Rep. **219**, 175 (1992).

[10] T. W. Hansch, M. D. Levenson, and A. L. Schawlow, Phys. Rev. Lett. **26**, 946 (1971).

[11] G. S. Agarwal and T. N. Dey, Laser & Photonics Reviews **3**, 287 (2009).

[12] G. Alzetta, A. Gozzini, L. Moi, and G. Orriols, Nuovo Cimento B **36**, 5 (1976).

[13] S. E. Harris, J. E. Field, and A. Imamoglu, Phys. Rev. Lett. **64** 1107 (1990).

[14] K.-J. Boller, A. Imamoglu, and S. E. Harris, Phys. Rev. Lett. **66**, 2593 (1991).

[15] R. G. Beausoleilp, W. J. Munros, D. A. Rodriguess, and T. P. Spiller, J. Mod. Opt. **51**, 2441 (2004).

[16] L. V. Hau, S. E. Harris, Z. Dutton, and C. H. Behroozi, Nature **397**, 594 (1999).

[17] K. P. Heeg, J. Haber, D. Schumacher, L. Bocklage, H.-C. Wille, K. S. Schulze, R. Loet-zsch, I. Uschmann, G. G. Paulus, R. Rüffer, R. Röhlsberger, and J. Evers, Phys. Rev. Lett. **114**, 203601 (2015).

[18] D. F. Phillips, A. Fleischhauer, A. Mair, R. L. Walsworth, and M. D. Lukin, Phys. Rev. Lett. **86**, 783 (2001).

[19] T. N. Dey and G. S. Agarwal, Phys. Rev. A **67**, 033813 (2003).

[20] A. G. Truscott, M. E. J. Friese, N. R. Heckenberg, and H. Rubinsztein-Dunlop, Phys. Rev. Lett. **82**, 1438 (1999).

TH-1819_11612116

[21] R. R. Moseley, S. Shepherd, D. J. Fulton, B. D. Sinclair, and M. H. Dunn, Phys. Rev. Lett. **74**, 670 (1995).

[22] R. R. Moseley, S. Shepherd, D. J. Fulton, B. D. Sinclair, and M. H. Dunn, Phys. Rev. A **53**, 408 (1996).

[23] V. A. Sautenkov, H. Li, Y. V. Rostovtsev, and M. O. Scully, Phys. Rev. A **81**, 063824 (2010).

[24]] D. L. Zhou, L. Zhou, R. Q. Wang, S. Yi, and C. P. Sun, Phys. Rev. A **76**, 055801 (2007).

[25] O. N. Verma and T. N. Dey, Phys. Rev. A **91**, 013820 (2015).

[26] R. Kapoor and G. S. Agarwal, Phys. Rev. A **61**, 053818 (2000).

[27] D. D. Yavuz and N. A. Proite, Phys. Rev. A **76**, 041802(R)(2007).

[28] A. V. Gorshkov, L. Jiang, M. Greiner, P. Zoller, and M. D. Lukin, Phys. Rev. Lett. **100**, 093005 (2008).

[29] H. Li, V. A. Sautenkov, M. M. Kash, A. V. Sokolov, G. R. Welch, Y. V. Rostovtsev, M. S. Zubairy, and M. O. Scully, Phys. Rev. A **78**, 013803 (2008).

[30] E. Paspalakis and P. L. Knight, Phys. Rev. A **63**, 065802 (2001).

[31] J. A. Miles, D. Das, Z. J. Simmons, and D. D. Yavuz, Phys. Rev. A **92**, 033838 (2015).

[32] W. D. Phillips, Rev. Mod. Phys. **70**, 721 (1998).

[33] K. S. Johnson, J. H. Thywissen, W. H. Dekker, K. K. Berggren, A. P. Chu, R. Younkin, and M. Prentiss, Science **280**, 1583 (1998).

[34] S. A. Carvalho and L. E. E. de Araujo, Phys. Rev. A **83**, 053825 (2011).

[35] W. Duan, L. Zhao, and S. F. Yelin, Phys. Rev. A **82**, 013809 (2010).

[36] M. D. Lukin, S. F. Yelin, M. Fleischhauer, and M. O. Scully, Phys. Rev. A **60**, 3225 (1999).

[37] C. Y. Ye, A. S. Zibrov, Yu. V. Rostovtsev, and M. O. Scully, Phys. Rev. A **65**, 043805 (2002).

[38] E. A. Korsunsky, N. Leinfellner, A. Huss, S. Baluschev, and L. Windholz, Phys. Rev. A **59**, 2302 (1999).

[39] Y. Niu, S. Gong, R. Li, Z. Xu, and X. Liang, Opt. Lett. **30**, 3371 (2005).

[40] O. N. Verma and T. N. Dey, Phys. Rev. A **91**, 013820 (2015).

[41] J. Sheng, X. Yang, U. Khadka and M. Xiao, Opt. Exp. **19**, 17059 (2011).

[42] C. Liu, S. Gong, D. Cheng, X. Fan, and Z. Xu, Phys. Rev. A **73**, 025801 (2006).

[43] R.-G. Wan, T.-Y. Zhang, and J. Kou, Phys. Rev. A **87**, 043816 (2013).

[44] N. Radwell, T. W. Clark, B. Piccirillo, S. M. Barnett, and S. Franke-Arnold, Phys. Rev. Lett. **114**, 123603 (2015).

TH-1819_11612116

[45] G. S. Agarwal, Springer Tracts in Modern Physics, **70** (1974).

[46] H. M. Gibbs, Phys. Rev. Lett. **29**, 459 (1972).

[47] D. Hockel, and O. Benson, Phys. Rev. Lett. **105**, 153605 (2010).

[48] G. Alzetta, S. Gozzini, A. Lucchesini, S. Cartaleva, T. Karaulanov, C. Marinelli and L. Moi, Phys. Rev. A **69**, 063815 (2004).

[49] L. V. Hau, S. E. Harris, Z. Dutton, and C. H. Behroozi, Nature Phys. **397**, 594 (1999).

[50] D. L. Fisher and T. Tajima, Phys. Rev. Lett. **71**, 4338 (1993).

[51] M. Shuker, O. Firstenberg, R. Pugatch, A. Ron, and N. Davidson, Phys. Rev. Lett. **100**, 223601 (2008).

[52] S. Schiemann, A. Kuhn, S. Steuerwald, and K. Bergmann, Phys. Rev. Lett. **71**, 3637 (1993).

[53] E. S. Fry, X. Li, D. Nikonov, G. G. Padmabandu, M. O. Scully, A. V. Smith, F. K. Tittel, C. Wang, S. R. Wilkinson, and S. Y. Zhu, Phys. Rev. Lett. **70**, 3235 (1993).

[54] J. E. Thomas, P. R. Hemmer, S. Ezekiel, C. C. Leiby, Jr., R. H. Picard, and C. R. Willis, Phys. Rev. Lett. **48**, 867 (1982).

[55] S. Knappe, V. Shah, P. D. D. Schwindt, L. Hollberg, J. Kitching, Li-Anne Liew, and J. Moreland, Appl. Phys. Lett. **85**, 1460 (2004).

[56] M. V. Berry and N. L. Balazs, Am. J. Phys. **47**, 264 (1979).

[57] G. A. Siviloglou, J. Broky, A. Dogariu, and D. N. Christodoulides, Phys. Rev. Lett. **99**, 213901 (2007).

[58] J. Durnin, J. J. Miceli Jr., and J. H. Eberly, Phys. Rev. Lett. **58**, 1499 (1987).

[59] D. McGloin and K. Dholakia, Contemp. Phys. **46**, 15 (2005).

[60] J. C. Gutiérrez-Vega, M. D. Iturbe-Castillo, and S. Chávez-Cerda, Opt. Lett. **25**, 1493 (2000).

[61] P. Zhang, Y. Hu, T. Li, D. Cannan, X. Yin, R. Morandotti, Z. Chen, and X. Zhang, Phys. Rev. Lett. **109**, 193901 (2012).

[62] M. A. Bandres, J. C. Gutiérrez-Vega, and S. Chávez-Cerda, Opt. Lett. **29**, 44 (2004).

[63] P. K. Vudyasetu, R. M. Camacho, and J. C. Howell, Phys. Rev. Lett. **100**, 123903 (2008).

[64] M. Kiffner, J. Evers, and M. S. Zubairy, Phys. Rev. Lett. **100**, 073602 (2008).

[65] K. T. Kapale and G. S. Agarwal, Opt. Lett. **35**, 2792 (2010).

[66] T. N. Dey and J. Evers, Phys. Rev. A **84**, 043842 (2011).

[67] T. N. Dey and G. S. Agarwal, Opt. Lett. **34**, 3199 (2009).

TH-1819_11612116

[68] R. R. Moseley, S. Shepherd, D. J. Fulton, B. D. Sinclair, and M. H. Dunn, Phys. Rev. A **53**, 408 (1996).

[69] J. Cheng and S. Han, Opt. Lett. **32**, 1162 (2007).

[70] L. Zhang, T. N. Dey, and J. Evers, Phys. Rev. A **87**, 043842 (2013).

[71] O. N. Verma, L. Zhang, J. Evers, and T. N. Dey, Phys. Rev. A **88**, 013810 (2013).

[72] D.-S. Ding, Z.-Y. Zhou, and B.-S. Shi, Opt. Lett. **39**, 240 (2014).

[73] M. Cao, L. Zhang, Y. Yu, F. Ye, D. Wei, W. Guo, S. Zhang, H. Gao, and F. Li, Opt. Lett. **39**, 2723 (2014).

[74] T. F. Scott, B. A. Kowalski, A. C. Sullivan, C. N. Bowman, and R. R. McLeod, Science, **324**, 913 (2009).

[75] T. L. Andrew, H.-Y. Tsai, and R. Menon, Science, **324**, 917 (2009).

[76] S. W. Hell, Nat. Biotechnol., **21**, 1347 (2003).

[77] S. W. Hell, Science, **316**, 1153 (2007).

[78] T. N. Dey and G. S. Agarwal, Phys. Rev. A **76**, 015802 (2007).

[79] S.-C. Tian, Z.-H. Kang, C.-L. Wang, R.-G. Wan, J. Kou, H. Zhang, Y. Jiang, H.-N. Cui, and J.-Y. Gao, Opt. Commun. **285**, 294 (2012).

[80] A. D. Bandrauk and H. Shen, J. Phys. A: Math. Gen. **27**, 7147 (1994).

[81] G. P. Agrawal and D. N. Pattanayak, J. Opt. Sci. Am. **69**, 575 (1979).

[82] P. Vaveliuk, B. Ruiz, and A. Lencina, Opt. Lett. **32**, 927 (2007).

[83] G. Molina-Terriza, J. P. Torres, and L. Torner, Phys. Rev. Lett. **88**, 013601 (2003).

[84] J. Leach, M. J. Padgett, S. M. Barnett, S. Franke-Arnold, and J. Courtial, Phys. Rev. Lett. **88**, 257901 (2002).

[85] K.-P. Marzlin and W. Zhang, Phys. Rev. Lett. **79**, 4728 (1997).

[86] J. W. R. Tabosa and D. V. Petrov, Phys. Rev. Lett. **83**, 4967 (1999).

[87] H. He, M. E. Friese, N. R. Heckenberg, and H. Rubinsztein-Dunlop, Phys. Rev. Lett. **75**, 826 (1995).

[88] L. Paterson, M. P. MacDonald, J. Arlt, W. Sibbett, P. E. Bryant, and K. Dholakia,Science **292**, 912 (2001).

[89] P. Zupancic, P. M. Preiss, A. Lukin, M. E. Tai, M. Rispoli, R. Islam , and M. Greiner, Opt. Express **24**, 013881 (2016).

[90] U. T. Schwarz, M. A. Bardres, and J. C. G. Vege, Opt. Lett. **29**, 1870 (2004).

[91] D. Naidoo, K. A. Ameur, M. Brand, and A. Forbes, Appl. Phys. B. **106**, 683 (2012).

[92] M. Sakamoto, K. Oka, R. Morita, and N. Murakami, Opt. Lett. **38**, 3661 (2013).

TH-1819_11612116

[93] L. Burger, and A. forbes, Opt. Express **16**, 12707 (2008).

[94] I. A. Litvin, L. Burger, and A. forbes, Opt. Express **15**, 14065 (2007).

[95] A. Jesacher, S. Furhapter, S. Bernet, and M. R. Marte, Opt. Express **12**, 4129 (2004).

[96] C. H. J. Schmitz, K. Uhrig, J. P. Spatz, and J. E. Curtis, Opt. Express **14**, 6604 (2006).

[97] S. F. Arnold, J. Leach, M. J. Padgett, V. E. Lembessis, D. Ellinas, A. J. Wright, J. M. Girkin, P. Ohberg, and A. S. Arnold, Opt. Express **15**, 8619 (2007).

[98] L. Marrucci, C. Manzo, and D. Paparo, Phys. Rev. Lett. **96**, 163905 (2006).

[99] F. Renzoni, W. Maichen, L. Windholz, and E. Arimondo, Phys. Rev. A **55**, 3710 (1997).

[100] S. J. Buckle, S. M. Barnett, P. L. Knight, M. A. Lauder, and D. T. Pegg, Opt. Acta **33**, 1129 (1986).

[101] D. V. Kosachiov, B. G. Matisov, and Y. V. Rozhdestvensky, J. Phys. B **25**, 2473 (1992).

[102] G. S. Agarwal, T. N. Dey, and S. Menon, Phys. Rev. A **64**, 053809 (2001).

[103] H. Li, V. A. Sautenkov, Y. V. Rostovtsev, G. R. Welch, P. R. Hemmer, and M. O. Scully, Phys. Rev. A **80**, 023820 (2009).

[104] D. V. Kosachiov and E. A. Korsunsky, Eur. Phys. J. D **11**, 457 (2000).

[105] K. V. Rajitha, T. N. Dey, S. Das, and P. K. Jha, Opt. Lett. **40**, 2229 (2015).

[106] S. Davuluri and Y. Rostovtsev, Phys. Rev. A **88**, 053847 (2013).

[107] L. Li and G. X. Huang, Eur. Phys. J. D **58**, 339 (2010).

[108] A. Eilam, A. D. Wilson-Gordon, and H. Friedmann, Opt. Lett. **34**, 1834 (2009).

[109] A. Mair, J. Hager, D. F. Phillips, R. L. Walsworth, and M. D. Lukin, Phys. Rev. A **65**, 031802 (2002).

[110] L. Margalit, M. Rosenbluh, and A. D. Wilson-Gordon, Phys. Rev. A **87**, 033808 (2013).

[111] A. G. Truscott, M. E. J. Friese, N. R. Heckenberg, and H. Rubinsztein-Dunlop, Phys. Rev. Lett. **82**, 1438 (1999).

[112] D. Bortman-Arbiv, A. D. Wilson-Gordon, and H. Friedmann, Phys. Rev. A **63**, 031801(R) (2001).

[113] P. W. Milonni, J. H. Eberly, Laser Physics, Wiley, 2010.

[114] D. Budker, D. F. Kimball, V. V. Yashchuk, and M. Zolotorev, Phys. Rev. A **65**, 055403 (2002).

[115] E. E. Mikhailov, I. Novikova, Y. V. Rostovtsev, and G. R. Welch, Phys. Rev. A **70**, 033806 (2004).

TH-1819_11612116

[116] T. N. Dey, and J. Evers, Phys. Rev. A **84**, 043842 (2011).

[117] M. Woerdemann, C. Alpmann, M. Esseling and C. Denz, Laser Photonics. Rev. **7**, 839 (2013).

[118] A. Vaziri, J. W. Pan, T. Jennewein, G. Weihs, and A. Zeilinger, Phys. Rev. Lett. **91**, 227902 (2003).

[119] K. T. Gahegan, and, G. A. Swartzlander, Opt. Lett. **21**, 827 (1996).

[120] M. Padgett and R. Bowman, Nat. Photon. **5**, 343 (2011).

[121] M. P. Macdonald, L. Paterson, K. V. Sepulveda, J. Arlt, W. Sibbett, and K. Dholakia, Science, **296**, 1101 (2002).

[122] L. Paterson, M. P. Dacdonald, J. Arlt, W. Sibbett, P. E. Bryant, and K. Dholakia, Science, **292**, 912 (2001).

[123] D. J. Stevenson, F. G. Moore, and K. Dholakia, Journal of Biomedical optics, **15**, 041503 (2010).

[124] S. Sharma and T. N. Dey, Phys. Rev. A **96**, 033811 (2017).

[125] S. Sharma and T. N. Dey, Phys. Rev. A **96**, 053813 (2017).

[126] V. Ivanov and Y. Rozhdestvensky, Phys. Rev. A **81**, 033809 (2010).

[127] V. Ivanov, Y. Rozhdestvensky, and K.-A. Suominen, Phys. Rev. A **90**, 063802 (2014).

[128] Z. Zhu, W.-X. Yang, X.-T. Xie, S. Liu, S. Liu, and R.-K. Lee, Phys. Rev. A **94**, 013826 (2016).

[129] H. Zhang and K.-K. Liu, J. R. Soc. Interface **5**, 671 (2008).

[130] J. Gea-Banacloche, Y.-Q. Li, S.-Z. Jin, and M. Xiao, Phys. Rev. A **51**, 576 (1995).

[131] K. -J. Boller, A. Imamoglu, and S. E. Harris, Phys. Rev. Lett. **66**, 2593 (1991).

[132] J. E. Field , K. H. Hahn, and S. E. Harris Phys. Rev. Lett. **67**, 3062 (1991).

[133] M. O. Scully, Phys. Rev. Lett. **67**, 1855 (1991).

[134] M. D. Lukin, M. Fleischhauer, A. S. Zibrov, H. G. Robinson, V. L. Velichansky, L. Hollberg, and M. O. Scully, Phys. Rev. Lett. **79**, 2959 (1997).

[135] J. Kitching, H. G. Robinson, L. Hollberg, S. Knappe, and R. Wynands, J. Opt. Soc. Am. B **18**, 1676 (2001).

[136] S. Knappe, V. Shah, P. D. D. Schwindt, L. Hollberg, J. Kitching, Li-A. Liew, and Moreland, Appl. Phys. Lett. **85**, 1460 (2004).

[137] A. Kasapi, M. Jain, G.Y. Yin, and S. E. Harris, Phys. Rev. Lett. **74**, (1995).

[138] O. Schmidt, R. Wynands, Z. Hussein, and D. Meschede, Phys. Rev. A **53**, R27 (1996).

TH-1819_11612116

[139] L. J. Wang, A. Kuzmich, and A. Dogariu, Nature(London) **406**, 277 (2000).

[140] A. Dogariu, A. Kuzmich, and L. J. Wang, Phys. Rev. A **63**, 053806 (2001).

[141] R. W. Boyd, and D. J. Gauthier, Prog. Opt. **43**, 497 (2002).

[142] L. V. Hau, S. E. Harris, Z. Dutton, and C. H. Behroozi, Nature **397**, 594 (1999).

[143] M. M. Kash, V. A. Sautenkov, A. S. Zibrov, L. Hollberg, G. R. Welch, M. D. Lukin, Y. Rostovtsev, E. S. Fry, and M. O. Scully, Phys. Rev. Lett. **82**, 5229 (1999).

[144] A. V. Turukhin, V. S. Sudarshanam, M. S. Shahriar, J. A. Musser, B. S. Ham, and P. R. Hemmer, Phys. Rev. Lett. **88**, 023602 (2002).

[145] M. S. Bigelow, N. N. Lepeshkin, and R. W. Boyd, Phys. Rev. Lett. **90**, 113903 (2003).

[146] J. Tidstrom, P. Janes, and L. M. Andersson, Phys. Rev. A **75**, 053803 (2007).

[147] M. Hosseini, B. M. Sparkes, G. Campbell, P. K. Lam, and B. C. Buchler, Nat. Commun. **2**, 174 (2011).

[148] L. Thevenaz, Nat. Photonics **2**, 474 (2008).

[149] H. R. Thorsheim, J. Weiner, and P. S. Julienne, Phys. Rev. Lett. **58**, 2420 (1987).

[150] J. Weiner, V. S. Bagnato, S. Zilio, and P. S. Julienne, Rev. Mod. Phys. **71**, 1 (1999).

[151] K. M. Jones, E. Tiesinga, P. D. Lett, and P. S. Julienne, Rev. Mod. Phys. **78**, 483 (2006).

[152] T. Kohler, K. Goral, and P. S. Julienne, Rev. Mod. Phys. **78**, 1311 (2006).

[153] C. Chin, R. Grimm, P. S. Julienne, and E. Tiesinga, Rev. Mod. Phys. **82**, 1225 (2010).

[154] R. Dumke, J. D. Weinstein, M. Johanning, K. M. Jones, and P. D. Lett, Phys. Rev. A **72**, 041801 (2005).

[155] K. Winkler, G. Thalhammer, M. Theis, H. Ritsch, R. Grimm, and J. H. Denschlag, Phys. Rev. Lett. **95**, 063202 (2005).

[156] J. C. J. Koelemeij, and M. Leduc, Eur. Phys. J. D. **60**, 3174 (2004).

[157] S. Moal, M. Portier, N. Zahzam, and M. Leduc, Phys. Rev. A **75**, 033415 (2007).

[158] K. Aikawa, D. Akamatsu, M. Hayashi, K. Oasa, J. Kobayashi, P. Naidon, T. Kishimoto, M. Ueda, and S. Inouye, Phys. Rev. Lett. **105**, 203001 (2010).

[159] T. V. Tscherbul, T. Calarco, I. Lesanovsky, R. V. Krems, A. Dalgarno, and J. Schmiedmayer, Phys. Rev. A **81**, 050701 (2010).

[160] U. Fano, Phys. Rev. **124**, 1866 (1961).

TH-1819_11612116

[161] A. Vardi, D. Abrashkevich, E. Frishman, and M. Shapiro, J. Chem. Phys. **107**, 6166 (1997).

[162] X. Li, M. Gacesa, W. Dupre, and G. A. Parker, New J. Phys. **14**, 073001 (2012).

[163] M. Mackie, and J. Javanainen, Phys. Rev. A **60**, 3174 (1999).

[164] E. Kuznetsova, M. Gacesa, P. Pellegrini, S. F. Yelin, and R. Cote, New J. Phys. **11**, 055028 (2009).

[165] B. Deb, and G. S. Agrawal, J. Phys. B: At. Mol. Opt. Phys. **42**, 215203 (2009).

[166] B. Deb, and A. Rakshit, J. Phys. B: At. Mol. Opt. Phys. **42**, 195202 (2009).

[167] G. S. Agarwal, *Quantum Optics* (Cambridge University Press, New York, 2013).

[168] A. Raczynski, M. Rzepecka, J. Zaremba, and S. Z. Kaniasty, Opt. Commun. **266**, 552 (2006).

[169] J. G. Danzl, E. Haller, M. Gustavsson, M. J. Mark, R. Hart, N. Bouloufa, O. Dulieu, H. Ritsch, and H.-C. Nagerl, Science **321**, 1062 (2008).

[170] S. E. Harris, Phys. Today **50**(7), 36 (1997).

[171] A. Simoni, F. Ferlaino, G. Roati, G. Modugno, and M. Inguscio, Phys. Rev. Lett. **90**, 163202 (2003).

[172] A. Simoni, M. Zaccanti, C. D'Errico, M. Fattori, G. Roati, M. Inguscio, and G. Modugno, Phys. Rev. A **77**, 052705 (2008).

[173] C. Chin, V. Vuletic, A. J. Kerman, and S. Chu, Phys. Rev. Lett. **85**, 2717 (2000).

[174] C. Chin, V. Vuletic, A. J. Kerman, S. Chu, E. Tiesinga, P. J. Leo, and C. J. Williams, Phys. Rev. A **70**, 032701 (2004).

[175] S. Inouye, M. R. Andrews, J. Stenger, H.-J. Miesner, D. M. Stamper-Kurn, and W. Ketterle, Nature(London) **392**, 151 (1998).

[176] A. Marte, T. Volz, J. Schuster, S. Durr, G. Rempe,E. G. M. van Kempen, and B. J. Verhaar, Phys. Rev. Lett. **89**, 283202 (2000).

TH-1819_11612116

List of publications

1. S. Sharma, B. Deb, T. N. Dey, "*Subluminal light propagation through an ultracold atom–molecule coupled resonant medium*", J. Phys. B: At. Mol. Opt. Phys. **48**, 175502 (2015).

2. S. Sharma, and T. N. Dey, "*Phase-induced transparency-mediated structured-beam generation in a closed-loop tripod configuration*", Phys. Rev. A **96**, 033811 (2017).

3. S. Sharma, and T. N. Dey, "*Kerr field induced tunable optical atomic waveguide*", Phys. Rev. A **96**, 053813 (2017).

4. S. Sharma, and T. N. Dey, "*Controlled light shaping via phase dependent electromagnetically induced transparency,*" (communicated.)

Schools and Conferences attended

1. ICTS school on frontiers in light matter interaction (ICTS-LMI2014), held at Indian Association for cultivation of science during 8-18 December 2014.

2. ICTS Discussion Meeting on frontiers in light matter interaction (ICTS-LMI2014), held at Indian Association for cultivation of science during 19-22 December 2014.

3. 4th international conference on current developments in atomic, molecular, optical and nano physics with application (CDAMOP-2015), held at Delhi University during 11-14 March 2015.

4. XXVII IUPAP Conference on Computational Physics (CCP-2015), held at IIT Guwahati during 2-5 December 2015.

TH-1819_11612116